Summer 2017

Effect of fracture heterogeneity on proppant transport and settling mechanism

Dhurgham Abdulameer Kadhim

Follow this and additional works at: https://scholarsmine.mst.edu/masters_theses

Part of the Petroleum Engineering Commons

Department:

Recommended Citation

Kadhim, Dhurgham Abdulameer, "Effect of fracture heterogeneity on proppant transport and settling mechanism" (2017). *Masters Theses*. 7691.
https://scholarsmine.mst.edu/masters_theses/7691

EFFECT OF FRACTURE HETEROGENEITY ON PROPPANT TRANSPORT AND

SETTLING MECHANISM

by

DHURGHAM ABDULAMEER KADHIM

A THESIS

Presented to the Faculty of the Graduate School of

MISSOURI UNIVERSITY OF SCIENCE AND TECHNOLOGY

In Partial Fulfillment of the Requirements for the Degree

MASTER OF SCIENCE IN PETROLEUM ENGINEERING

2017

Approved by

Dr.Shari Dunn-Norman, Advisor
Dr.Abdulmohsin Imqam, Co-advisor
Dr. Ralph Flori
Dr. Mingzhen Wei

ABSTRACT

Proppant transport modeling through fractures with slickwater fluid systems assumes uniform and homogeneous fracture widths by implying constant fluid behavior at wall boundaries. Hydraulic fracturing mineback operations have demonstrated that induced fractures are heterogeneous and varying in width. This work investigates the impact of fracture width heterogeneity, roughness, and leak-off on ceramic proppant transport and settling, using proppant distribution concepts of Equilibrium Dune Level (EDL) and equilibrium Dune Length (EDX). Experimental work was conducted to investigate the impact of fracture width heterogeneity by varying fracture width along two plexiglass sheets. To mimic actual hydraulic fractures, the injection side was designed as the largest width, and the width of the opposite end was reduced. The ratio between the injection and tip side widths was varied to study the effect of changing fracture width. One ratio was used as a base to study the effect of varying wall roughness and leak-off on the proppant placement. Results of this work demonstrate the impacts of reservoir heterogeneity, wall roughness, and leak off on proppant conveyance and distribution. Fracture width and wall roughness have a significant effect on proppant distribution along a fracture. Increasing width heterogeneity and roughness provide a better proppant distribution and thus better fracture propped conductivity. The effect of leak-off on proppant distribution was monitored, and it showed that proppant followed water movement. Consequently, average water volume that left the slot was affected by proppant distribution.

ACKNOWLEDGMENTS

IN THE NAME OF ALLAH, THE MOST GRACIOUS, THE MOST MERCIFUL

I am eternally thankful to Allah for supporting me to accomplish this research.

I would like to express my extreme appreciation to The Higher Committee for Education Development in Iraq (HCED) for awarding me a fully funded scholarship. I offer my sincere gratitude for the learning opportunity provided by them.

I am grateful to each of my thesis committee members for their professional guidance and encouragement: Dr. Shari Dunn-Norman; Dr. Abdulmohsin Imqam; Dr. Ralph Flori; and Dr.Mingzhen Wei. I am especially indebted to my advisor, Dr. Shari Dunn-Norman, for all support and encouragement that she provides. I would not be able to pursue my goal without her assistance. I am especially appreciative to Dr.Abdulmohsin Imqam who drew for me the way of success in this project during his hectic schedules.

I would like to thank Unconventional Resources Technology (URTeC) for acceptance a relevant paper at the 2017 Unconventional Resources Technology Conference in Austin, Texas.

To whom gave me life and continuously influences how I live, my parents, I am forever grateful. I hope they have been satisfied with me. I would like to express my appreciation for all incorporeal support provided by my brothers and my sister.

To each person in the research group, my deepest gratefulness. Many thanks to my friends for propelling me and encouraging me to endeavor to reach my goal.

Finally, to my precious, patient, and supportive wife, my cordial gratitude. During rough times, your encouragement and support enabled me to complete this research. For those angels who implants the smile on my face my lovely kids, my love and gratitude.

TABLE OF CONTENTS

LIST OF FIGURES

LIST OF TABLES

NOMENCLATURE

Symbol	Description
a	Relative capacity parameter, dimensionless
k_f	Fracture permeability, md
W	Fracture width, ft
k	Reservoir permeability, md
x_f	Fracture half length, ft
s_f	The equivalent skin effect, dimensionless
F_{CD}	Dimensionless fracture conductivity
v_s	Particle settling velocity, cm/s
g	Gravitational constant, 980 cm/s^2
ρ_p	Particle density, gm/cc
ρ_f	Fluid density, gm/cc
d_p	Particle diameter, cm
μ_f	Fluid viscosity, poise
$V_{equilibrium}$	Equilibrium velocity, ft/min
Q	Injection rate, bbl/min
w	Fracture slot width, cm
h_o	The height of cross-sectional area above-settled sand, ft
θ_r	Angle of repose
FPV	Fracture pore volume, dimensionless
EDL	Equilibrium dune level, dimensionless
EDX	Equilibrium dune length, dimensionless

l	Fracture slot length, cm
h	Fracture slot height, cm
v_w	Settling rate corrected for presence of walls, cm/s
v_s	Settling rate of particle in stokes flow, cm/s
a	Particle radius, cm
t	Fracture width, cm
P	Pressure, psi
ρ	Slurry density, m/cc
m_p	Proppant mass, gm
m_w	Water mass, gm
v_p	Proppant volume, cc
v_w	Water volume, cc
g	Acceleration due to gravity, 980.6 cm/s^2
v	Slurry horizontal velocity, ft/s
K_L	Loss coefficient, dimensionless
d	Smaller dimeter pipe, cm
D	Bigger diameter pipe, cm
D_e	Equivalent diameter, cm
μ	Slurry viscosity, poise
Q_s	Slurry flowrate, cm^3/s
$V_\emptyset$	Settling rate of concentrated particle, cm/s
$\emptyset$	Proppant concentration (volume of solid/volume of mixture)

1. INTRODUCTION

Hydraulic fracture is a technique using high-pressurized fluid to create a crack which acts as a conduit channel inside a specific interval of a formation, usually oil/gas shale formation. It was introduced to the oil industry by Clark in 1948 (Jones and Britt, 2009). This technology was commercially accepted by 1950. Today hydraulic fracture is applied in most oil and gas wells, with more than 1 million fracturing jobs in the United States, and 2.5 million fractures worldwide, based on an estimation by Society of Petroleum Engineers (King, 2012).

The fracturing objective is to create conductive channels in oil/gas shale reservoirs. In 1961 Pratt showed a relationship between effective wellbore radius, r'_{wD} , and a relative capacity parameter, a, (Economides et al., 2013); a and r'_{wD} are defined in (1) and (2) respectively:

$$a = \frac{\pi k x_f}{2 k_f W} \tag{1}$$

$$\acute{r}_{wD} = \frac{\acute{r}_w}{x_f} \tag{2}$$

$$\acute{r}_w = r_w e^{-s_f} \tag{3}$$

where

    a: Relative capacity parameter, dimensionless

    k_f: Fracture permeability, md

    W: Fracture width, ft

    k: Reservoir permeability, md

x_f: Fracture half length, ft

s_f: The equivalent skin effect, dimensionless.

The relationship between relative capacity parameter and effective well radius is illustrated in Figure 1.1. Pratt showed that a has an inverse relationship with r'_{wD}. Large values of a imply small fracture permeability-width product or large reservoir permeability-fracture length product, hence a large conductivity fracture. Pratt shows that a flat part of the curve where an "infinite conductivity fracture" was achieved. This occurs where r'_{wD} is 0.5 and $a = 0.01$.
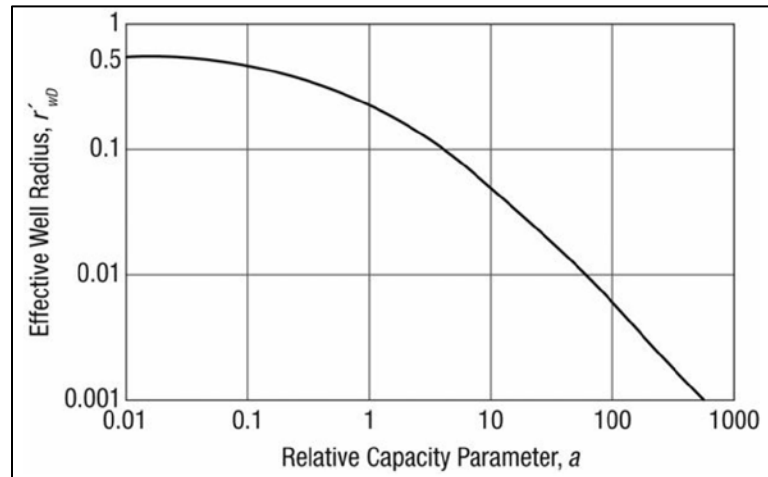
Figure 1.1. The relationship between Relative Capacity Parameter and Effective Well Radius (Economides et al., 2013)

Cinco-Ley and Samaniego-V. (1981) introduced the dimensionless fracture conductivity term (F_{CD}). F_{CD} can be calculated by (4) (Marquardt et al., (1991):

$$F_{CD} = \frac{k_f W}{k x_f} \tag{4}$$

where

F_{CD}: Dimensionless fracture conductivity.

F_{CD} is the inverse of a so the curve flips around, as shown in Figure 1.2. At $r'_{wD} = 0.5$, F_{CD} ≥ 20, and an infinite conductivity fracture exists. At this point, well production is not improved by increasing fracture conductivity, k_fW. For shale formations where reservoir permeability is very small, $k < 0.001$ mD, F_{CD} will be large and the fracture acts as infinite conductivity fractures. Increasing x_f is the important for better fracture performance. In essence, there is no need to inject high proppant concentration, and thus, viscous fluid should not be used in such cases. Hence, slickwater fracturing, which can produce long fracture length with low fracture conductivity is utilized in shale field development.
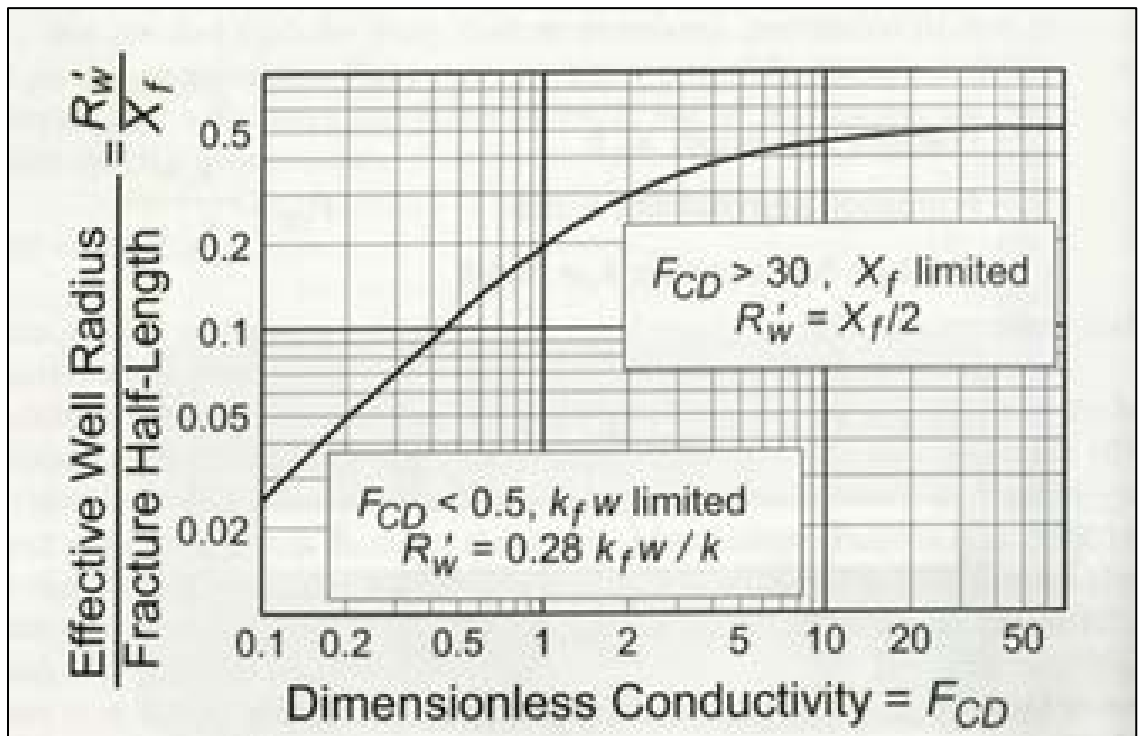
Figure 1.2. Effective Wellbore Radius VS. Dimensionless Fracture Conductivity (Jones and Britt, 2009)

The type of fracturing fluid and leak-off affects fracture fluid efficiency, which controls fracture half-length. Fracture height is affected by two factors:

- Stress differences between the pay formation and the surrounding zones.

- Fluid viscosity

Proppant type has a significant effect on fracture conductivity and well productivity. This chapter will be dedicated to slickwater properties, proppant type and proppant distribution along a fracture.

1.1. FRACTURING FLUID

Selecting a fracturing fluid depends on formation characteristics like grain composition, cementation factors between grains, stress gradient and the compatibility between injected fluids and the formation. The most common fracturing fluids are oil-based fluids and water based fluids. Due to the low cost and environmental benefits of water based fluids, most hydraulic fracturing is performed with this fluid (Harris, 1988). Based on gelling agents and other additives, water based fracturing fluids may be either slickwater (water with polyacrylamide for friction reduction), linear gel (water with some polymer added) water based crosslinked polymers, or a hybrid fluid (a combination of above mentioned types). Each of these types of fracturing fluids may use different additives and chemicals.

The purpose of using additives in fracturing fluids is to control undesirable reactions, such as downhole corrosion or friction during pumping, or to enhance fracture productivity by improving proppant-carrying capacity, which improves proppant distribution. Fracture fluid additives can also help minimize formation damage. The most commonly used additives in hydraulic fracturing are viscosifiers or crosslinkers, pH control, fluid-loss additives, gel breakers, surfactants, clay stabilizers, biocides (Harris,

1988). Each of these additives can be used in different concentrations based on the formation and fracture design. The functions of these additives are briefly described here:

- Viscosifiers or crosslinkers: these additives increase fluid viscosity to enhance proppant carrying capacity. In viscosifiers, guar and cellulose are used to add a polymer which viscosifies the fluid, so that larger sand concentrations can be pumped. The greatest proppant carrying capacity comes from crosslinking the polymers. For crosslinkers, aluminum, antimony, borate, etc., are utilized to increase fluid viscosity, but for environmental reasons borate is preferred over the metallic crosslinkers. Viscosifiers decompose at temperatures above 225°F. The products of this decomposition reduced fluid viscosity. To stabilize fluid viscosity, a chemical stabilizer like methanol is added. Using crosslinked-fracturing fluid with high sand concentration leads to high fracture width and conductivity, most typically used in stimulating high permeability reservoirs.

- Ph control: to control gel properties by influencing initial polymer gelation rate, viscosity stabilization, bacteria growing control, gel break properties.

- Fluid-loss additives: to minimize fluid loss into the formation by controlling filter cake forming rate. Upon contact, some of the fracturing fluid, called 'spurt', enters into the formation before a filter cake forms and reduces the fluid loss. If pore openings are big as in high permeable reservoirs, using proppant size close to the size of the pore openings is suggested.

- Gel breakers: when using a crosslinked fracturing fluid, gel breakers are included to break the crosslinked bonds of the fluid after fracture closure. This allows the

well to clean up and, therefore, enhances fracture conductivity by reducing fluid viscosity in the placed fracture.

- Surfactants: to lower interfacial tension and capillary pressure, promote fluid recovery and facilitate compatibility between the fracturing and reservoirs fluids.
- Clay stabilizers: to prevent clay sloughing and fines migration.
- Biocides: to control the growth of aerobic and anaerobic bacteria in gelled fluids.

Many studies and field treatments have been conducted to identify fracturing fluids that yield optimum economical profit for a particular reservoir. Parker (1990) developed a comparison between different types of gelled fluids. He found that crosslinked fluids generated thinner filter cake than other types of gelled fluids. As a result, he found crosslinked fluids provide higher conductivity than linear gel but may lead to high damage of the proppant pack. Water frac treatments, which use water and only a polyacrylamide friction reducer, have proven most beneficial in unconventional resources. For example, water frac treatments became the primary fracturing fluid for the impermeable gas reservoirs in the East Texas Cotton Valley (Smith et al., 2001). Shelley et al. (2008) used a statistical analysis to compare crosslinked gel and slickwater fracturing fluids used in the Barnett shale formation and their impact on production. They found that injected proppant concentration depends on the type of fracturing fluid. In slickwater, 50,000 lb to 200,000 lb can be injected while it ranged from 1,000,000 lb to 1,800,000 lb for cross-linked fluids. Median production for the first year shows that wells treated by slickwater produced 23,000 Mcf/ac-ft, while wells treated with crosslinked fluids produced 15,000 Mcf/ac-ft. Treated water (slickwater) fracturing provides more economical profit than hybrid-treated water and linear gel fracturing based on a study provided by Alqatrani, etal. (2016) on

Glauconite formation on Tierra del Fuego. This study showed that slickwater treatment added $230,000 profit to the average revenue of Glauconite hybrid treatment stimulation.

Based on the previous work, slickwater provides better well productivity among all types of fracturing fluids in unconventional shale reservoirs. Slickwater is considered the least additives-containing fluid (i.e., it is environmentally friendly). In general, slickwater fracturing fluids contain some chemical and additives, illustrated in Figure 1.3. Beside the high productivity of the slickwater-treated wells, slickwater treatment meets environmentally responsible mandates (Paktinat et al., 2011).
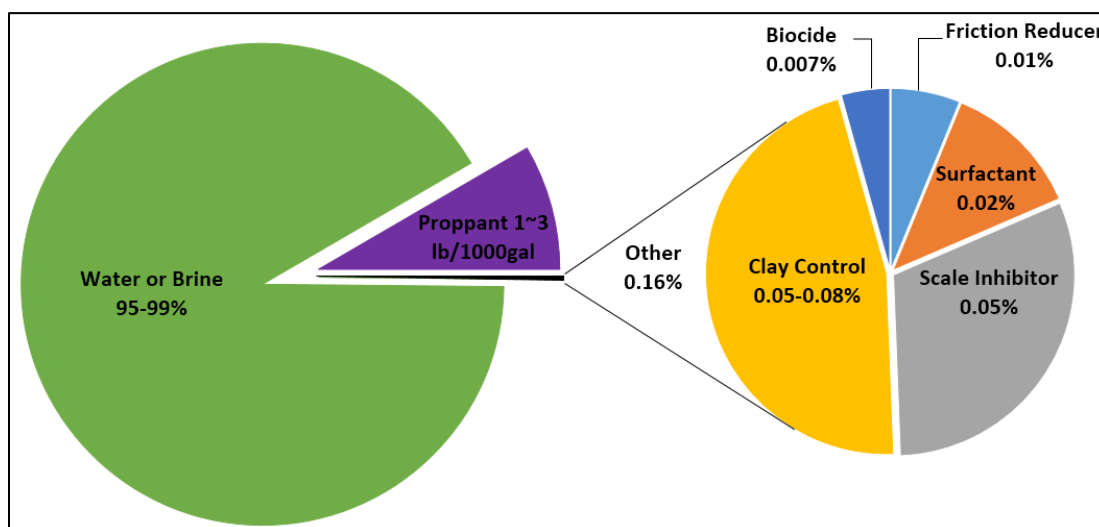
Figure 1.3. Slickwater Composition and Allowed Carried Proppant Concentration (modified from Paktinat et al., 2011)

However, slickwater is considered an imperfect transport fluid when it comes to moving proppant. Crosslinked fluids are considered 'perfect transport fluids' and can carry large concentrations of sand. Slickwater is inefficient, and sand settles very quickly in such fracturing fluid. However, slickwater can carry up to 3 ppg (Figure 1.3) proppant, which creates sufficient fracture conductivity ($k_f W$).

1.2. PROPPANT

Proppant is granular material, which is pumped into a formation after mixing with a fracturing fluid. Proppant serves two functions. First, it holds the created fracture open after pump pressure is released, to allow hydrocarbon to flow through the fracture. Secondly, proppant is designed to provide a certain fracture conductivity (kfw). Because of the variation in underground formation environments (e.g. pressure, temperature and stresses), proppant manufacturers have developed many kinds of proppant to meet the needs of the oil/gas industry. Each proppant type can withstand a range of in-situ stresses. Sand is commonly sufficient in formation closure stresses of up to 4000-6000 psi, and ceramic proppant is used at higher downhole stresses.

The selection of proppant is an important element in fracturing treatment. Well productivity is related to fracture conductivity. Fracture conductivity is affected by many factors, including:

1. The size of proppant particle.

2. Proppant microstructure

3. The shape of proppant grains.

4. Volume of grains.

5. Proppant coverage (surface area, lb/ft^2).

The available types of proppant belong to one of the following categories: basic types of proppants, modified proppants, multifunctional proppants, proppant agglomerates, self-suspending proppants and in-situ generation of proppant (Liang et al., 2016). Liang explained detailed information about these categories, which are summarized in Table 1.1. Ceramic proppant can be categorized into four groups based on specific gravity (S.G), as

shown in Table 1.2. Increasing alumina content enables proppant to withstand higher closure pressure.

Table 1.1Proppant Types (modified from Liang et al., 2016)

Category	Type	Brief description
Basic types of proppants	Sand (frac sand/silica sand	Cheap, uniformity in size and shape and capable to withstand pressure up to 6000 psi.
	Ceramic proppant	More expensive than sand, uniform in size and shape, capable to withstand closure pressure up to 10,000 psi. Higher porosity, permeability and conductivity than sand.
Modified proppants	Resin coated proppant (RCP)	Advantages: broken grain can be trapped inside the coating and prevent proppant flowback by connecting proppant with each other. Disadvantage: cannot withstand high temperature or high temperature degradation.
	Ultra-lightweight proppant (ULW)	Advantage: reduced proppant settling to enable slickwater to carry proppant deep inside the formation even with low flowrate. S.G ranges from 0.8 to 2.59.
Multifunctional proppants	Traceable proppant	Advantage: provides detailed information about fracture height growth and where proppants were placed in a multistage fracturing treatment.
	Infused porous ceramic proppants	Advantage: minimize wasting chemical during proppant transport, enhance the chemical elution profile and induce longer treatment life.
	Slow-released breaker	Advantage: slows breaker reaction rate and induces better cleanup for the residue gel because breakers are positioned on the proppant surface and in contact with the gel directly.
	Multiphase flow enhancer	Advantage: modifying proppant surface to be neutral-wet instead of being water-wet to increase hydrocarbon recovery.
	Contaminant removal	Mingling some contaminant elimination chemical on the surface of proppant grains or inside the pores of porous proppants.
Proppant agglomerates	Proppant agglomerates	Coating proppant with hydrophobic material to bind proppant as conglomerates when they are wetted by an aqueous media. Gas presence in those agglomerates reduces bulk density.
Self-suspending proppants	Self-suspending proppants (SSP)	Advantage: enhance proppant transport, minimize the required amount of proppant and enhance fracture conductivity.
In-situ generation of proppant	In-situ generation of proppant	Generating proppant solids free by using chemical that can form spherical grains inside the formation. These grains provide a pathway for hydrocarbon to flow, withstand high closure pressure and cannot be crushed because of its permanent elasticity.

Table 1.2. Description of ceramic proppant types (Liang et al., 2016)

Type of Ceramic proppant	S.G, fraction	Alumna content, %
Lightweight ceramic (LWC)	2.55 to 2.71	45 to 50
Intermediate density ceramics (IDC)	~3.27	70 to 75
High density ceramics (HDC)	~3.5	80 to 85
Ultra-high-strength proppant (UGSP)	~3.9	~ 10

Cobb and Farrell (1986) presented a long-term test (70-80 days) under realistic conditions to reveal how conductivity changes with time. In their study, two kinds of sintered bauxite and intermediate ceramic proppant are exposed to brine for four weeks. Closure pressure and test temperature were 50 MPa and 100°C respectively. The results of the test are shown in Figure 1.4. At the end of the test, this figure reveals that productivity decreased about 30% for sintered bauxite while it was reduced about 65 % for intermediate ceramic.
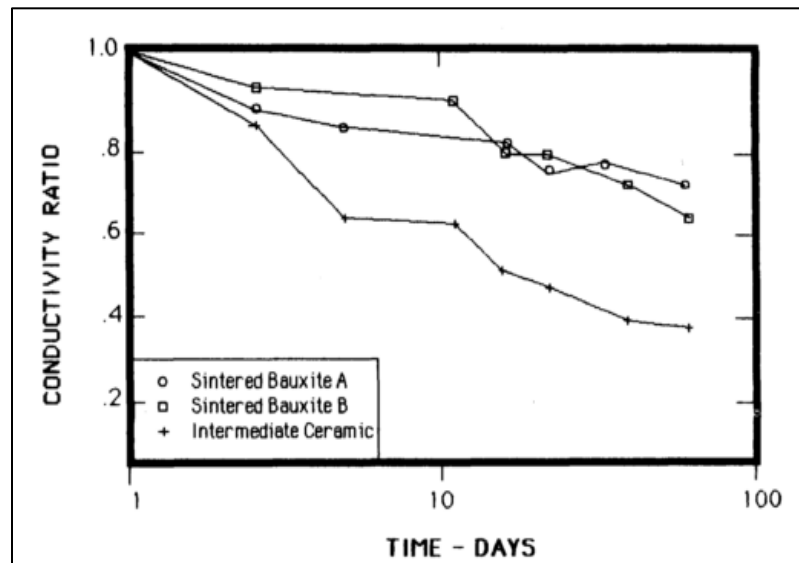
Figure 1.4. Effect of 50 MPa of Closure Stress on Conductivity of Three Types of Proppant (Cobb and Farrell, 1986)

McDaniel (1986) reported experimental results about the effect of reducing temperature under a specific closure stress. Intemediate strength ceramic (ISC Proppant), resin coated sand (RC Sand) and ottawa sand were used in this study. The results of the tests are shown in Figure 1.5. They found that ISC proppant is better than the others for all ranges of temperautre, and no effect was observed for cool-down on fracture conductivity on all types of proppant.
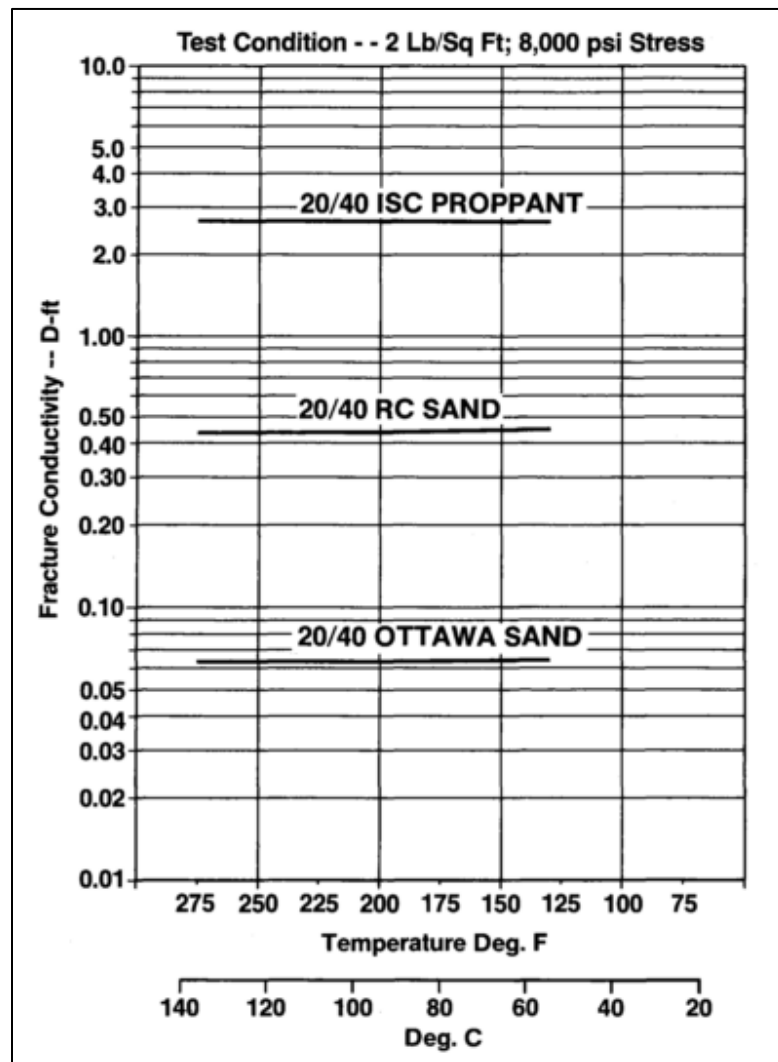
Figure 1.5. Temperature Effect on the Conductivity of Different Types of Proppant (McDaniel, 1986)

Vincent (2009) presents experimental data describing a relationship between conductivity and stress applied on different types of proppant and sand (Figure 1.6). This figure shows that ceramic exhibited higher conductivity than RCP sand and Ottawa sand. The highest measured conductivity occurs using premium sieve lightweight ceramic. Increasing the formation closure stress reduces conductivity in all types of proppant.
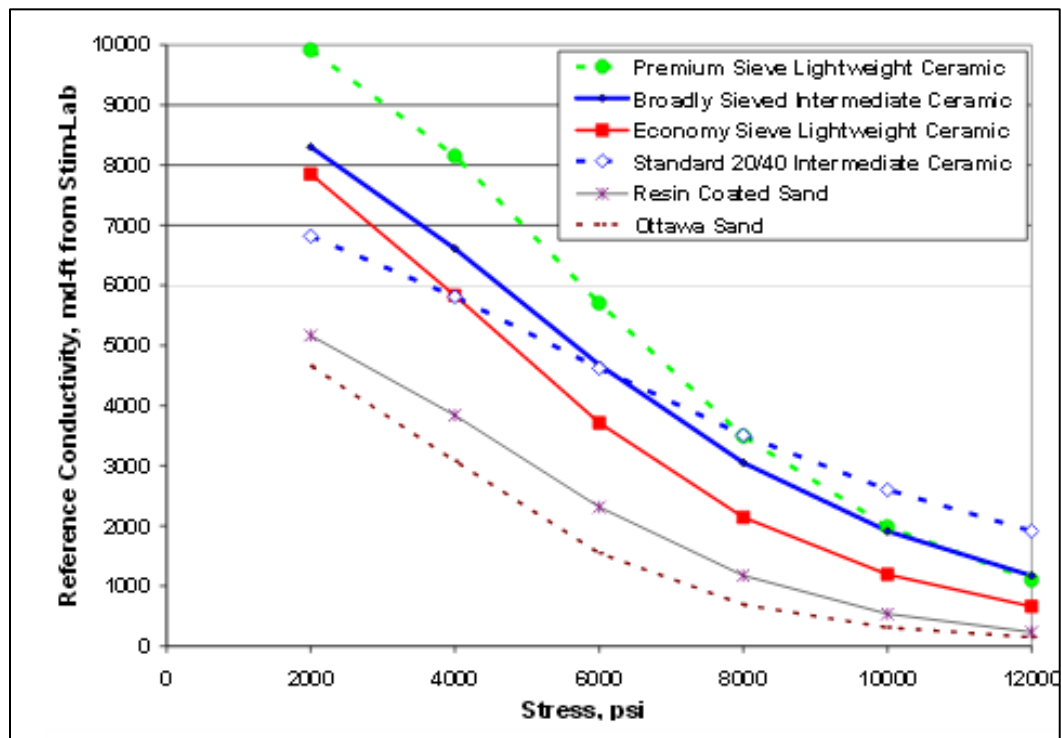
Figure 1.6. Effect of Proppant Type on Conductivity (Vincent, 2009)

Proppant size also affects fracture conductivity. Mack et al. (2014) explained a relationship between conductivity and stress for different types of proppant. Figure 1.7 reveals how increasing stress could reduce conductivity. At very low stresses, larger proppant gave higher conductivity. By increasing stress, 20/40 sand has a much lower conductivity than 50/60 advanced ceramic proppant (ACP).
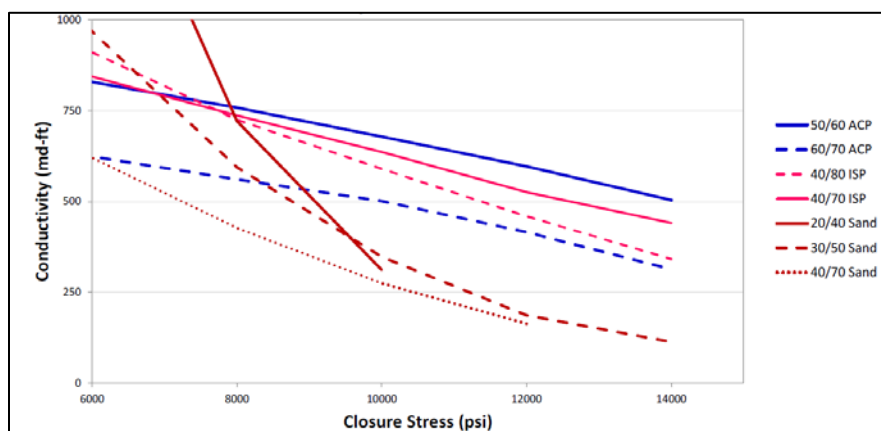
Figure 1.7. Large Proppant has higher Conductivity than Small Proppant (Mack et al., 2014)

1.3. PROPPANT TRANSPORT, DISTRIBUTION AND SETTLING

Based on previous studies and field reports, fracture conductivity is directly related to proppant distribution. Carroll Jr. and Baker (1979) suggested that particle size distribution in relation to the formation pore size distribution should be considered as an affecting factor on fracture conductivity. Proppant distribution and deposition are functions of particle size, current speed, flow regime (laminar or turbulent) and the density contrast between the proppant and the fluid. The Open University Course Team (1999) classified the transport of particles flowing in a stream into four categories: sliding, rolling, saltation and suspension. Figure 1.8(a) explains sliding and rolling transport, and Figure 1.8(b) illustrates saltation and suspension transport. Sliding and rolling occur at low flowing velocity. In these modes, proppant grains are in continuous contact with the bottom of a fracture or the bed that was formed due to previous settled proppant. Salton grains which have higher velocity jumped off the surface in different trajectory. These three categories collectively formed the proppant dune or proppant pile. Suspended particles are the particles that travel for a long distance and merely come in contact with the pile. Suspended

particles have higher velocity than the others do. After losing the kinetic energy, these grains will settle at the top of the dune.

(a) (b)
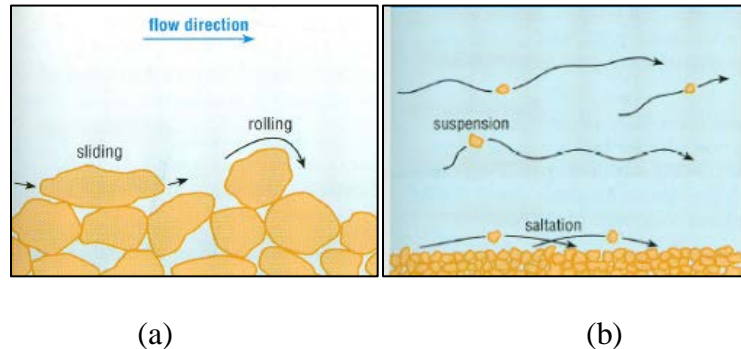
Figure 1.8. Modes of Proppant Transport (The Open University Course Team, 1999). (a) Rolling Sliding Mode (b) Saltation and Suspension Mode

Coker and Mack (2013) provide an explanation about these mechanisms. In viscous fluid, suspension is the most common proppant transport mechanism because most proppant will be suspended in that fluid and will settle slowly to form a bank. Suspension is affected by density and particle diameter. When the carrying fluid is slickwater, or other thin fluids, proppant settling becomes faster than in viscous fluids. Creeping (sliding and/or rolling) and saltation will be important. Saltation is controlled by the coefficient of restitution (CoR). CoR is defined as the velocity of the object that leaves the surface after collision to the velocity of that object entering the collision. See Section 2.2 for more information about CoR. Creeping is dominated by friction.

On the other hand, proppant grains settle in one of two manners either hindered or free settling. McMechan and Shah (1991) defined free settling as the settlement of proppant that occurs without any effect of container walls or surrounding particles. If the settling was under the influence of either container boundaries or/and surrounding particles, particle movement will be impeded. This process is defined as hindered settling.

Clark and Zhu (1996) defined the term N_c which is the rate of the horizontal force divided by the vertical slurry settling force:

$$N_c = \frac{F_h}{F_v} \tag{5}$$

This concept is embedded in the current research.

1.4. OBJECTIVES

The main objective of this study is to provide a clear and rigorous interpretation for proppant behavior inside a fracture. Building fracture models with a width variation along the fracture more accurately simulates field fracture geometry. The objectives of this study can be summarized as follows

- Studying the effect of fracture width heterogeneity, injection side width, wall roughness and leak-off on proppant distribution.
- Monitoring proppant movement and distribution inside the fracture.
- Describing proppant transport mechanisms along the fracture slot.

The results obtained from this research provide more comprehensive details regarding proppant behavior inside the fracture slot and an interpretation of the proppant movement along the fracture slot, for heterogeneous fractures including friction and leak-off.

1.5. THE SCOPE OF THIS RESEARCH

This study is an experimental work conducted to understand proppant transport through a fracture slot. Proppant pile buildup rate was investigated through varying fracture width heterogeneity, injection side width, friction and leak-off. The shortcoming of

previous work lies in assuming fracture homogeneity, and studying proppant transport using homogeneous fracture models. This work provides heterogeneous fracture modeling, combined with an investigation of how friction and leak-off may affect proppant distribution in heterogeneous fractures. Using the slurry injection fracture pore volume (FPV) strategy provided an exact description for proppant flow behavior. Proppant height distribution was described for each slurry FPV to get a better determination for the effect of fracture width heterogeneity, injection side width and fracture leak-off on proppant transport and settlement. Furthermore, leak-off effect on injection pressure and the tendency of water to exit the slot were precisely monitored. A new settling and transport mechanism has been identified. The construction of this study to accomplish the scope of this research is summarized by Figure 1.9.
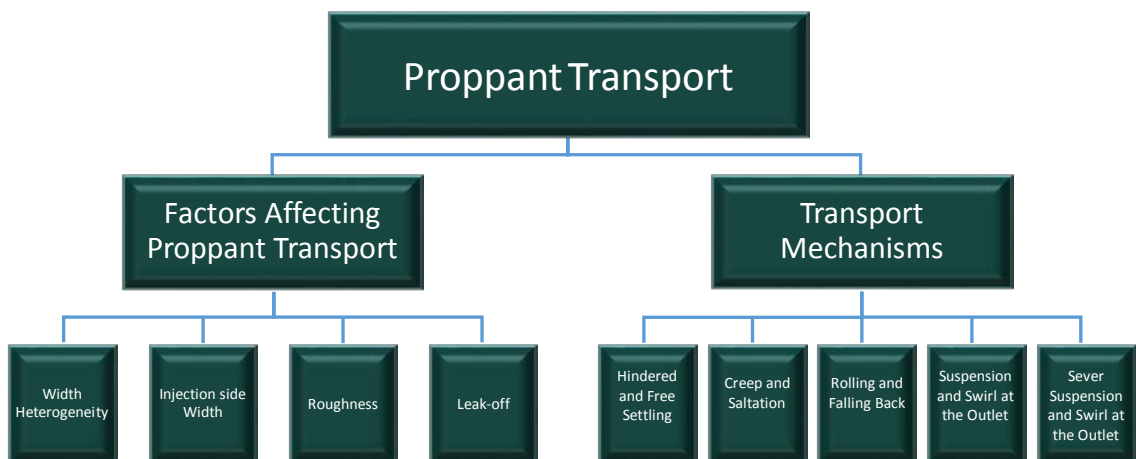
Figure 1.9. Research Scope

2. LITERATURE REVIEW

Slickwater-proppant transport became preferable for use in hydraulic fracturing in the oil and gas industry due to its low cost from not needing polymer crosslinking. Adding crosslinkers to fracturing fluids to enhance fluid ability to carry more proppant deep into the formation adds more residue in fractures. That residue has an inverse effect on fracture conductivity; therefore, slickwater has better productivity enhancement than viscous fluid because of its resulting high permeability. The limitation of using slickwater to transport proppant is its inability to carry proppant for a long distance inside the formation. Proppant carried by slickwater settles readily and closer to the wellbore than in viscous fluids and does not follow stoke's law. Thus, studying proppant transport by slickwater is crucial and an important topic.

2.1. FACTORS AFFECTING PROPPANT TRANSPORATION

Several attempts have been made to give a thorough understanding of proppant distribution and its settling velocity. Particle settling velocity typically is calculated by Stoke's law and Newton's equation (Barree and Conway, 1995). Stoke's law and Newton's equations are listed below in (6) and (7), respectively. Stoke's law is applicable for single particle, viscous Newtonian fluids and a low particle Reynolds number, $R_{ep} \leq 2$. Newton's equation is valid for single particle and high particle Reynolds number, $R_{ep} \geq 500$. Since proppant mostly settles in groups of grains, particles will be affected by each other and therefore settling velocity will be affected too (Gadde et al., 2004). Thus, these two equations are not truly accurate:

$$v_s = \frac{g(\rho_p - \rho_f)d_p^2}{18\mu_f} \tag{6}$$

$$v_s = 1.74\left(\frac{g(\rho_p - \rho_f)}{\rho_f}\right)^{0.5} d^{0.5} \tag{7}$$

where

v_s: Particle settling velocity, cm/s

g: Gravitational constant, 980 cm/s^2

ρ_p: Particle density, gm/cc

ρ_f: Fluid density, gm/cc

d_p: Particle diameter, cm

μ_f: Fluid viscosity, poise.

The first proppant experiment was presented by Kern et al. (1959) to study sand transport in two plexiglass sheets. They focused on defining equilibrium velocity and sand distribution for various velocities and viscous fluids. They built a vertical fracture with a width of 0.25 inch. They mixed 10-20 and 20-40 mesh sized sand and 20-40 steel shot with water in some of their experiments and water and CMC (carboxymethylcellulose), in others. They found that injected sand settled immediately when slurry entered the slot. Before reaching equilibrium velocity, injected sand contributed building dune height. After reaching equilibrium velocity, all injected sand increased dune length and settled away from the wellbore. They concluded that large sand should be injected earlier in a fracture job or during the entire fracture job because they found that larger sand washed over the small sand and did not settle near the wellbore. At equilibrium velocity, they concluded that leak-off and sand concertation were the two primary factors controlling dune height at

equilibrium velocity. Leak-off results in fluid loss into that formation and reduced fluid horizontal velocity. As a result, leak-off increases sand concentration. A mathematical correlation for equilibrium velocity was the result of their work. The correlation can be applicable for vertical and rectangular fracture. The correlation is illustrated in (8):

$$V_{equilibrium} = \frac{13.4 \, Q}{w h_o} \tag{8}$$

Equilibrium sand height at a specific velocity can be estimated by (9):

$$h_o = \frac{13.4 \, Q}{w V_{equilibrium}} \tag{9}$$

where

$V_{equilibrium}$: Equilibrium velocity, ft/min

Q: Injection rate, bbl/min

w: Fracture slot width, cm

h_o: The height of cross-sectional area above-settled sand, ft.

Swanson (1967) introduced an equation to calculate free settling velocity by using an empirical trial and error method. His equation is explained in (10). His formula is applicable for a wide range of particle Reynolds number.

$$v_o = \frac{v_N}{\alpha} \left(\frac{1}{1 + \frac{\sqrt{48}\beta\mu_f}{d\rho v_N}} \right) \tag{10}$$

where

$$v_N = \sqrt{\frac{4gd(\rho_p - \rho_f)}{3\rho_f}} \tag{11}$$

α, β: Boundary layer coefficients, for sand $\alpha = 1.277$, $\beta = 2.8$.

Many experiments and models have been constructed to give a qualitative visualization of proppant motion and settling inside a fracture. Clark and Quadir (1981) used some experimental data to calculate proppant-settling velocity using various equations. He found that ignoring the effect of shear on fluid viscosity results in lower particle settling velocity and longer propped length. Choosing the right formula is a critical because each equation may yields different results.

An experimental study was conducted by Liu and Sharma (2005) to investigate proppant transport and settling as a result of changing the ratio of proppant size to fractures width. Various fluid rheological properties and types of fluids were used in their study. Roughness effect was investigated as well. From their study, they found the following:

- Proppant horizontal velocity is less than fluid horizontal velocity, but it is higher than average fluid velocity for small particles where fracture wall effect is low, and less than average fluid velocity where fracture wall effect is significant.

- Increasing proppant size will increase fracture wall effect, and the proppant will be more retarded.

- As proppant diameter becomes close to the fracture width, settling velocity can be reduced dramatically.

- Fracture wall has a great impact when the interaction between proppant and fracture walls increases, which happens in higher fluid viscosity.

- "Reverse-Hybrid-Frac" by displacing high viscous fluid by water carrying proppant enhances the horizontal transport of proppant.

- Wall effects correlation for two categories: one for the ratio of proppant diameter to fracture thickness less than 0.9 and the other when the ratio is greater than 0.9, which means that the border-line is 0.9.

- Particle horizontal movement is retarded by a rough wall more than a smooth wall.

Because of the importance of slickwater in oil industry, recent studies have been dedicated to investigate the effect of some factors on proppant motion and settling in slickwater. Some of these studies were conducted by designing an experimental model, and others by simulating a fracture with a 3D simulator.

On the modeling side, Gadde et al. (2004) built a 3-D hydraulic fracture simulator to study the effect of fluid velocity, proppant size, fluid rheology and fracture width on settling velocity in water fracs. They found that bigger proppant size, lower proppant concentration and wider fractures increase settling. A short propped length can be achieved because of that high settling velocity that results from using slickwater. They also found that, Stoke's law is applicable whens when the particle Reynolds number is less than than 2 ($R_{ep} < 2$). If Rep > 2, Stoke's Law will overestimate settling velocities because it does not include the effect of turbulence, fracture wall, proppant concentration and inertial effects. By using

A CFD model was built by Tsai et al. (2013) to represent fracture width heterogeneity with a large scale. In this model, flow rate of 18.75 bpm and 75 bpm were used to pump propant densities of 1.0, 1.35 and 2.65 S.G. They found that proppant with a density similar to that of water followed water and settled at the end of the fracture. Increasing proppant density showed early proppant settlement. The unwanted early settling behavior for heavy proppant can be minimized by increasing flow rate. They suggested

that including roughness and fracture leak-off in future study can give better understanding for simulated gas and oil reservoirs.

Another experimental study was provided by Dayan et al. (2009). They addressed questions about slurry traveling through a network of pathways. They observed that the most significant factors that can control proppant distribution in a fracture are fracture heterogeneity and leak-off. They recommended studying these two factors in detail in future work.

Based on our review of historical work of proppant transport and settling in slickwater fluid, there is still a lack of knowledge in the phenomenon. Assuming homogeneous fracture in previous experimental works might affect proppant settling and dune buildup calculations. In this study, fracture width heterogeneity has been considered in all investigated factors. In addition, many questions related to leak-off need to be answered. For example, the effect of leak-off location on water tendency to leave a fracture slot needs to be explored. Roughness effect on proppant transport has not been completely addressed. The previous work examined wall roughness effect on proppant horizontal velocity by displacing gelled fluid by water. In this study, the effect of wall roughness on proppant horizontal and vertical velocity was inspected.

2.2. PROPPANT TRANSPORT MECHANISMS

Proppant placement and distribution is considered to have the main effect on fracture conductivity and well productivity. Many works to study the mechanisms of proppant transport and proppant settlement were presented. In this section, some of these experiments will be explained.

An economic model was built by Coker and Mack (2013) to identify prodcution benefit from a stimulated well. They described proppant transport mechanisms as one of three categories: creeping, saltation or suspension. Creeping can be improved by reduced friction, saltation can be enhanced by increasing CoR, and suspension can be improved by reducing proppant size and density.

Mack et al. (2014) constructed a transparent slot to study injected proppant and sand behavior. Different types of proppant and different mesh sizes were injected at different flow rates. They injected advanced ceramic proppant (ACP), conventional proppant (Intermediate Strength Proppant ISP), and sand with slickwater separately. The theory of the three kinds of proppant movement, creep, saltation and suspension, was validated. The proppant settled immediately at low flowing velocity. Increasing flowing velocity caused the proppant to move farther. At even higher velocities, saltation and bounce motion can be observed. Furthermore, they have found the opposite for proppant deposition. They concluded that large proppant should be tailed in the job because it settled in the near-wellbore zone. They found that the best correlation to calculate proppant settling velocity is McCabe and Smith's correlation. Their correlation is illustrated in (12). This correlation is valid for a broad range of Reynolds number ($2 < R_e < 500$) and represents most cases that can be faced in hydraulic fracturing.

$$v_s = \left[\frac{0.072 g (\rho_p - \rho_f) d_p^{1.6}}{\rho_f^{0.4} - \mu_f^{0.6}} \right]^{0.71} \tag{12}$$

In addition, they found the optimum type of proppant that should be used with slickwater in a hydraulic fracture to give better proppant distribution. The comparison between these three types of proppant was based on resuspension probability for each type.

They determined that proppant distribution and transport are functions of coefficient of restitution, (*CoR*) and friction coefficient (*f*). Coefficient of restitution and friction coefficient are illustrated in (13) and (14), respectively. They found that advanced ceramic proppant can be transported deeper than the others because of its high coefficient of restitution and friction coefficient. They stated that ceramic proppant is better than sand in transport, even sand that has high (*CoR*) because of the high friction of sand. They measured (*CoR*) by dropping a proppant grain from a certain height and measuring the distance that proppant bounced off after hitting the surface. Friction coefficient was determined by measuring the angle between the horizontal surface and pile surface of proppant that was poured through an orifice of 0.4 cm located in a plastic hourglass

$$CoR = \frac{v_{after}}{v_{initial}} = \sqrt{\frac{h_{bounce}}{h_{initial}}} \tag{13}$$

$$f = tan\theta_r \tag{14}$$

Where:

θ_r: Angle of repose

Proppant suspension is almost the only mechanism that improves proppant transport. Some researchers devoted their work to proppant suspension improvement. Zhou et al. (2014) presented the results of preformed gel system on suspension of intermediate strength proppant particles (ISPPs). Static proppant settling experiments were conducted to examine the performance of performed gel on suspending proppant under 180°F for different periods. His results showed that this type of fluid can suspend proppant better than gel guar and provide better cleanup than crosslink fluids. Cleanup performance

reached to 90% under 2000 psi closure pressure. Improved suspension and better proppant distribution resulted in higher fracture surface area. Improving proppant distribution and cleanup enhanced led to better well productivity.

Similarly, Sun et al. (2015) conducted static and dynamic experiments to test the ability of a new fracturing fluid system, referred to as "soft particle fluid", on proppant carrying efficiency. In this technology, proppant grains were entangled by the void space that formed between particle fluids, as shown in Figure 2.1. The new mechanism diminished the gravity effect and carried proppant as a moving piston in a visualization dynamic experiment. Improving proppant transport promotes propped surface area, minimizes the volumes of treating fluid, and boosts fracture conductivity. The efficiency of cleanup reached to 97%. This fluid was used in the field. Well results were utilized in a simulator to offer more information about proppant suspension by the soft particle fluid.
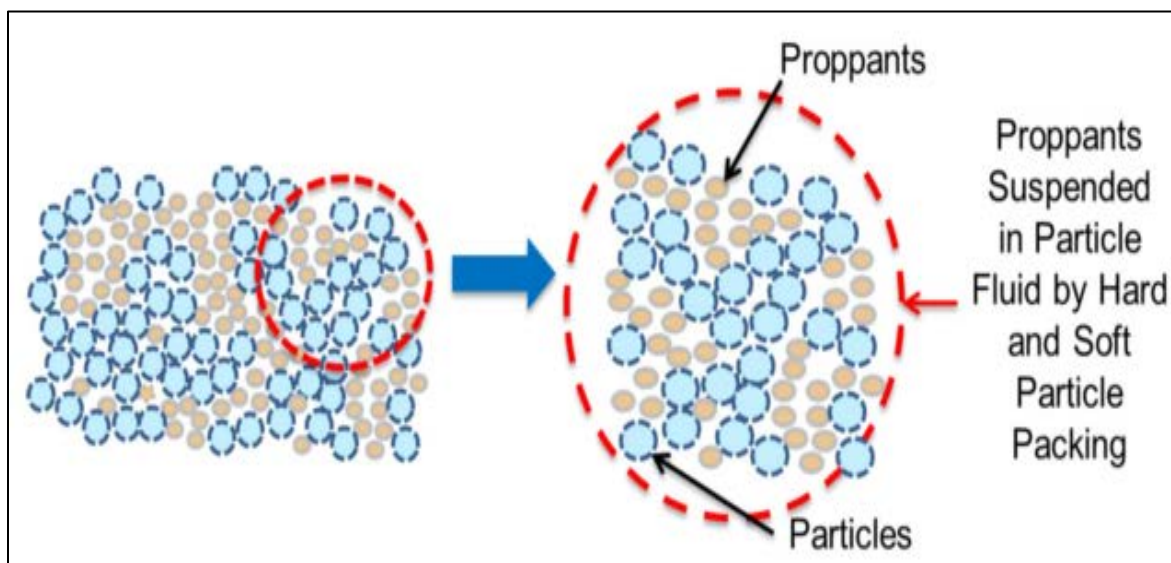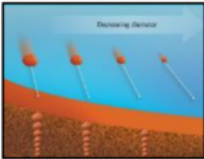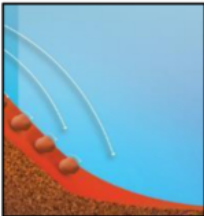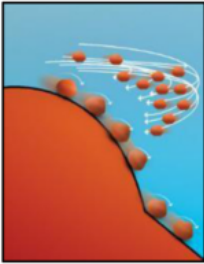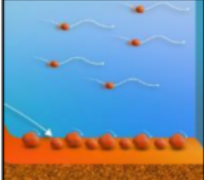
Figure 2.1. Proppant Suspension within the Void Space of Fluid Particle (Sun et al., 2015)

Alotaibi and Miskimins (2015) built a network of primary, secondary and tertiary fracture. They mixed sand with a 30/70 mesh size with slickwater. Different velocities and proppant concentrations were used to study proppant dune build up criteria. From their study they determined the following:

- They developed the term "Equilibrium Dune Level (EDL)" which is the ratio of equilibrium dune height to fracture slot height multiplied by 100%.

- They found that sand was sorted from the smallest settled at the bottom of the fracture to the largest at the top.

Table 2.1. Dune Development Stages' Features (Alotaibi and Miskimins, 2015)

Stage	EDL, %	Dune shape	Transport mechanism	Relative proppant size range	Proppant size distribution	
					Vertically	Horizontally
1	0-10		Hindered settling	Smallest size range	Increasing	No change
2	10-75		Free settling + Rolling	Mostly mid to large size range	Layers of small and large proppant with a downward slope	
3	75-97		Rolling + free settling + Suspension	Mostly large with partially mid-size range	No certain sorting was observed	
4	97-100		Rolling + Saltation	The largest size range		

- The required process to reach EDL was classified into four stages based on proppant transport mechanism, dune build-up rate, dune shape and particle size distribution. See Table 2.1.

- Sand settled at different angles based on the the size of the sand. The settling angle is the angle between the horizontal plane and particle settling direction. Large grains have higher settling angle than small grains.

- They developed correlation to calculate equilibrium dune level based on slurry velocity and proppant concentration.

Based on field data presented by Warpinski et al. (1982) it is clear that fracture width varies along fracture length due to in-situ stress variations. The shortcoming of historical hydraulic fracture proppant experiments has been the assumption of a homogeneous fracture width in proppant transport with a slickwater fluid. This study considers fracture width heterogeneity in all models. Roughness and leak-off effects are handled separately. Ceramic proppant is mixed with slickwater and an FPV strategy provided is used for a more precise description of proppant placement mechanisms.

3. EXPERIMENT DESCRIPTION AND PROCEDURE

A small experimental model was used to study proppant transport behavior. This in-house experimental design was chosen to represent field scale in lab scale. Different types of data and interpretations have been incorporated in this study to investigate proppant settling and transport mechanisms. This chapter details the experimental setup and precedure.

3.1. EXPERIMENTAL APARATUS

An experimental model was constructed to collect precise data about proppant movement and settling mechanisms using ceramic proppant in slickwater. Figure 3.1 reveals a schematic for the apparatus. The apparatus consists of a nitrogen tank, an accumulator, a pressure sensor, a pressure gauge, two valves, flow lines, a video camera and the fracture slot. The main reason for using nitrogen as a driving force is to see its effect on proppant distribution. Nitrogen allows proppant to penetrate deeper into a fracture because it improves proppant buoyancy (Boyer et al., 2014).
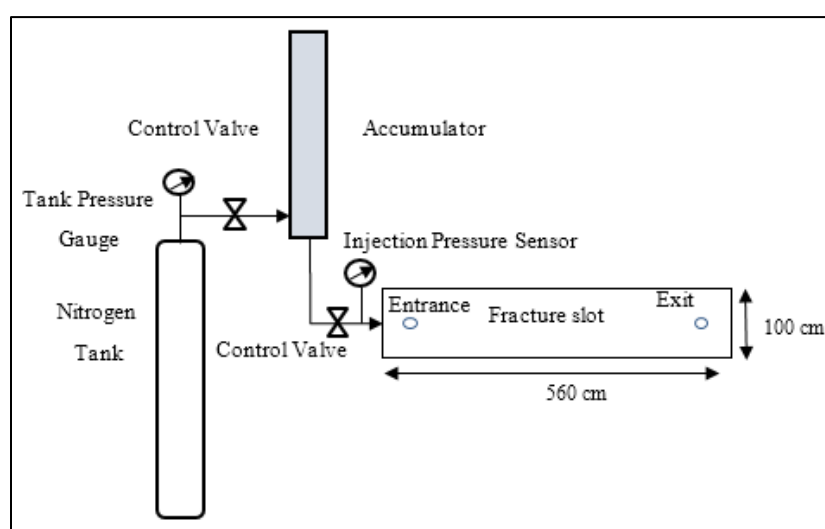
Figure 3.1. Schematic for the Apparatus

3.1.1. The Fracture Slot. A small transmit cell (565 mm long and 100 mm high) has been constructed, as shown in Figure 3.2. This cell was created by using two transparent plexiglass sheets separated by a rectangular rubber frame. The space between these two plaxiglass sheets is made by the rubber. The inner dimensions of the rubber define the slot dimensions. Two apertures were drilled in the middle height of one sheet of this apparatus. One of these apertures was an inlet, and the other one was an outlet for the slot. Each aperture was 50 mm from the end of the slot. The diameter of the entrance and exit holes was 11 mm.
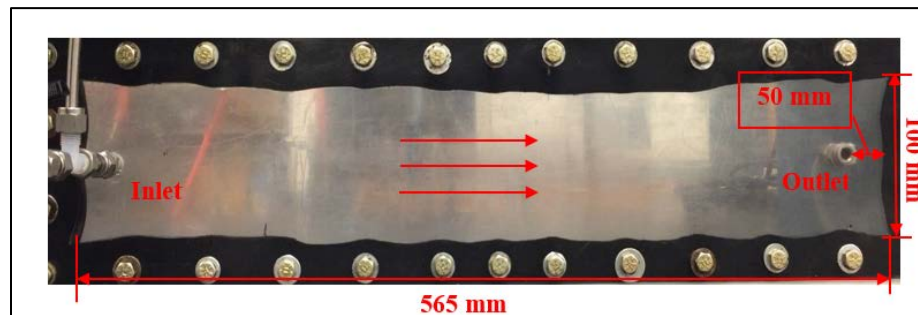
Figure 3.2. Apparatus Slot Description

3.1.2. The Accumulator. The accumulator is an enclosed container used to mix proppant and water together before injecting them into the fracture slot. A schematic of the accumulator is illustrated in Figure 3.3. It consisted of two seals, a cylindrical container and two holes. One hole was located one inch from the bottom on the sidewall of the accumulator. This hole was used to connect the nitrogen tank to the accumulator. The location of the hole enabled nitrogen to generate a turbulent movement inside the accumulator to mix proppant with water. The second hole was located 1 inch (25.4 mm) off the bottom of the accumulator and connects to the fracture slot. Proppant and water

were mixed together inside the accumulator container by injecting nitrogen. Then, nitrogen

was used to move the slurry into the fracture slot. Injection pressure was 55 psi.
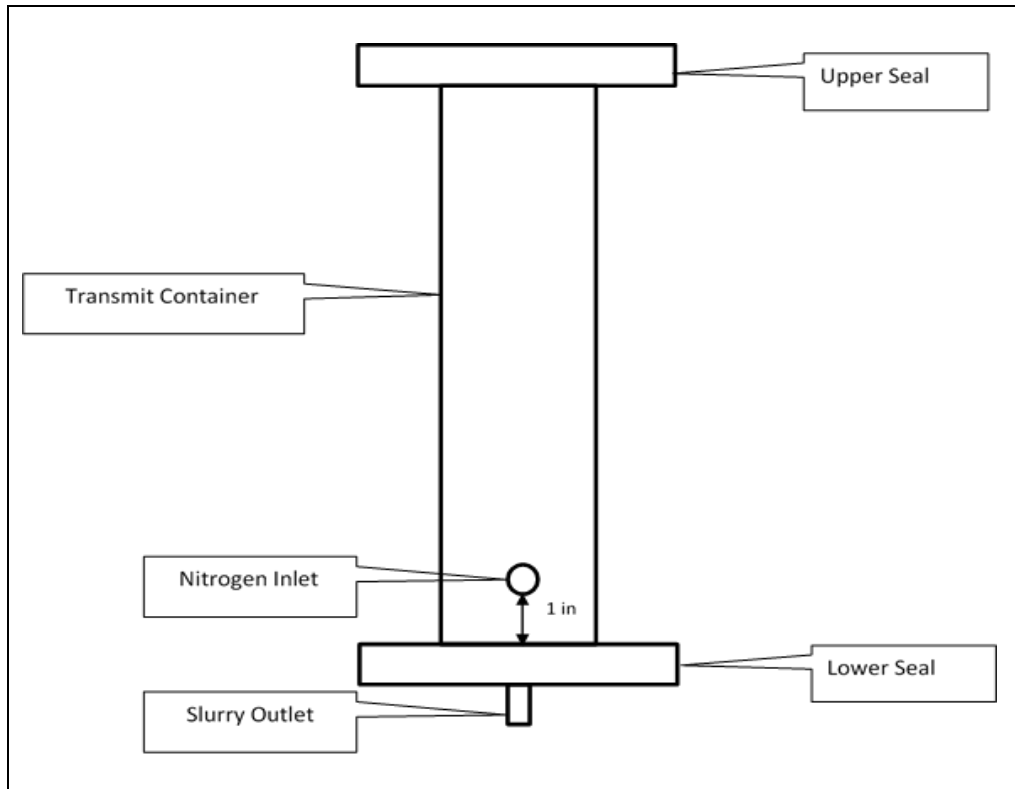
Figure 3.3.Schematic for the Accumulator

3.1.3. Pressure Sensor.   A highly accurate pressure sensor, a USB data logger

whose name is myPCLab and made by NOVUSUK, was connected to the inlet of the slot

to measure injection pressure. A cable was connected to a computer for recording pressure

data. This sensor can feel 0.01 psi and can read every 0.01 second.

3.2.   SLURRY DESCRIPTION

The slurry used in this study consists of slickwater and ceramic proppant without

any additives; 25 gm of Ceramic proppant with 40/70 mesh size and apparent density of

2.59 gm/cc was used with 250 ml of slickwater to give 100000 ppm or 0.83 lb/gal. This

proppant crushes at 7.5 API or 1.3 Kpsi. Proppant sieve distribution and proppant diameter

for each mesh size are given in Table 3.1. The slurry was mixed in the accumulator, and

injected into the fracture slot using nitrogen as previously shown.

Table 3.1. Seive Distribution

US mesh	Wt% Retained	Diameter, µm
40	4.8	420
45	25.2	354
50	46.8	297
60	21.4	250
70	1.7	210
100	0.1	149

3.3. EXPERIMENTAL PROCEDURE

Proppant dune height was measured for each slurry fracture pore volume, FPV.

FPV is the ratio of injected slurry volume to the fracture volume. FPV is shown in (15) and

slurry volume is defined in (16):

$$FPV = \frac{Slurry\ volume}{Fracture\ volume} \tag{15}$$

$$Slurry\ volume = \frac{proppant\ wieght(25gm)}{proppant\ density(2.59\frac{gm}{cc})} + water\ volume(250gm) \tag{16}$$

Concepts of EDL and EDX, previously defined by Alotaibi and Miskimins, (2015)

are used in this study. The general procedures followed in this work include:

1. Injecting multiple slurry FPVs to reach either the EDL (when dune height is stable and no more settlement or erosion occurs) or the point where the slot was completely filled. EDL can be calculated by (17).

2. Reading the height of proppant pile along the fracture slot after injecting each slurry FPV. Proppant pile height was measured by digitizing the photos of each slurry FPV.

3. Calculating proppant plateau extension and pile height (interest zone). Proppant plateau extension can be estimated by using Equilibrium Dune Length (EDX). EDX equation can be calculated using (18).

4. Calculating EDL, buildup angle, drawdown angle.

5. Calculating propped surface area in order to determine the effect of each factor on predicted fracture conductivity.

6. Monitoring the movement of proppant and its mechanism.

The slot-leaving slurry was also collected for more analysis. A pressure gauge was connected to a computer to record the pressure for each centisecond.

$$EDL = \frac{average\ dune\ height}{fracture\ height} \times 100\% \tag{17}$$

$$EDX = \frac{average\ dune\ length}{fracture\ length} \times 100\% \tag{18}$$

4. EXPERIMENTAL RESULTS AND ANALYSIS

Proppant transport in slickwater fracturing is a complex phenomenon. It is well documented that proppant settles very quickly in slickwater, especially the larger grains. Small grains can navigate farther, as will be explained later. Many factors control proppant settling velocity and horizontal movement such as the density difference between injected slurry and preexisting fluid$[(\rho_P - \rho_f)\, g]$, gravity force, proppant diameter, fracture thickness, fracture heterogeneity, wall roughness, fracture leak-off, and fluid rheology properties. In this study, four parameters were investigated in detail: fracture heterogeneity, fracture thickness, fracture wall roughness and fracture leak-off. The findings and highlights of the experimental results are shared in this chapter. Experimental design and factors are shared in Section 41. All experimental results and interpretations are presented in Section 4.2. A new settling mechanism is reported at the end of Section 4.2.

4.1. EXPERIMENTAL FACTORS

Four experimental models have been constructed to investigate how proppant distribution can be affected by fracture width heterogeneity, injection side width, fracture wall thickness and fluid efficiency or fracture leak-off. Table 4.1 summarizes all experiments conducted in this study. The base case model was a wall-smoothed heterogeneous fracture with no leak off.

Table 4.1. Summary for all Experiments of This Study

Factor investigated	Number of experiments	Description

Table 4.1. Summary for all Experiments of This Study (cont)

Fracture heterogeneity	3	Uniform fracture (homogeneous)	
		$H_{0.25L}$	
		$H_{0.75L}$	
Wall thickness	5	W_{in}/W_{out}	Uniform fracture
			1.2 (base case)
			2
			3
			4
Fracture wall roughness	3	Smooth wall (base case)	
		Low-roughened wall	
		High-roughened wall	
Leak-off	3	No leak-off (base case)	
		Low leak-off	
		High leak-off	

4.1.1. First Model (Fracture Heterogeneity Effect). Fracture heterogeneity was investigated by making the first quarter (25%) and then the first three quarters (75%) of the fracture slot wider on the inlet, than the remaining outlet distance. In the study, these distances are denoted $H_{0.25L}$ and $H_{0.75L}$. A uniform or homogeneous slot was used as the base case.

Figure 4.1 is a front-view schematic for each fracture, which it was the same for each model. Figure 4.2, Figure 4.3 and, Figure 4.4 are top-view schematics for the uniform fracture, $H_{0.25L}$, and $H_{0.75L}$, respectively.
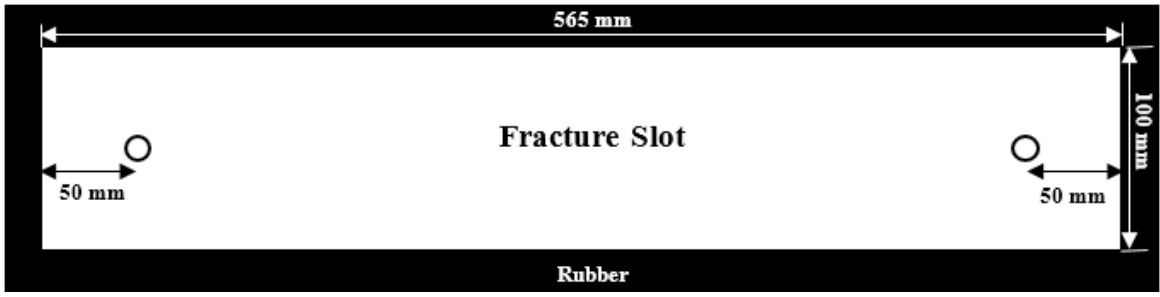
Figure 4.1. Front View of the Slot
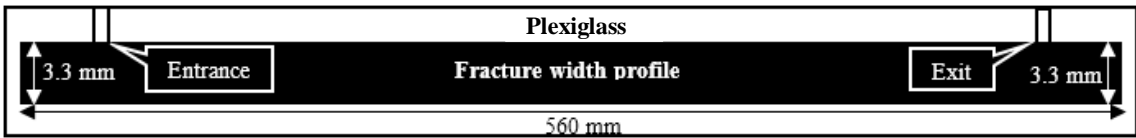
Figure 4.2. Top View of the Uniform Fracture
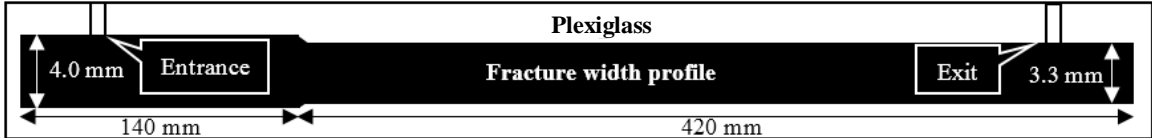
Figure 4.3. Top View of $H_{0.25L}$ Fracture
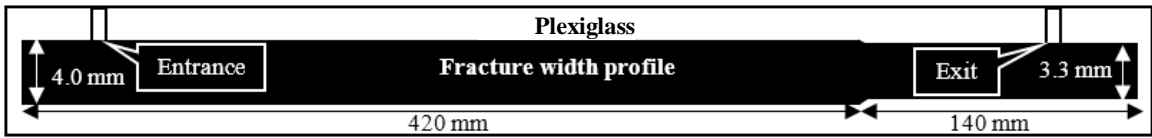
Figure 4.4. Top View of $H_{0.75L}$ Fracture

4.1.2. Second Model (Injection side Width Effect). The injection side width effect utilized a heterogeneous base case model. A ratio of the inlet width divided by the

outlet width, W_{in}/W_{out} was defined. The ratio was 1.2 for the base case. Then, the width of the injection side was changed in other experiments to be 6.6 mm, 9.9 mm and 13.2 mm keeping the opposite side width a constant 3.3 mm. This changed width ratio, W_{in}/W_{out} to approximately 2, 3 and 4 respectively. Figure 4.5, Figure 4.6 and Figure 4.7 show a schematic for the top view of these experiments respectively
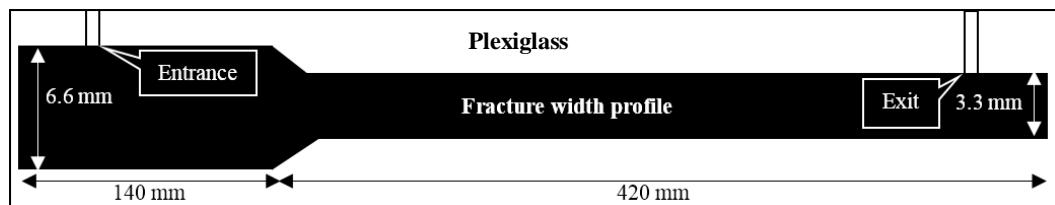
Figure 4.5. Top View of Fracture W_{in}/W_{out}=2
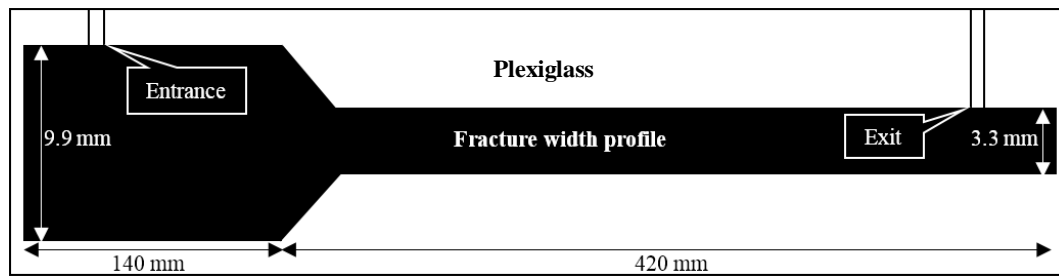
Figure 4.6. Top View of Fracture W_{in}/W_{out}=3
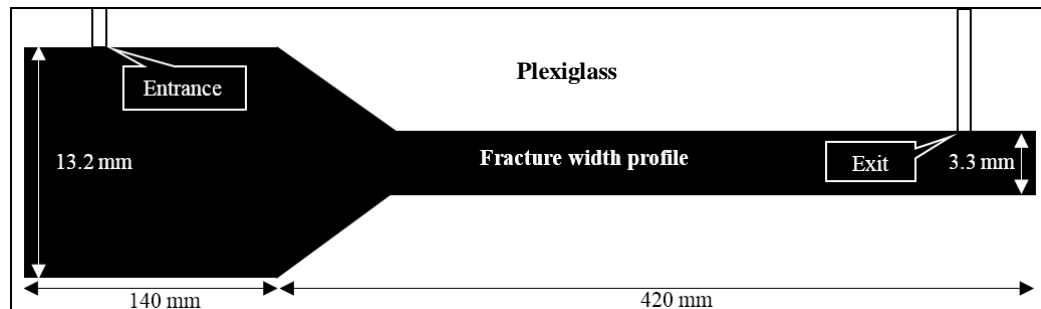
Figure 4.7. Top View of Fracture W_{in}/W_{out}=4

4.1.3. Third Model (Fracture Wall Roughness Effect). Three experiments were conducted to study the effect of fracture wall roughness, using a smooth fracture wall (base

case), low-roughened wall fracture and high-roughened wall fracture. Figure 4.8 illustrates low roughness fracture slot. Transparent waterproof sandpaper was affixed on the inner side of the two plexiglass sheets with no change in the other parameters to give low-roughened walls. High roughness fracture slot is shown in Figure 4.9. High roughness achieved by attaching 30/40 mesh size of sand on the inner side of the plexiglass using epoxy, keeping fracture width and other parameters as they were in the base case. The sand grains were manually placed in the epoxy.

Figure 4.8. Low Roughness Fracture Slot

Figure 4.9. High Roughness Fracture Slot

4.1.4. Fourth Model (Leak-Off Effect). Two experiments were designed to study fracture leak-off effect and compare results to a 'no leak-off' base case. These experiments used heterogeneous fractures. Figure 4.10 illustrates the design of the low leak-off slot. In

this experiment, four apertures were drilled in one plexiglasss sheet. One of these apertures was for injecting the slurry, and the other three were for water leak-off. A small wire mesh was inserted at the face of each aperture to keep proppant inside the slot while allowing water to leave the slot.
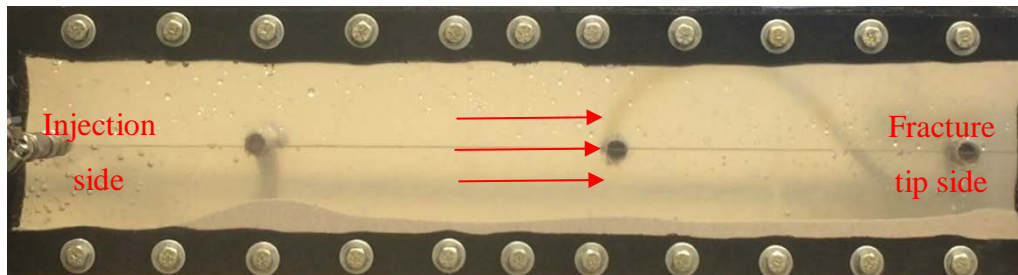
Figure 4.10. The Design of Low Fracture Leak-off Apparatus

Figure 4.11 shows the design of high leak-off slot and location of apertures. To represent high fracture leak-off, ten apertures instead of four were drilled in one plexiglass sheet to create severe leak-off effect. One of these holes was for injecting the slurry, and the other nine were for producing water. These apertures are categorized into three columns, based on the distance from the beginning of the slot, and three rows from the top to the bottom of the slot. Spots located in the first third of the slot length, from the injection side, were named as "one-third fracture length zone" ($Z_{1/3L}$); spots located in the second third of slot length were denoted as "two-third fracture length zone" ($Z_{2/3L}$); and spots located near slot end were referred to as "three-third fracture length zone" ($Z_{3/3L}$). Rows from top to bottom were numbered 1, 2, and 3 respectively. Thus, the marked aperture by a red circle in Figure 4.11 was named as "$Z_{1/3L}1$." Water from each aperture was collected and measured.

Figure 4.11. The Design of High Fracture Leak-off Apparatus

4.2. RESULT AND ANALYSIS

This section discusses the results of slurry injection into fracture heterogeneous slots. It examines the effect of fracture width heterogeneity, injection side width, fracture wall roughness, and fracture leak-off. The results included the measurements of proppant dune height, EDL, EDX, buildup and drawdown angle, and propped surface area along the fracture. Buildup angle is the angle between the horizontal surface and proppant pile from the injection side. Drawdown angle is the angle between the horizontal surface and the proppant pile from the fracture tip side. For fracture leak-off effect, the dependency of proppant distribution on water movement and its effect on how water left the slot are examined. The effect of leak-off on pressure profile was also monitored.

4.2.1. Effect of Fracture Width Heterogeneity. Three experiments have been performed to study fracture heterogeneity effect: uniform fracture, $H_{0.25L}$, and $H_{0.75L}$. Each experiment will be discussed in detail separately, in the same order**.** Table 4.2 shows the magnitude of each slurry FPV for each of the three experiments of this factor**.**

Table 4.2. FPV Number and Magnitude for the Effect of Changing Fracture Width Heterogeneity

FPV Number	FPV Magnitude		
	Uniform Fracture	$H_{0.25L}$	$H_{0.75L}$

Table 4.2. FPV Number and Magnitude for the Effect of Changing Fracture
Width Heterogeneity (cont)

FPV1	1.16	1.43	1.18
FPV2	2.32	2.87	2.37
FPV3	3.47	4.30	3.55
FPV4	4.63	5.73	4.73
FPV5	5.79	7.17	5.92
FPV6	6.95	8.60	7.10
FPV7	8.11	10.03	8.28
FPV8	9.26	11.47	9.47
FPV9	10.42	12.90	10.65
FPV10	11.58	14.33	11.84
FPV11	12.74	15.77	13.02
FPV12	13.90	17.20	14.20
FPV13	15.05	18.63	15.39
FPV14	16.21	20.06	16.57
FPV15	17.37	21.50	17.75
FPV16	18.53	22.93	18.94
FPV17		24.36	20.12
FPV18		25.80	21.30
FPV19			22.49
FPV20			23.67

4.2.1.1. Uniform fracture. The first slurry FPV is illustrated in Figure 4.12. The distance proppant travelled is represented by x-axis, and proppant height that was measured at that distance and is shown on the y-axis. The red circle marks the buildup slope where it was 0.21 and buildup angle was 11.87°. In this slurry FPV, most of injected proppant distributed horizontally rather than vertically.
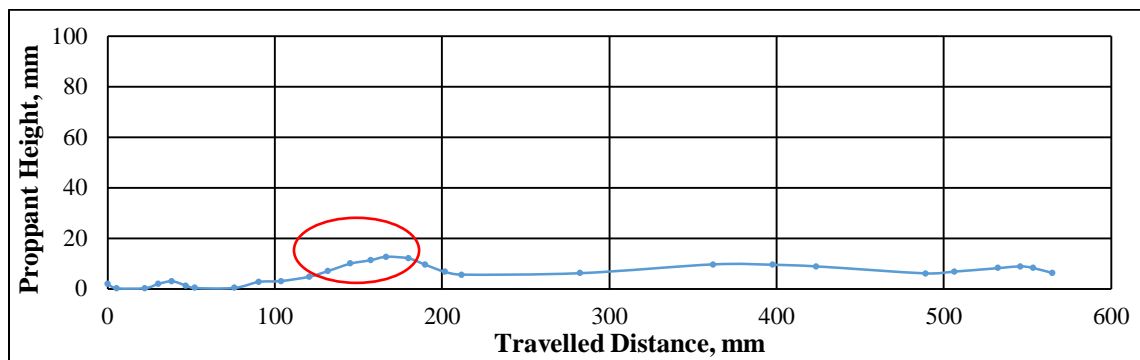
Figure 4.12. Proppant Distribution along the Uniform Fracture after the First FPV

Figure 4.13 illustrates proppant bed development as a function of slurry FPV. Buildup slope, plateau zone and drawdown slope are explained in the figure. Close to the injection side and before the plateau zone, buildup angles were formed. After the plateau, drawdown angles were formed. From FPV1 to FPV12, the height increment trend was constant in the plateau zone. At FPV12, the buildup slope was 0.49 with an angle of 25.97°, while drawdown slope was -0.2, with an angle of -11.44°. From FPV12 until FPV16, height distribution remains almost identical except little height increment.
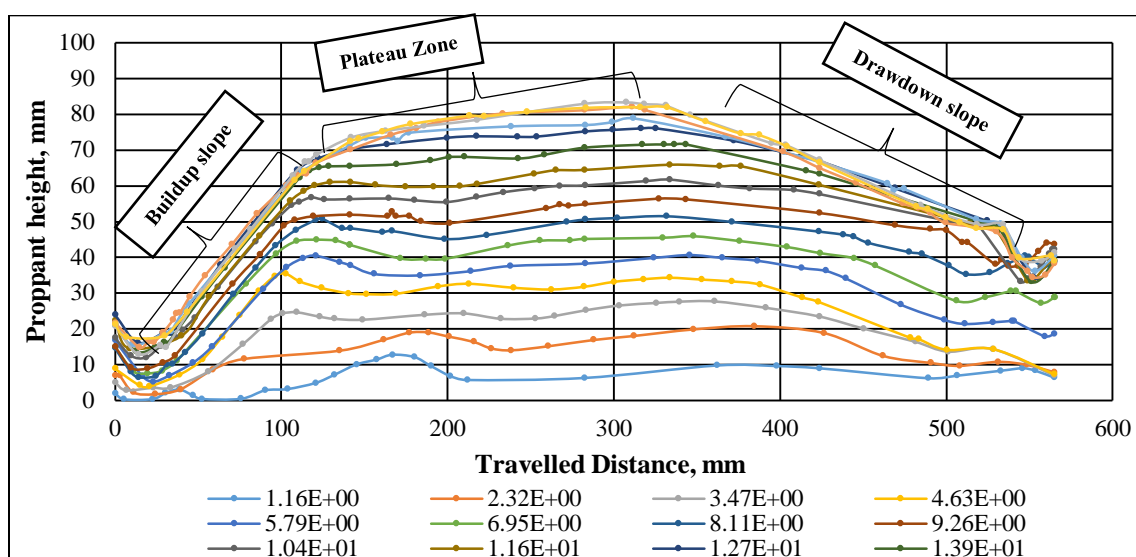
Figure 4.13. Proppant Distribution along the Slot after FPV16

Proppant distribution along the slot for the last slurry FPV is illustrated in Figure 4.14. The green marker points represent the first and last point on the dune to calculate EDL and EDX (plateau zone). At FPV16, EDL was achieved when no more settlement or erosion was noticed. The slope on the injected side, buildup slope, was 0.61, while the slope at the end side, drawdown slope, was -0.13.
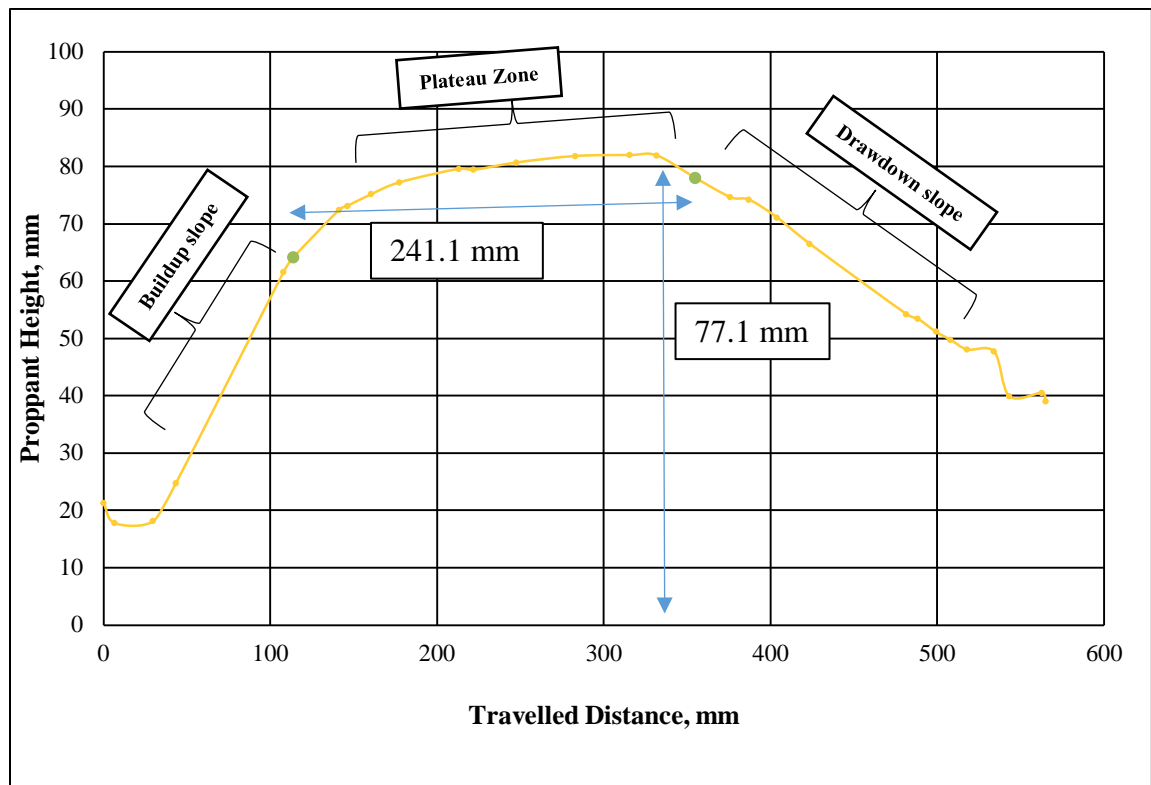
Figure 4.14. Proppant Distribution along the Uniform Fracture after FPV16

4.2.1.2. $H_{0.25L}$ fracture. In this fracture, the widest part of the fracture slots extends to the first quarter of the slot length. Figure 4.15 explains proppant pile development from the first slurry FPV until FPV12. The proppant pile incremental build rate was as constant, as in the uniform fracture from FPV1 to FPV12. After that, the pile tended to grow in length rather than in height until EDL was reached.
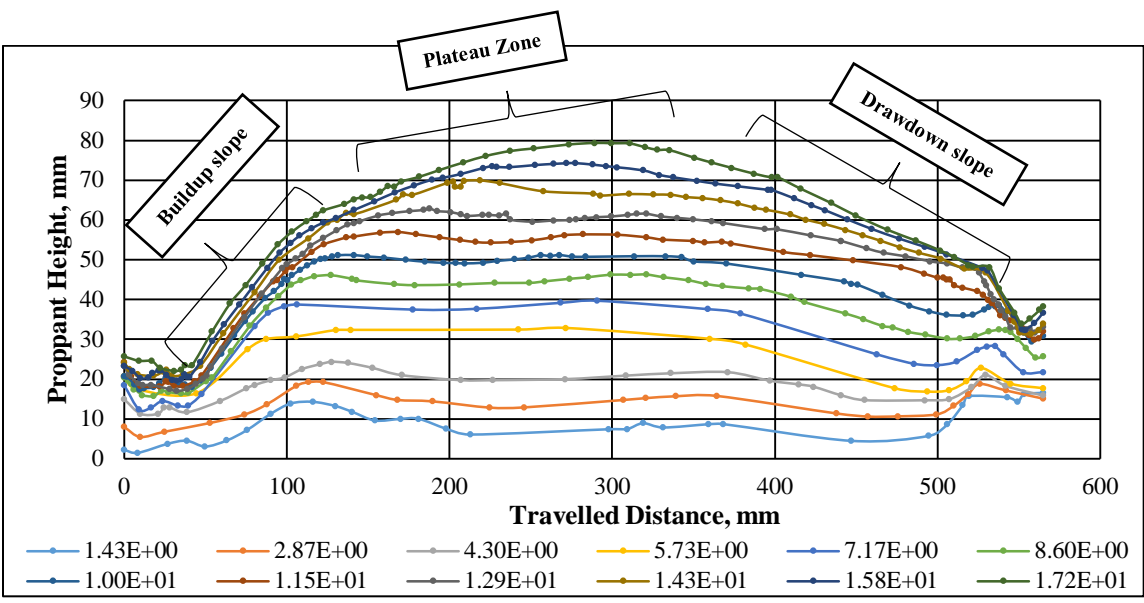
Figure 4.15. Proppant distribution along $H_{0.25L}$ Fracture during 12 Slurry FPVs

Figure 4.16 illustrates proppant distribution along the slot for all FPVs. After slurry FPV18, injected proppant increased proppant height and plateau length slightly. Most of the injected proppant was produced from the exit of the slot. Proppant erosion rate was higher than previous slurry FPVs.
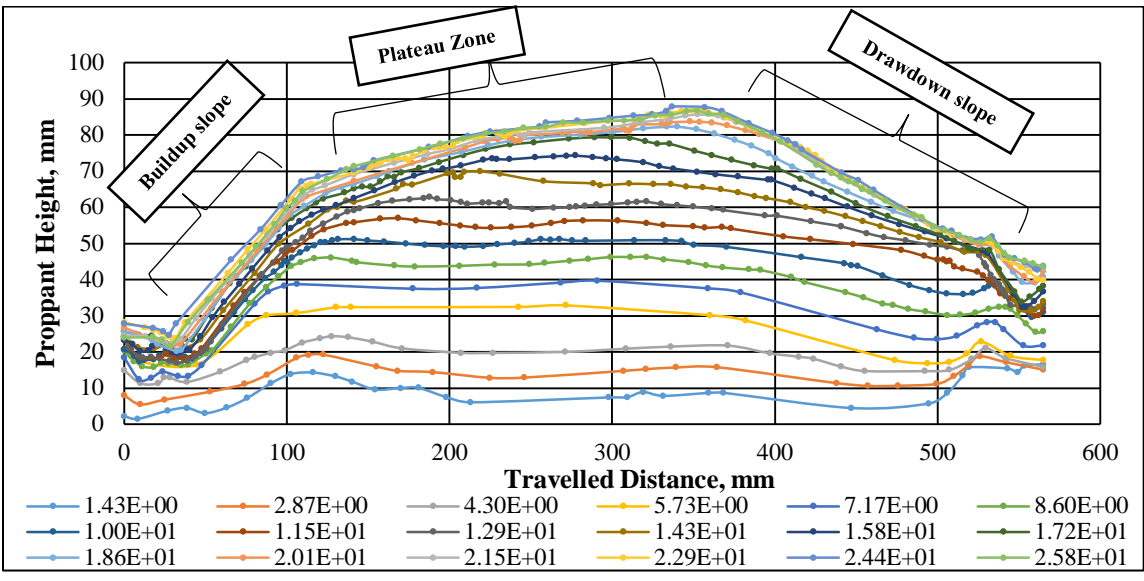
Figure 4.16. Proppant Distribution along the $H_{0.25L}$ Fracture after FPV18

Figure 4.17 illustrates proppant height distribution along $H_{0.25L}$ slot at the last slurry FPV. Plateau extended from 105.1 mm to 377.2 mm giving a plateau length equals to 272.1 mm. Average height of proppant pile was 79.4 mm. Buildup angle was 26.1°, and drawdown angle was -14.5°.
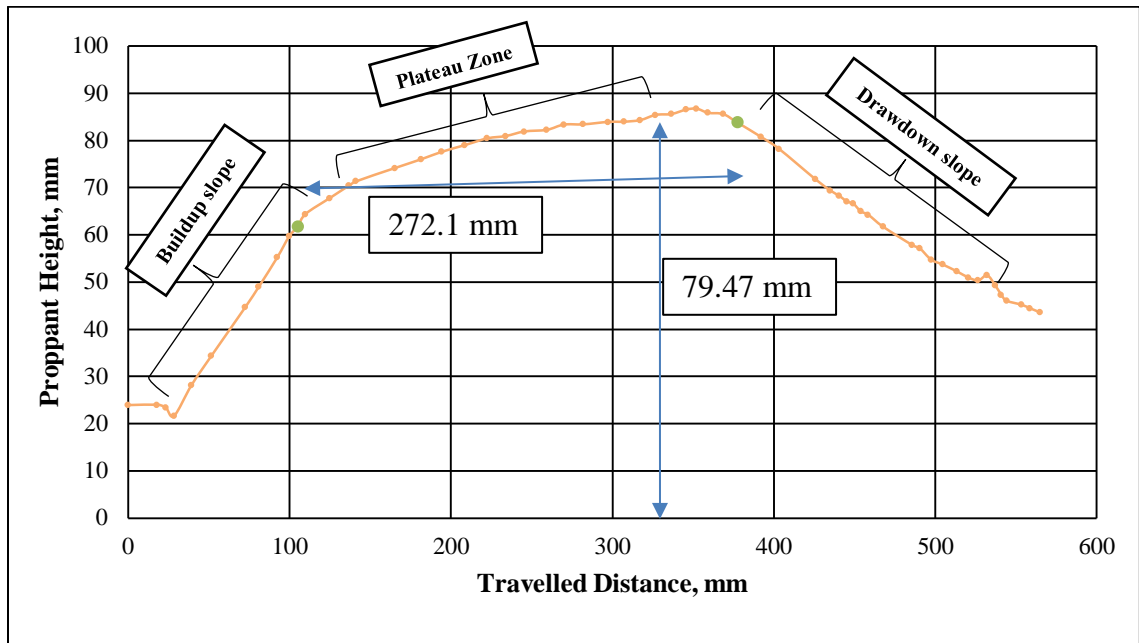
Figure 4.17. Proppant Distribution along the $H_{0.25L}$ Fracture after FPV18

4.2.1.3. $H_{0.75L}$ fracture. This fracture has more width heterogeneity than the previous two fractures. The widest part of the fracture slot extends to the first three-quarters of the slot length. Figure 4.18 shows the scenario of proppant settling and pile propagation along the fracture. The scenario of proppant pile development that was observed in the previous fractures was repeated in this fracture. From slurry FPV1 until slurry FPV12, proppant was growing in semi-stable rate. After slurry FPV12, most proppant elongated the pile horizontally, while vertical growth was negligible. At FPV20, EDL was achieved when proppant pile was stable in shape and dimensions.
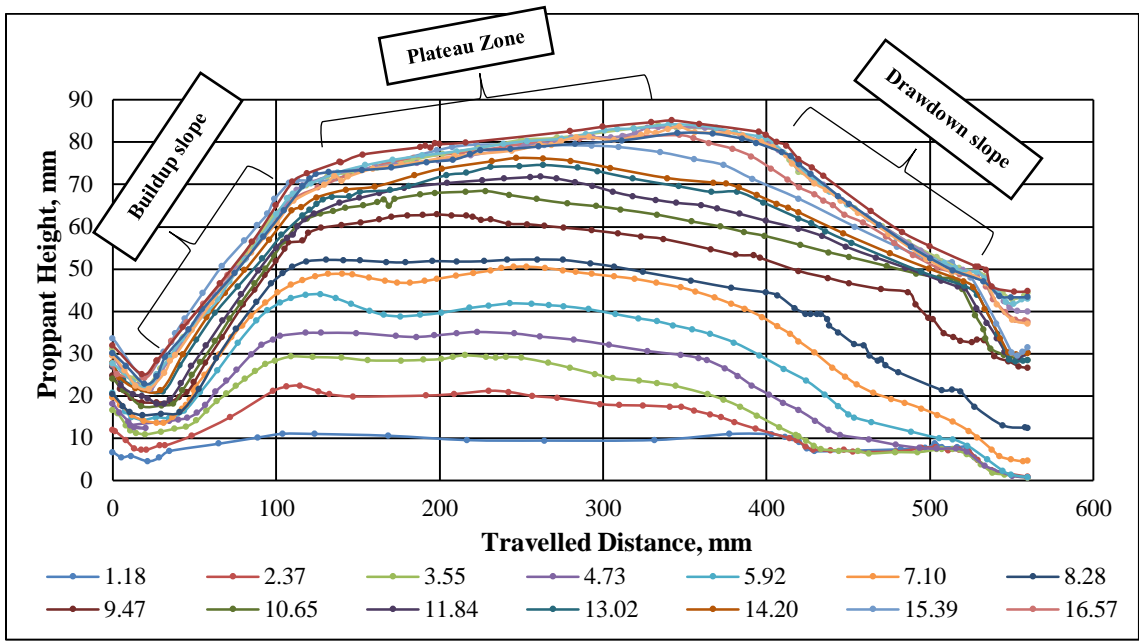
Figure 4.18. Proppant Distribution along $H_{0.75L}$ Fracture during All FPVs and after FPV20

Figure 4.19 illustrates pile height and length at EDL. Pile length and height were greater than the preceding experiments. The plateau of proppant pile extended from 99.9 mm to 419.9 mm. Proppant height was 79.5 mm, and proppant height was 297.2 mm. buildup angle was 27.20° while drawdown angle was -14.45°.
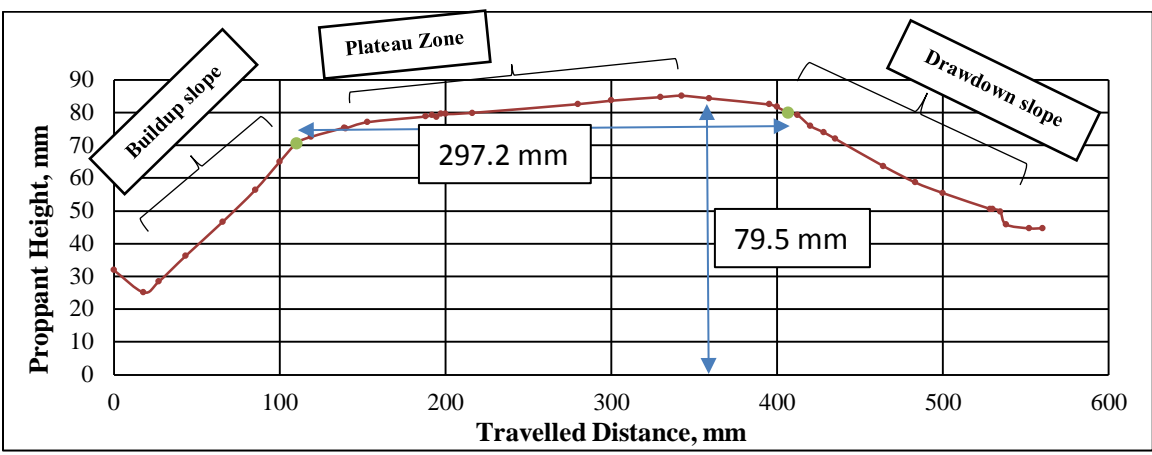
Figure 4.19. Proppant Distribution along an $H_{0.75L}$ Fracture after FPV20

4.2.1.4. Comparison between uniform, $H_{0.25L}$ and $H_{0.75L}$ fractures. Figure 4.20 shows proppant distribution along three different width heterogeneous slots at the last slurry FPV. This figure shows that fracture width heterogeneity can affect proppant distribution. The more fracture heterogeneity, the better proppant distribution can be achieved. The blue curve is for the uniform fracture, the red curve is for the $H_{0.25L}$ fracture and the purple curve is for $H_{0.75L}$ fracture. For the uniform fracture, pile height and extension was the least among these three fracture. The highest and longest pile was observed for $H_{0.75L}$ fracture.
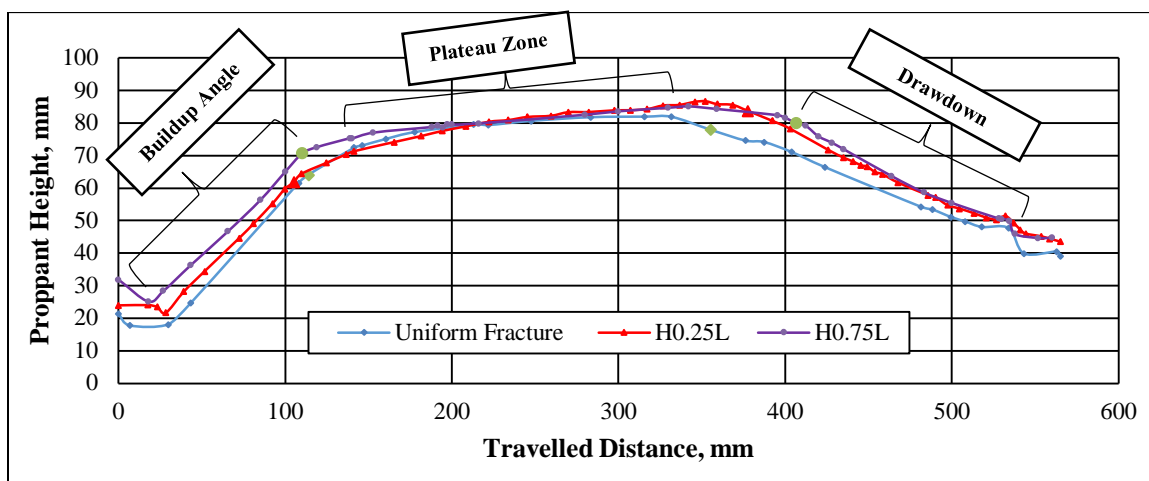
Figure 4.20. Proppant Distribution for the Last FPV for Each Fracture

Figure 4.21(a) shows how increasing fracture heterogeneity increased EDL. The lowest calculated EDL was for the uniform fracture (the blue point) while the highest EDL was for $H_{0.75L}$ fracture (the purple point). Figure 4.21(b) reveals the effect of fracture width heterogeneity on EDX. The EDX of the uniform fracture (the blue point) was 0.43 while it was 0.53 for $H_{0.75L}$ fracture (the purple point). The more heterogeneity, the higher EDX value.
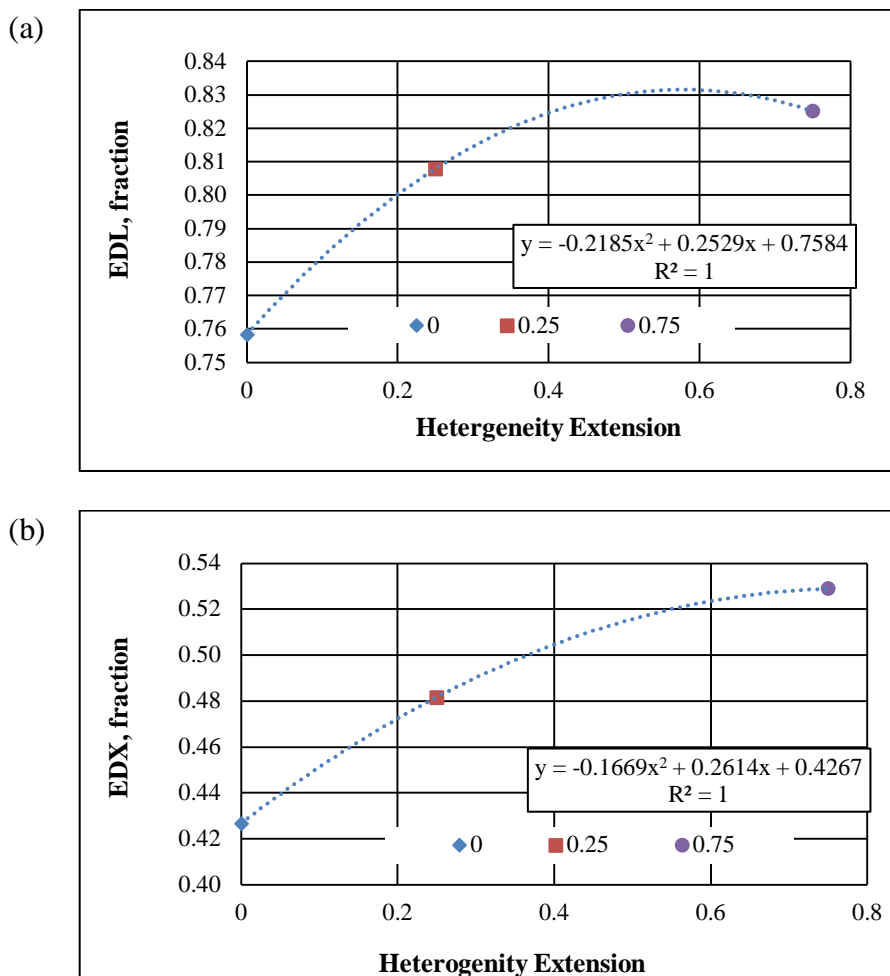
Figure 4.21. Effect of Fracture Width Heterogeneity on EDL and EDX. (a) Effect of Width Heterogeneity on EDL (b) Effect of Width Heterogeneity on EDX

The effect of fracture width heterogeneity on buildup and drawdown angles is illustrated in Figure 4.22(a) and Figure 4.22(b) respectively. In Figure 4.22(a), increasing width heterogeneity increased buildup slope. Buildup angle increased from 25.9° in the uniform fracture to 27.2° in $H_{0.75L}$ fracture. In Figure 4.22(b), the magnitude of drawdown angle increased due to increasing fracture width heterogeneity. Drawdown angle for the uniform fracture was -11.4°, and -14.4° for $H_{0.75L}$ fracture. Note that buildup angle is close to the injection side and the drawdown angle is close to the fracture tip side.

(a)

(b)
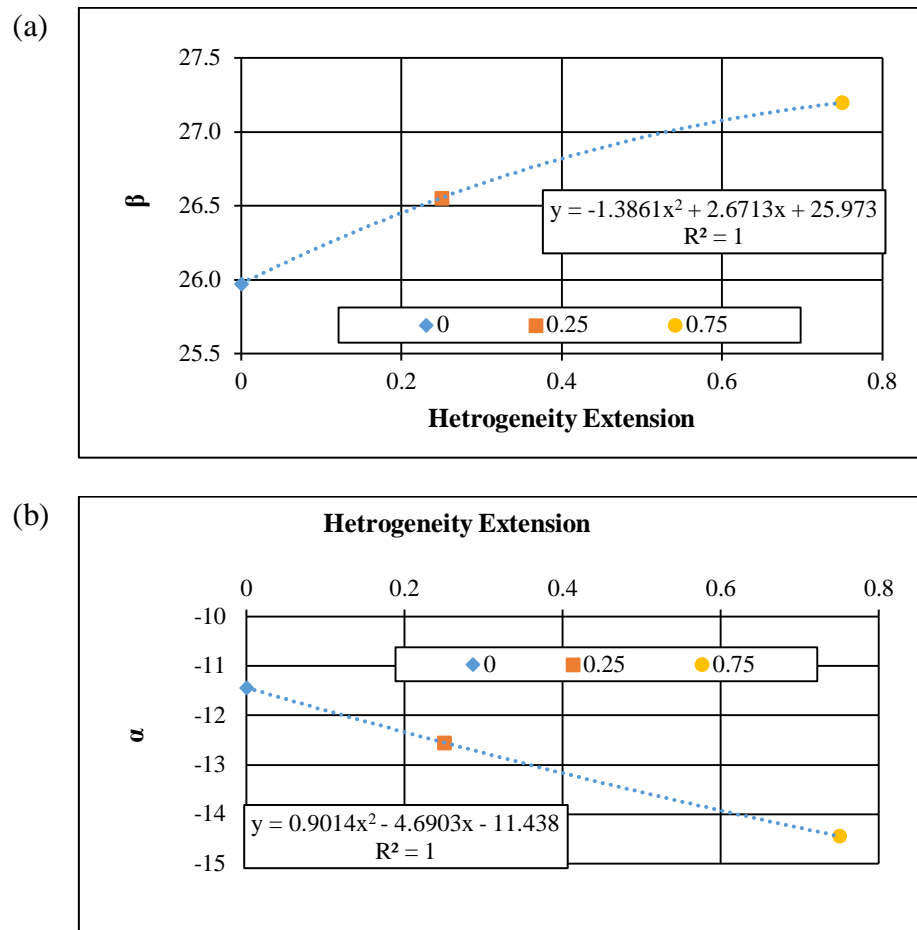
Figure 4.22. Effect of Fracture Width heterogeneity on Buildup and drawdown angle. (a) Heterogeneity Effect on Buildup Angle (b) Heterogeneity Effect on Drawdown Angle

Figure 4.23 and Figure 4.24 illustrate the influence of changing fracture width heterogeneity on surface area fraction. Surface area fraction is the ratio of propped surface area to fracture surface area. Propped surface area was calculated by inserting the reading of proppant height at each point in a trapezoidal code in MATLAB, while fracture surface area is the result of multiplying fracture height by fracture length. Surface area fraction and propped surface area can be calculated by (19) and (20) respectively:

$$Surface\ area\ fraction = \frac{Propped\ surface\ area}{Fracture\ surface\ area} \qquad (19)$$

$$Fracture\ surface\ area = l * h \qquad (20)$$

where

l: Fracture slot length, cm

h: Fracture slot height, cm.

Figure 4.23 shows surface area fraction (y-axis) as a function of slurry FPV (x-axis). The blue curve is for the uniform fracture, the red curve is for $H_{0.25L}$ fracture, and the purple curve is for $H_{0.75L}$ fracture. From FPV1 until FPV17, the uniform fracture showed higher propped surface area than $H_{0.25L}$ fracture and lower than $H_{0.75L}$ fracture. At slurry FPV18, the uniform fracture had the lowest propped surface area while $H_{0.75L}$ fracture still had the highest propped surface area.
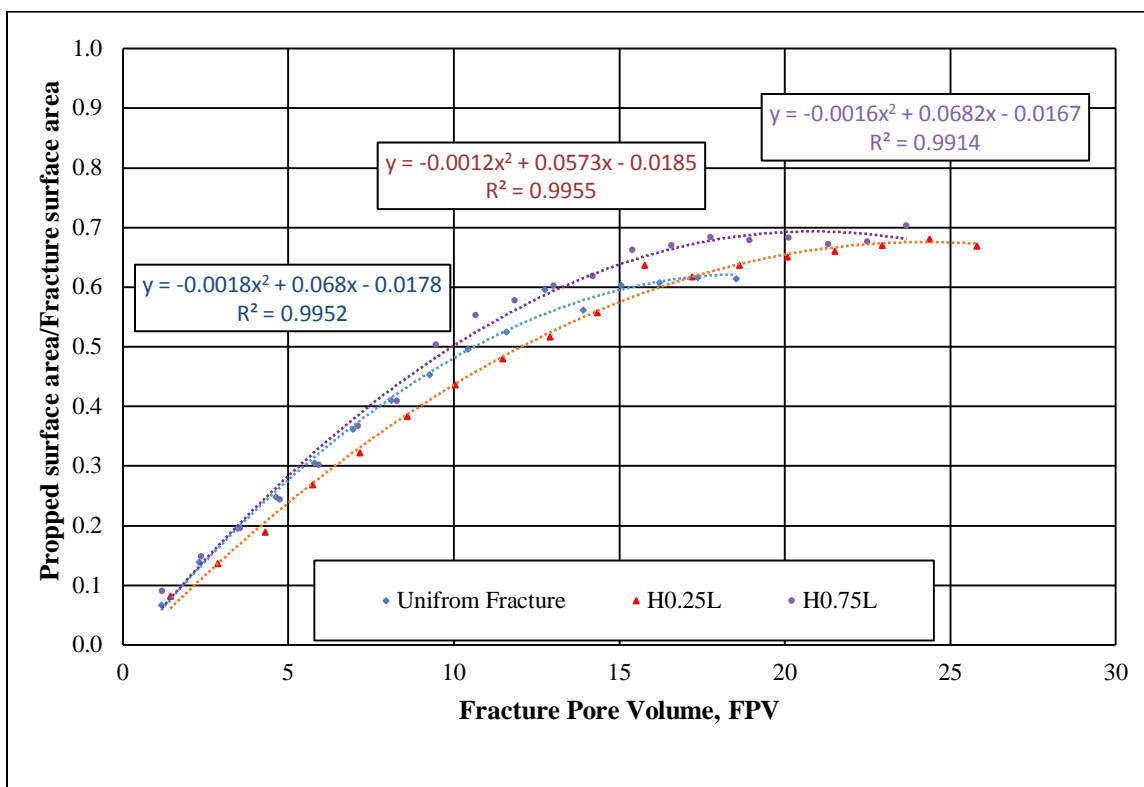
Figure 4.23. Surface Area Fraction vs. of Fracture Heterogeneity for Each FPV

Figure 4.24 explains the effect of fracture width heterogeneity on surface area fraction at the last slurry FPV. Surface area fraction increased from 0.61 for the uniform fracture to 0.7 for $H_{0.75L}$ fracture. Propped surface area is a function of EDL and EDX. As aforementioned above that increasing fracture width heterogeneity increased both EDL and EDX. Thus, the increment of surface area fraction can be considered a logical result.
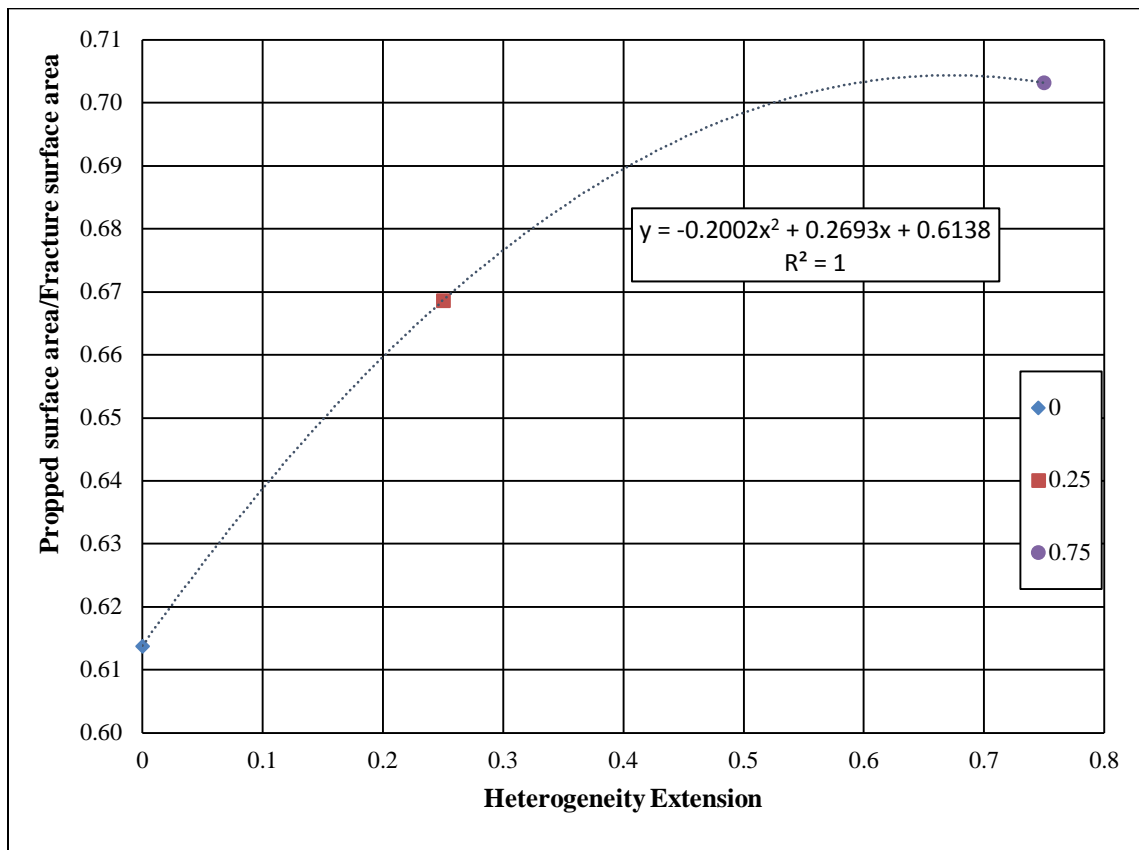
Figure 4.24. Surface Area Fraction vs. of Fracture Heterogeneity for the Last FPV

Table 4.3 shows a comparison among these three models. Proppant height was measured for each slurry FPV. At the injection side, the height of settled proppant increased from 0.34 mm in the uniform fracture to 5.48 mm in $H_{0.75L}$ fracture. At the fracture tip side, the height of settled proppant decreased from 16.5 mm in the uniform fracture to 0.5 in

$H_{0.75L}$ fracture. These numbers implied that increasing fracture width heterogeneity allowed more proppant to settle earlier. Consequently, increasing fracture heterogeneity would increase proppant settling velocity, and decrease slurry horizontal velocity. The proppant that was produced from each slot supports this analysis. For the uniform fracture, 0.53 gm left the slot in FPV1, while no proppant left the slot in FPV1 of the $H_{0.75L}$ fracture. This result is consistent with the results that was presented by Gadde et al. (2004), which examined the effect of fracture-width effect on proppant settling velocity. Their formula shows an inverse relationship between fracture wall thickness and proppant-settling velocity, as illustrated in (21):

$$v_w = v_s \left[0.563 \left(\frac{a}{t} \right)^2 - 1.563 \left(\frac{a}{t} \right) + 1 \right] \tag{21}$$

where

v_w: Settling rate corrected for presence of walls, cm/s

v_s: Settling rate of particle in Stokes flow, cm/s

a: Particle radius, cm

t: Fracture width, cm.

Proppant volume that settled in the uniform slot was 97.29 mm^3 while 113.25 mm^3 was settled in the $H_{0.75L}$ fracture slot. Increasing propped volume inside the slot increased proppant concentration inside the slot. Apparent concentration, actual concentration and concentration fraction are illustrated in (22), (23) and (24) respectively.

$$Apparent\ concentation = \frac{proppant\ weight}{h * l} \tag{22}$$

$$Actual\ concentration = \frac{proppant\ weight}{propped\ surface\ area} \tag{23}$$

$$Concentration\ fraction = \frac{apparent\ concentraion}{real\ concentraion} \qquad (24)$$

Table 4.3. Summary for all Results of Fracture Heterogeneity Effect

	Uniform fracture	$H_{0.25L}$	$H_{0.75L}$
Pile height at the injection side for first FPV, mm	0.34	1.49	5.48
Pile height at the fracture tip for first FPV, mm	16.5	16.18	0.50
Pile length, mm	241.11	272.14	296.19
Pile height, mm	77.13	79.47	79.54
EDL, fraction	0.76	0.81	0.83
EDX, fraction	0.43	0.48	0.53
Buildup slope, fraction	0.49	0.50	0.51
Buildup angle, degree	25.97	26.55	27.20
Drawdown slope, fraction	-0.20	-0.22	-0.26
Drawdown angle, degree	-11.44	-12.55	-14.45
Number of FPV	16	18	20
Proppant volume inside the slot, mm^3	97.29	97.58	113.25
Apparent concentration, lb/ft^2	0.02	0.93	1.11
Real concentration, lb/ft^2	0.03	1.39	1.58
Concentration fraction	0.61	0.66	0.70

4.2.2. Effect of Injection side Width. This factor was handled by changing the W_{in}/W_{out} ratio. In addition to the uniform fracture and the base case ($W_{in}/W_{out} = 1.2$), three more experiments were conducted by making W_{in}/W_{out} equal to 2, 3, and 4 for each experiment. In this section discusses the results of these experiments.. Table 4.4 illustrates the magnitude of each slurry FPV for $W_{in}/W_{out}=2$, $W_{in}/W_{out}=3$ and $W_{in}/W_{out}=4$**.**

Table 4.4. FPV Number and Magnitude for the Effect of Changing W_{in}/W_{out}

FPV Number	FPV Magnitude		
	$W_{in}/W_{out}=2$	$W_{in}/W_{out}=3$	$W_{in}/W_{out}=4$
FPV1	1.22	0.75	0.64
FPV2	2.43	1.51	1.28
FPV3	3.65	2.26	1.91
FPV4	4.87	3.01	2.55
FPV5	6.09	3.77	3.19
FPV6	7.30	4.52	3.83
FPV7	8.52	5.27	4.47
FPV8	9.74	6.03	5.11
FPV9	10.95	6.78	5.74
FPV10	12.17	7.53	6.38
FPV11	13.39	8.28	7.02
FPV12	14.61	9.04	7.66
FPV13	15.82	9.79	8.30
FPV14	17.04	10.54	8.93
FPV15	18.26	11.30	9.57
FPV16	19.48	12.05	10.21
FPV17	20.69	12.80	10.85
FPV18	21.91	13.56	11.49
FPV19	23.13	14.31	12.13
FPV20	24.34	15.06	12.76
FPV21		15.82	13.40
FPV22		15.06	12.76
FPV23		15.82	13.40
FPV24		15.06	12.76
FPV25			13.40
FPV26			12.76
FPV27			13.40

4.2.2.1. W_{in}/W_{out}=2. Figure 4.25 illustrates the scenario of proppant pile increment for a fracture of Win/W$_{out}$=2. This scenario was similar to the scenario of all experiments above in Section 4.2.1; the pile grew at a stable rate from the beginning until FPV12. After FPV12, most settled proppant contributed to extend the proppant pile horizontally more than vertically until reaching EDL.
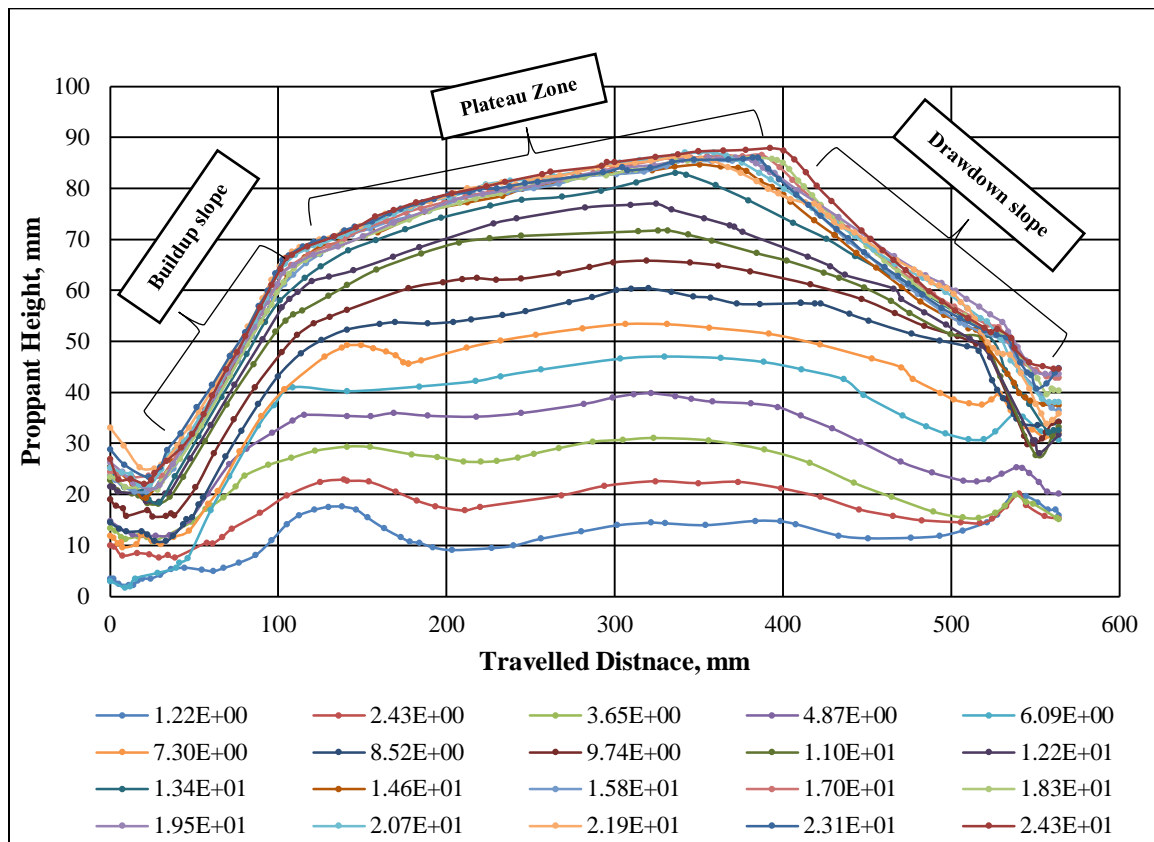
Figure 4.25. Proppant Distribution along W_{in}/W_{out}=2 Fracture after FPV20

Figure 4.26 clarifies pile height and plateau length for this slot at the last slurry FPV. The plateau proppant pile extended from 101.3 mm to 413.7 mm. Pile height was 81.0 mm and plateau length was 298.8 mm. Buildup and drawdown angles were 32.6° and -14.4° respectively.

Figure 4.26. Proppant Distribution along a $W_{in}/W_{out}=2$ Fracture after FPV20

4.2.2.2. Win /Wout=3. In this experiment, injection side width was 9.9 mm while the fracture tip side was 3.3mm. Figure 4.27 illustrates proppant development for each FPV. Proppant pile improvement strategy showed the same behavior as it explained in Section 4.2.1. From slurry FPV1 until slurry FPV8, proppant contributed by increasing pile height. Form slurry FPV9 until slurry FPV19, proppant extended the pile horizontally rather than vertically. Little augmenting in proppant pile was observed during this stage. From slurry FPV19 until slurry FPV24, pile shape was formed and EDL was achieved.

Figure 4.28 clarifies pile length and height at the last FPV. The extension of proppant pile plateau was measured from 133.2 mm until 384.7 mm. Pile height was 88.4 mm, and plateau length was 244.5 mm. Buildup angle was 27.8°, and drawdown angle was -14.3°.
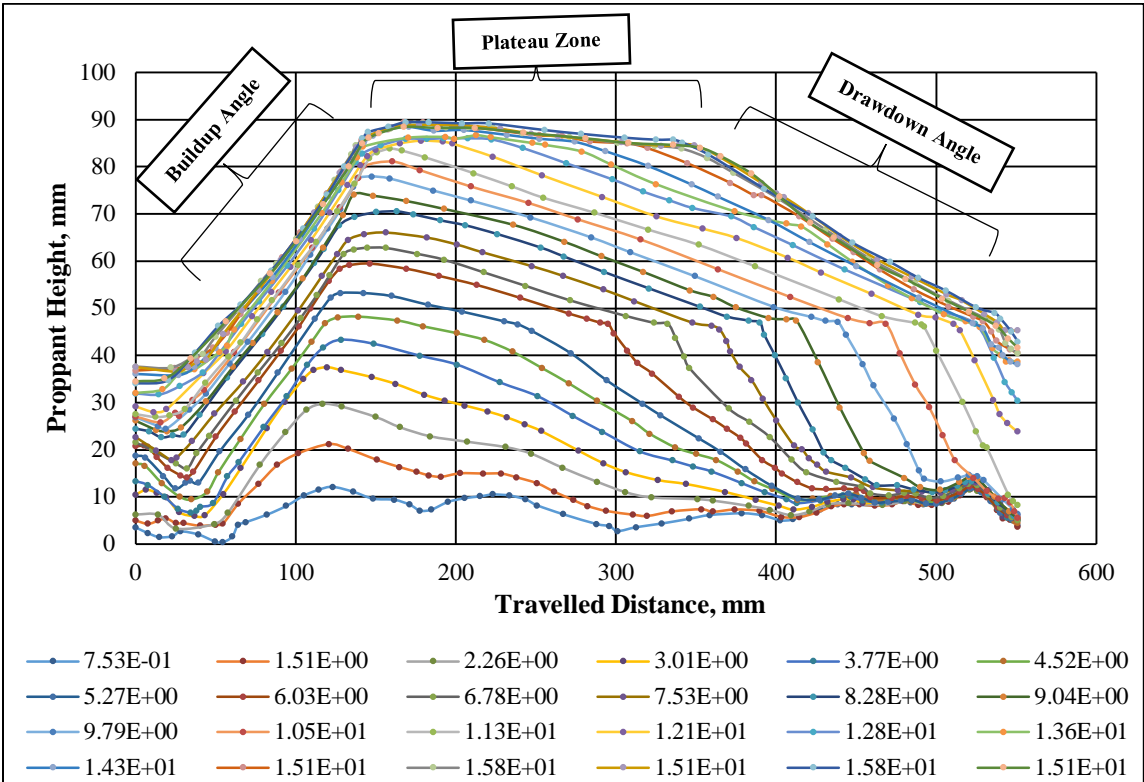
Figure 4.27. Proppant Distribution along $W_{in}/W_{out}=3$ Fracture after FPV24
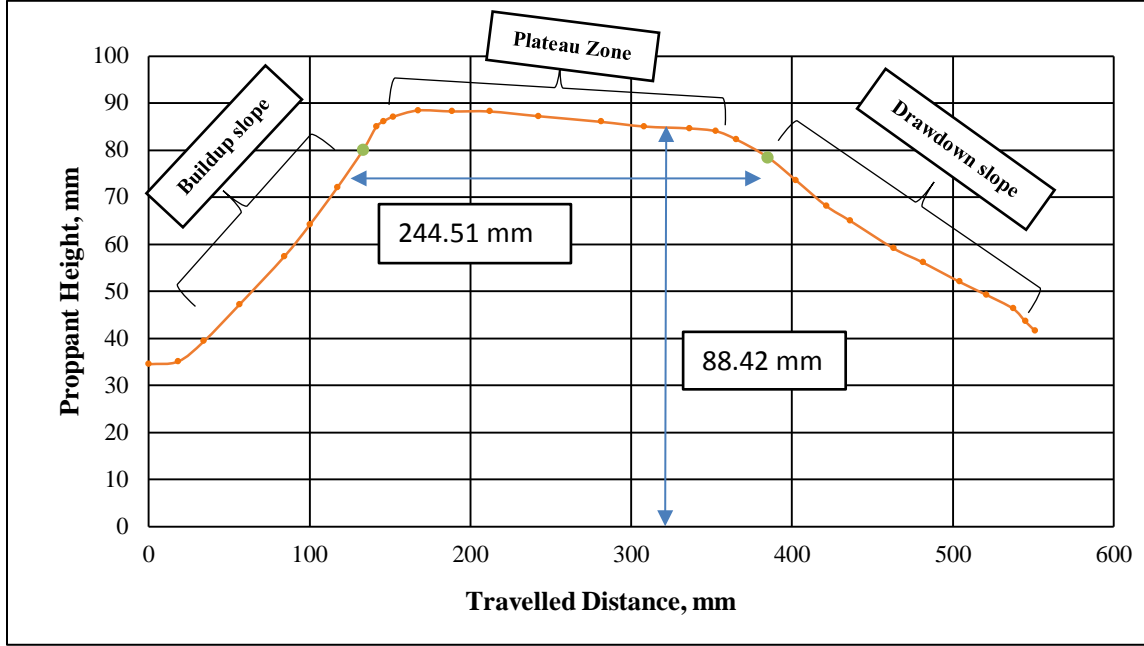
Figure 4.28. Proppant Distribution along a $W_{in}/W_{out}=3$ Fracture after FPV24

4.2.2.3. Win/Wout=4. In this model, the injection side width was 13.2 mm and the fracture tip side was constant. The width of fracture tip side was 3.3 mm. Figure 4.29 illustrates proppant distribution along the slot for all FPVs. From slurry FPV1 until FPV9, pile height increment faster than its increment during the next stages. From slurry FPV10 until slurry FPV16, proppant increased plateau length rather than pile height. After slurry FPV10, all injected slurry contributed to draw the last shape of proppant bed. At slurry FPV27, EDL was achieved and pile shape was constant.

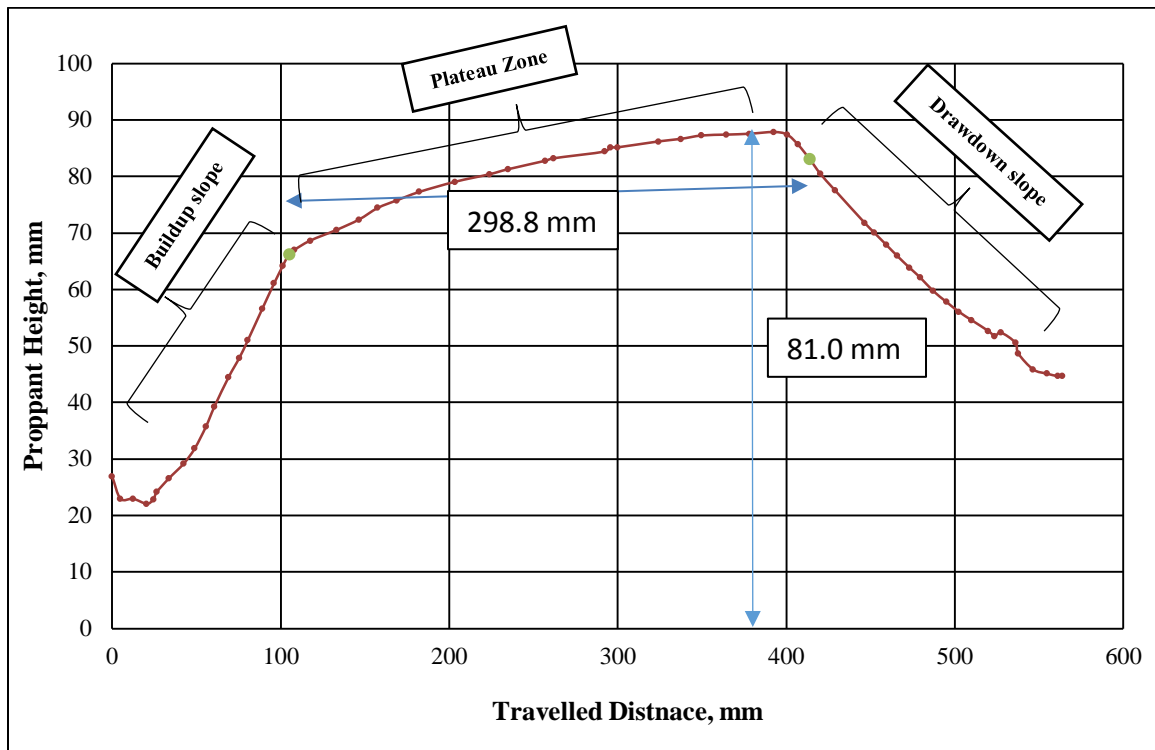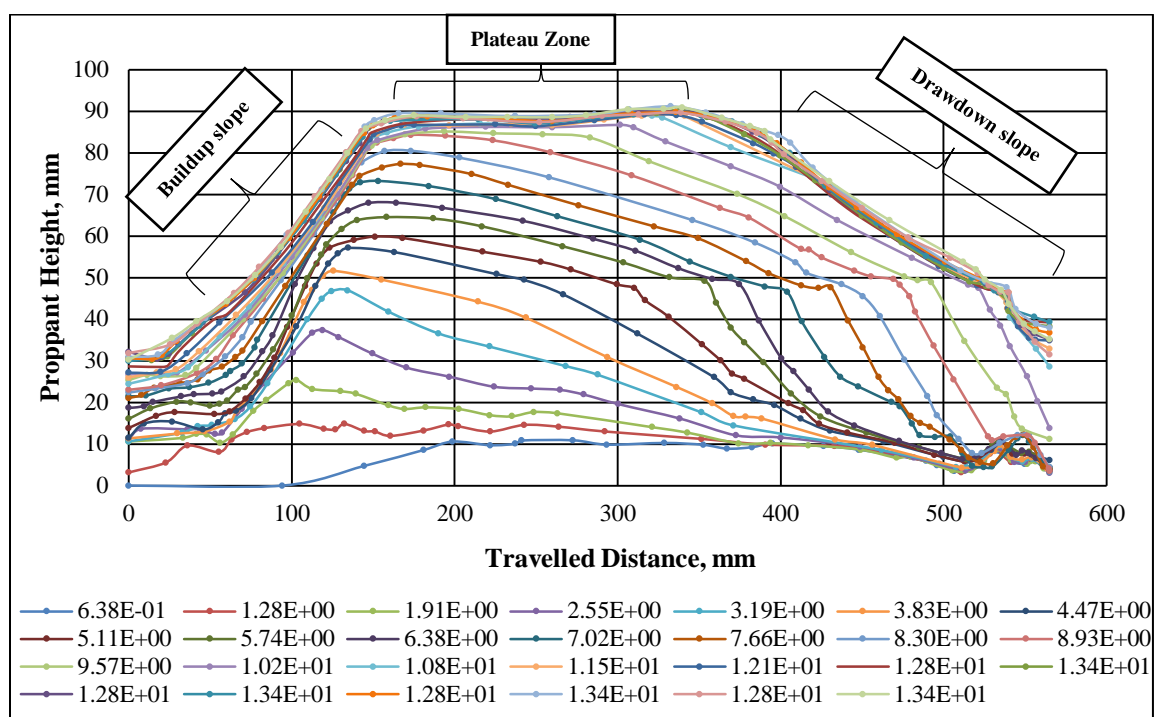Figure 4.29. Proppant Distribution along the W_{in}/W_{out}=4 Fracture after FPV27

Figure 4.30 shows pile length and height for the last FPV. The extension of proppant pile plateau was from 174.9 mm to 540.0 mm. Proppant height was 85.05 mm, and plateau length was 251.5 mm. Buildup and drawdown angles were 24.8°, and -13.9° respectively.
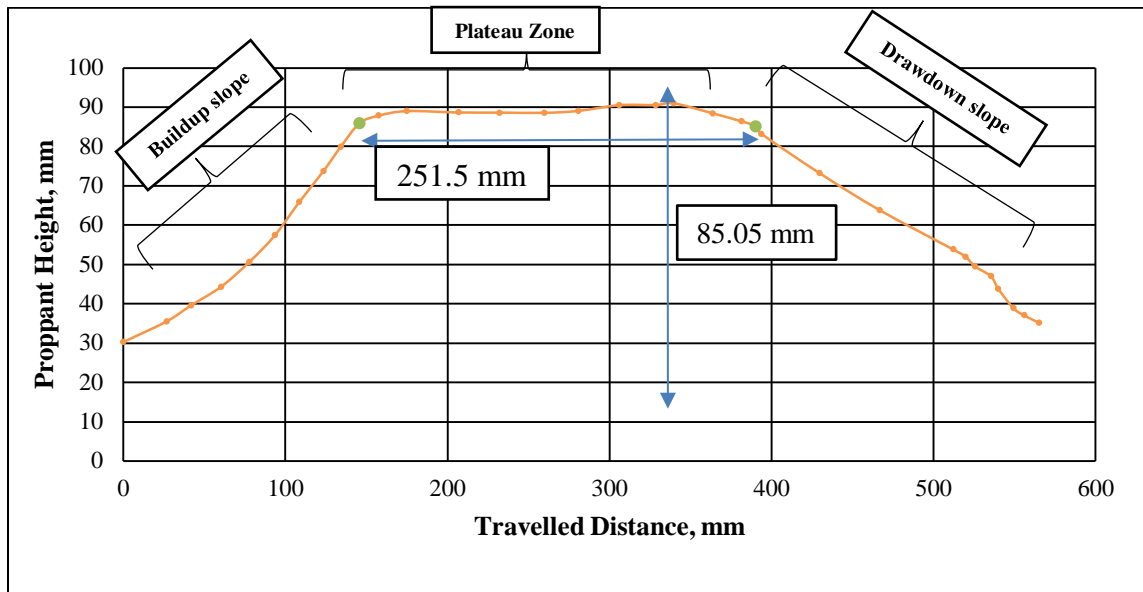
Figure 4.30. Proppant Distribution along a W_{in}/W_{out}=4 Fracture after FPV27

4.2.2.4. Comparison between a uniform, $W_{in}/W_{out} = 1.2$, $W_{in}/W_{out} = 2$, W_{in}/W_{out} =3 and $W_{in}/W_{out} = 4$.

As previously discussed the width ratio, W_{in}/W_{out}, was varied by changing the width of fracture injection side and keeping the tip side width constant. This design gave different values for W_{in}/W_{out}. Figure 4.31 shows proppant distribution along the slot at the last slurry FPV where x-axis is the travelled distance along the slot, and y-axis is proppant dune height at that point. The green marker points represent the first and last point on the dune to calculate EDL and EDX (plateau zone). Close to the injection side and before the plateau zone, buildup angles were formed. After the plateau, drawdown angles were formed. The lower curve is for the uniform fracture and the upper curve is for W_{in}/W_{out}=4. This figure shows that the highest pile is for the highest W_{in}/W_{out}, and vice versa. The more fracture width ratio, the better proppant distribution can be achieved. Results showed that injection side width affected proppant distribution. Increasing injection side width leads to reduction in slurry horizontal velocity because of increasing

cross-sectional area, while it augments proppant-settling velocity due to diminishing particle-wall and particle-particle friction effects. Increasing proppant settling velocity would increase the amount of settled proppant close to the injection side especially for early slurry FPVs while reducing slurry horizontal velocity would minimize erosion rate especially for last slurry FPVs.
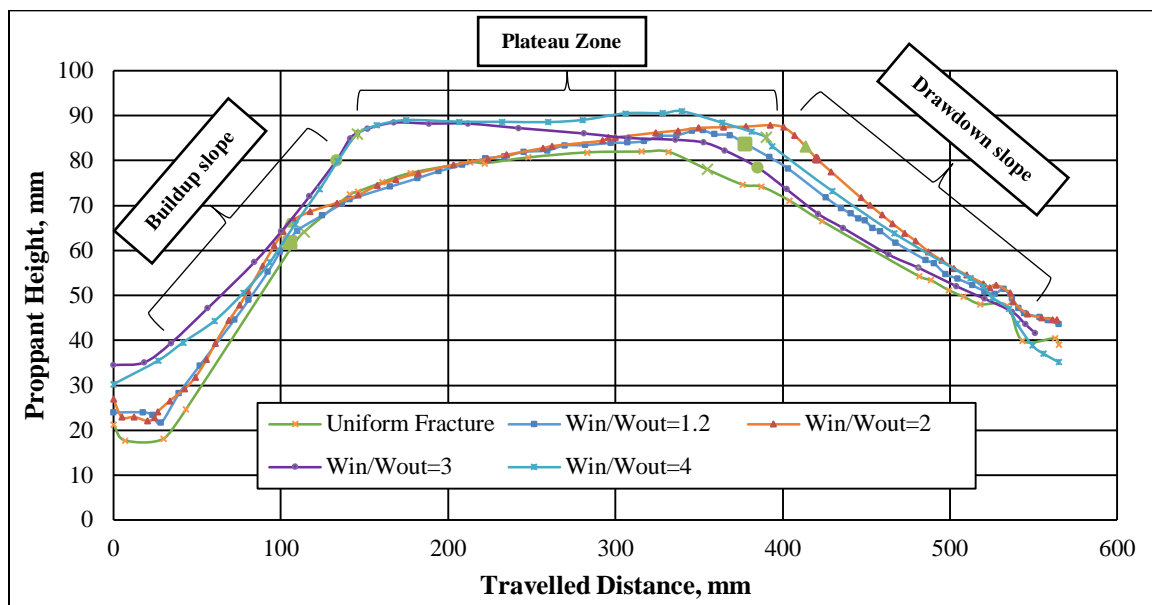
Figure 4.31. Proppant Distribution along Five Fractures with Different W_{in}/W_{out}

Figure 4.32(a) shows a direct relationship between W_{in}/W_{out} and EDL value. As W_{in}/W_{out} increased, cross-sectional area increased too. Consequently, proppant-settling rate increased and erosion rate decreased causing increasing EDL value. Figure 4.32(b) shows maximum EDX value is reached at $W_{in}/W_{out} = 2$. Increasing W_{in}/W_{out} allows for more proppant to precipitate. Below $W_{in}/W_{out} = 2$, increasing settling rate improved the pile plateau extension, EDX. Beyond $W_{in}/W_{out} = 2$, proppant-supportive forces from the fracture walls decrease and, therefore, EDX also decreases.

(a)

(b)
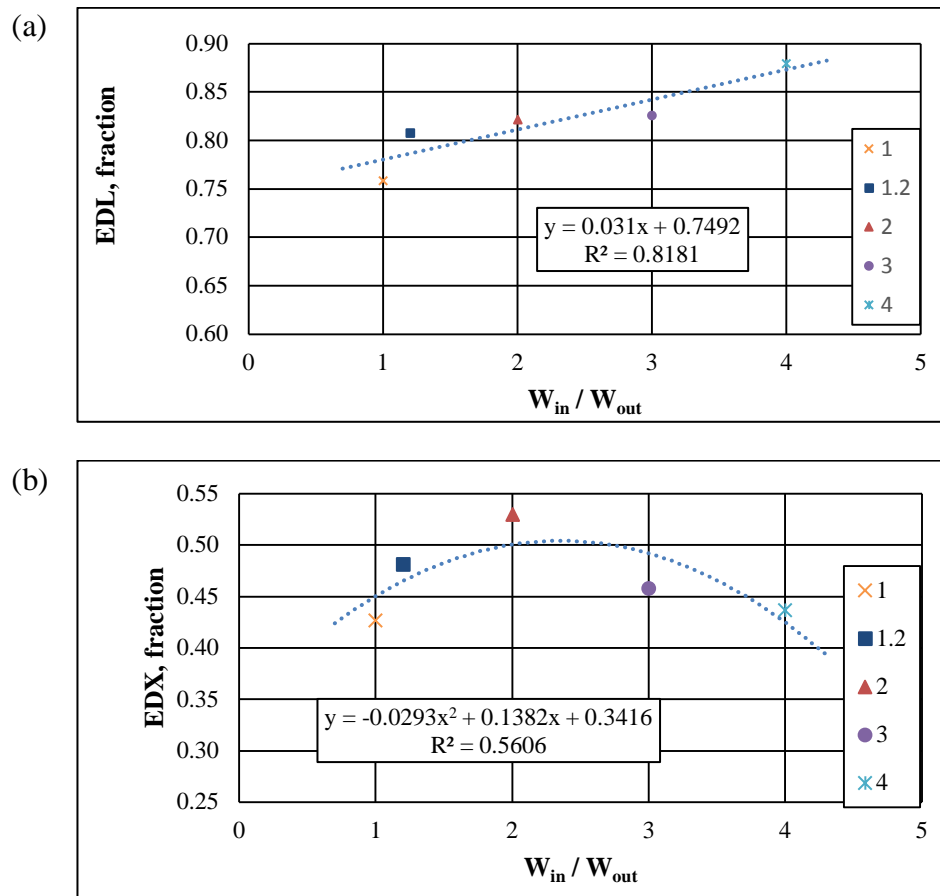
Figure 4.32. Effect of W_{in}/W_{out} on EDL and EDX. (a)W_{in}/W_{out} effect on EDL (b) W_{in}/W_{out} effect on EDX

The behavior of EDX as an effect of changing injection side width can be seen on buildup and drawdown angles. Figure 4.33(a) and Figure 4.33(b) illustrate the effect of changing W_{in}/W_{out} (x-axis) on buildup and drawdown angles (y-axis), respectively. The maximum slope for the pile was observed when $W_{in}/W_{out}=2$. Increasing this ratio more than two increased EDL and reduced EDX as were shown in Figure 4.33(a) and Figure 4.33(b). Consequently, increasing W_{in}/W_{out} above two caused a reduction in pile steep slope in both injection and end fracture side. Note that build-up slope is close to the injection side and the drawdown slope is close to the fracture tip side.
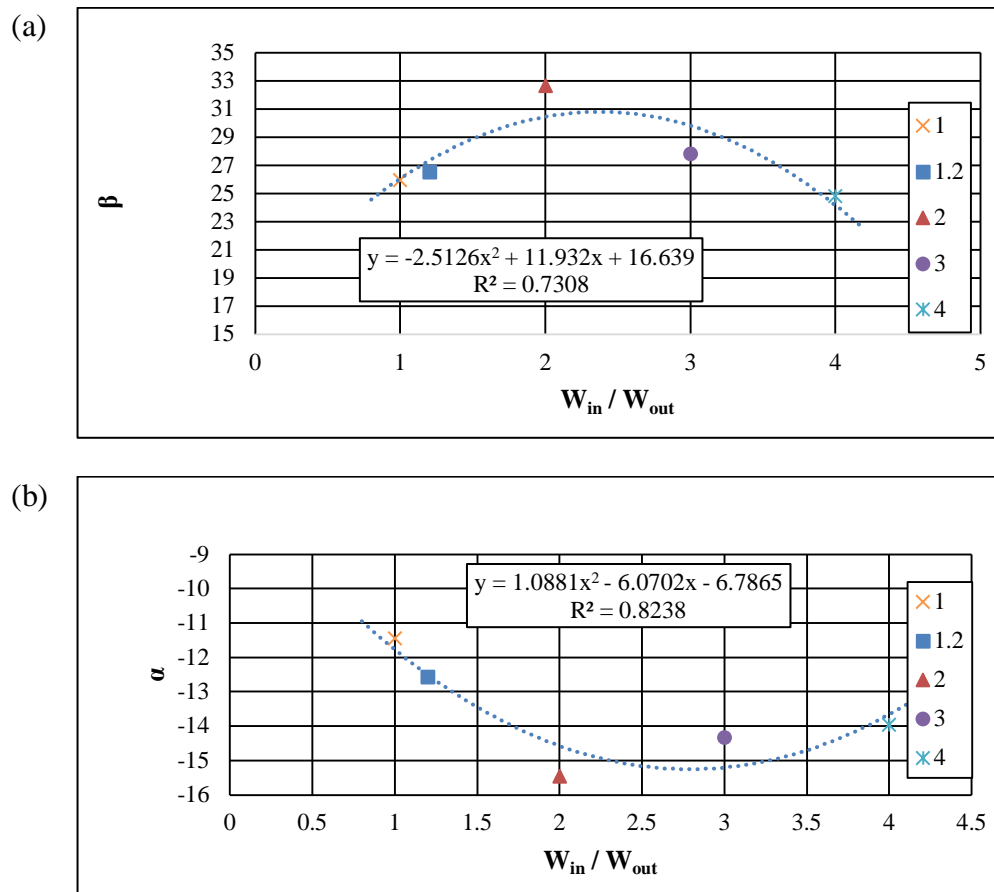
Figure 4.33. Effect of W_{in}/W_{out} on buildup and drawdown angle. (a) W_{in}/W_{out} Effect on Buildup Angle (b) W_{in}/W_{out} Effect on Drawdown Angle

The effect of changing W_{in}/W_{out} on propped surface area and proppant distribution is illustrated in Figure 4.34 and Figure 4.35. Figure 4.34 shows surface area fraction for five experiments have different W_{in}/W_{out} at each slurry FPV. The lower curve is for the uniform fracture, and the upper curve is for $W_{in}/W_{out}=4$ fracture. At the last slurry FPV, surface area fraction for the uniform fracture was 0.614 while it was 0.711 for $W_{in}/W_{out}=4$. Figure 4.35 explains propped surface area at the last FPV for the same experiments. Increasing W_{in}/W_{out} improved proppant distribution along the slot as illustrated in Figure 4.31. Consequently, propped surface area increased due to increasing W_{in}/W_{out}.

Thus, more injection side width gives higher propped surface area and surface area fraction.

Surface area fraction is the ratio of propped surface area to fracture surface area, as in (25):

$$Surface\ area\ fraction = \frac{Propped\ surface\ area}{Fracture\ surface\ area} \tag{25}$$

where, propped surface area is the area of fracture that covered by proppant. Propped surface area was calculated by inserting the reading of proppant height at each point in a trapezoidal code in MATLAB. While fracture surface area is the result of multiplying fracture height by fracture length as illustrated in (26):

$$Fracture\ surface\ area = l * h \tag{26}$$

where

l: fracture length (mm)

h: fracture height (mm).
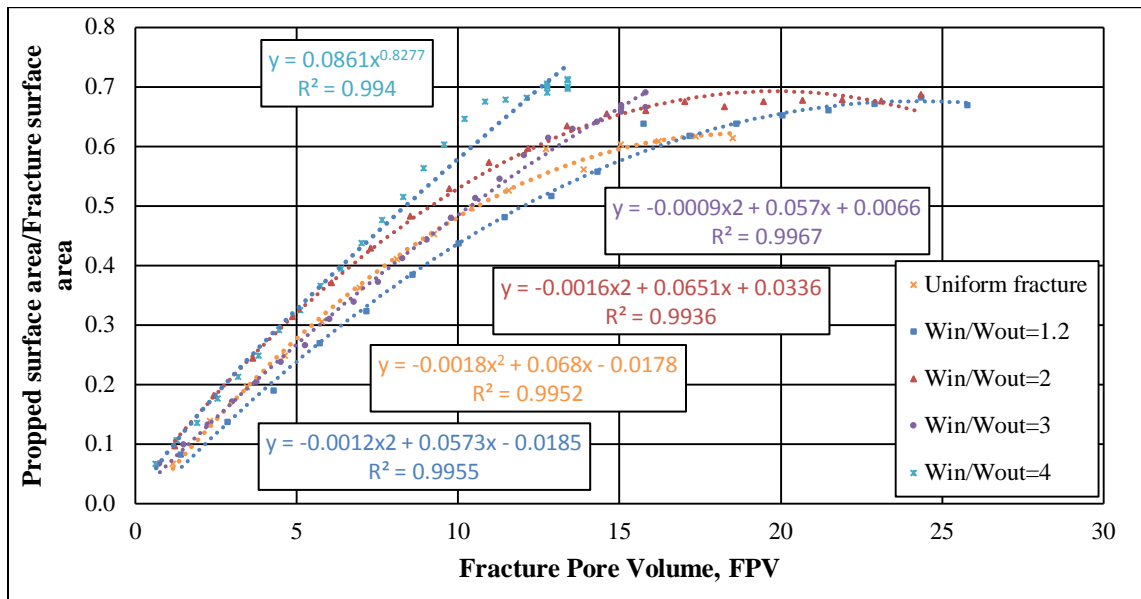
Figure 4.34. Effect of W_{in}/W_{out} on the Surface Area Fraction
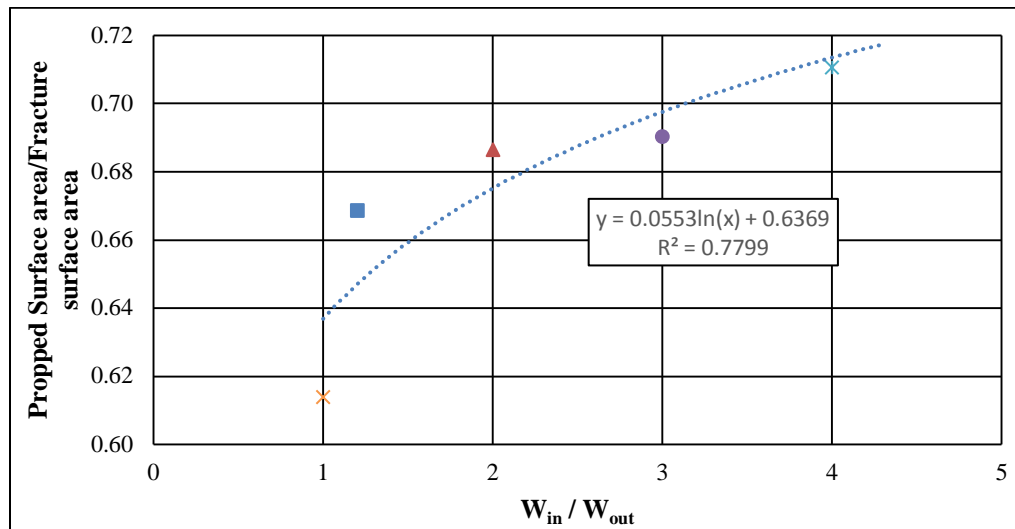
Figure 4.35. Effect of W_{in}/W_{out} on Surface Area Fraction for Last FPV

Table 4.5 shows that increasing W_{in}/W_{out} increased the amount of proppant that precipitates close to the injection side while it decreases at the fracture tip side. For instance, the pile height of proppant that settled at the injection side of the slot of $W_{in}/W_{out}=1$ was 0.34 mm whereas it was 3.7 mm for the slot whose $W_{in}/W_{out}=4$. At the fracture tip side, proppant height was 16.5 mm for the slot with $W_{in}/W_{out}=1$, but it was 3.64 mm for the slot whose $W_{in}/W_{out}=4$. The correlation that proposed by Gadde et al. (2004) shows an invertse relationship between fracture width and proppant-settling velocity, as illustrated in (19). Although increasing injection side width reduces settling velocity, the reduction in slurry horizontal velocity that resulted from increasing cross sectional area was dominant. This behavior allowed for more proppant to settle as W_{in}/W_{out} was increased.

Since increasing W_{in}/W_{out} allowed for more proppant to settle down in the slot, the required FPV to reach EDL, and apparent and real concentration of proppant volume inside the slot increased too.

Table 4.5. Comparison between Three Fractures with Different W_{in}/W_{out}

	Uniform Fracture	W_{in}/W_{out} =1.2	W_{in}/W_{out} =2	W_{in}/W_{out} =3	W_{in}/W_{out} =4
Pile height at the injection side for 1st FPV, mm	0.34	1.49	3.50	3.56	3.70
Pile height at the fracture tip 1st FPV, mm	16.50	16.18	15.87	3.97	3.64
Pile length, mm	241.11	272.14	298.86	251.50	244.51
Pile height, mm	77.13	79.47	81.02	85.05	88.42
EDL, fraction	0.76	0.81	0.82	0.83	0.88
EDX, fraction	0.43	0.48	0.53	0.46	0.44
Buildup slope, fraction	0.49	0.50	0.64	0.53	0.46
Buildup angle, degree	25.97	26.55	32.68	27.81	24.81
Drawdown slope, fraction	-0.20	-0.22	-0.28	-0.26	-0.25
Drawdown angle, degree	-11.44	-12.55	-15.44	-14.32	-13.95
Number of FPV	16	18	20	24	27
Proppant volume inside the slot, cm^3	97.29	97.58	121.65	163.92	165.03
Apparent concentration, lb/ft^2	0.02	0.93	1.16	1.54	1.55
Real concentration, lb/ft^2	0.03	1.39	1.69	2.24	2.19
Concentration fraction	0.61	0.67	0.687	0.690	0.71

4.2.3. Effect of Fracture Roughness. In this section, three experimental results will be shared. In addition to the model of the base case that had smooth fracture wall, two more experiments have been conducted. Results of the base case are shown in Section4.2.1.2. This section will be dictated to display the results of the low roughness and the high roughness and a comparison for the three models. Table 4.6 illustrates the magnitude of each slurry FPV for low and high roughness experiments.

Table 4.6. FPV Number and Magnitude for the Effect of Changing Wall Roughness

FPV Number	FPV Magnitude		
	Smooth	Low Roughness	High Roughness
FPV1	1.43	1.52	1.30
FPV2	2.87	3.05	2.61
FPV3	4.30	4.57	3.91
FPV4	5.73	6.10	5.22
FPV5	7.17	7.62	6.52
FPV6	8.60	9.15	7.83
FPV7	10.03	10.67	9.13
FPV8	11.47	12.19	10.43
FPV9	12.90	13.72	11.74
FPV10	14.33	15.24	13.04
FPV11	15.77	16.77	14.35
FPV12	17.20	18.29	15.65
FPV13	18.63	19.82	16.96
FPV14	20.06	21.34	18.26
FPV15	21.50	22.86	19.57
FPV16	22.93	24.39	20.87
FPV17	24.36	25.91	22.17
FPV18	25.80		

4.2.3.1. Low roughness. Figure 4.36 demonstrates proppant distribution along the slot for all FPVs. From slurry FPV1 until slurry FPV6, proppant increased pile height regularly. Additionally, no settled proppant was observed at the injection side during these six FPVs. After FPV6, proppant started to settle close to the inception side, and incremental growth of the pile height dwindled. At slurry FPV17, the final shape of the dune was drawn, and EDL was achieved.
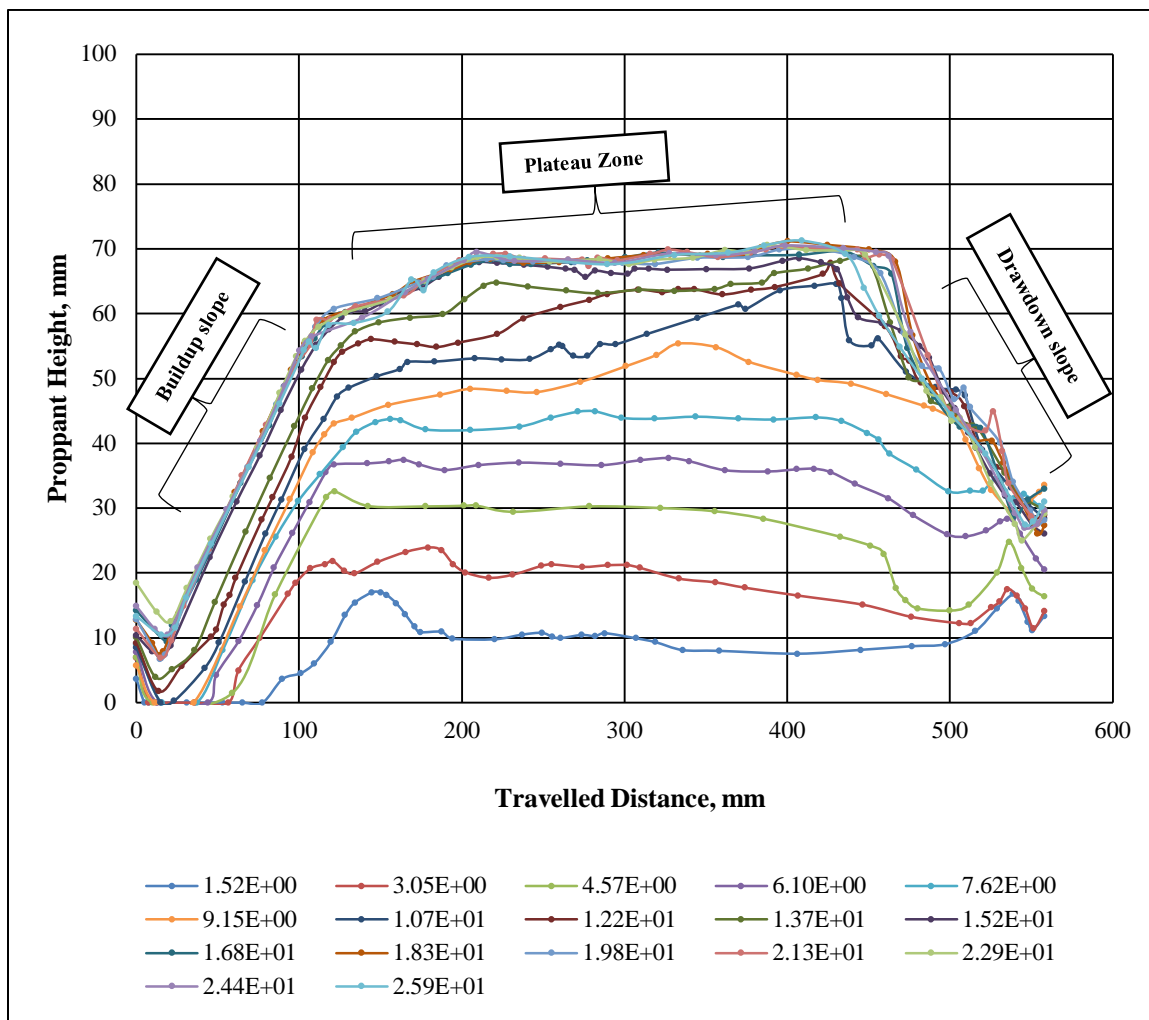
Figure 4.36. Proppant Distribution along the Low Roughness during All FPVs and after FPV17.

Proppant length and height are exhibited in Figure 4.37. Proppant pile plateau was extended from 106.3 mm to 447.2 mm. Plateau length was 340.6 mm, and pile height was 65.7 mm. Buildup and drawdown angles were 27.8° and -15.9° respectively.
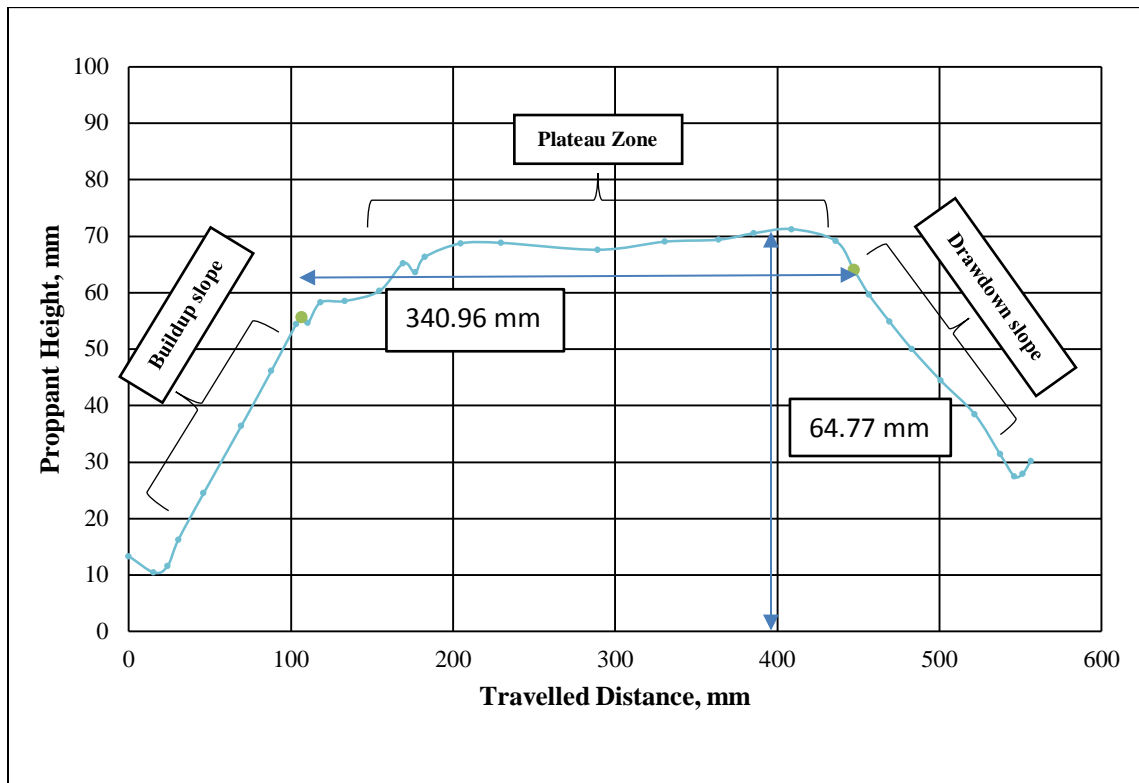
Figure 4.37. Proppant Distribution along the Low Roughness after FPV17

4.2.3.2. High roughness. More increments in fracture roughness caused different proppant distribution, as shown in the Figure 4.38. This figure illustrates proppant pile development during all slurry FPVs. During the 11 slurry FPVs, no settled or little settled proppant was observed at the injection side of the fracture. From slurry FPV1 until FPV7, proppant pile building had a constant rate. The building rate of proppant pile increased at the late slurry FPVs. In the late slurry FPVs, most injected proppant extended proppant dune until EDL was achieved.
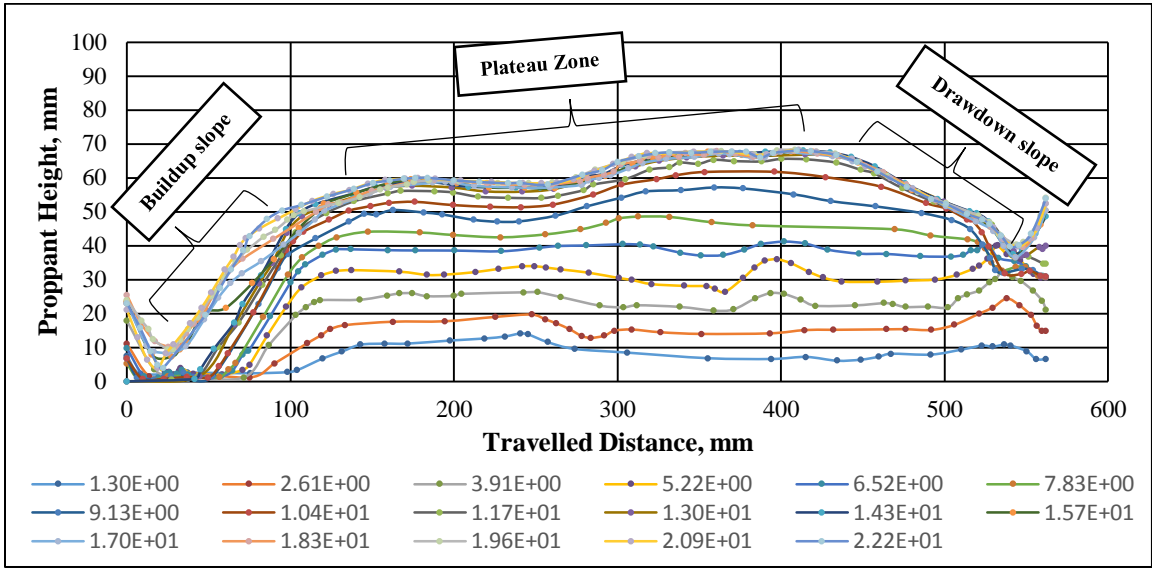
Figure 4.38. Proppant Distribution along the High Roughness after FPV17

Figure 4.39 shows the pile height and plateau length at the last slurry FPV. The extension of the plateau was from 85.7 mm to 446.3 mm. Pile height was 61.7 mm, and plateau length was 360.5 mm. Buildup and drawdown angles were 31.1° and -13.9° respectively.
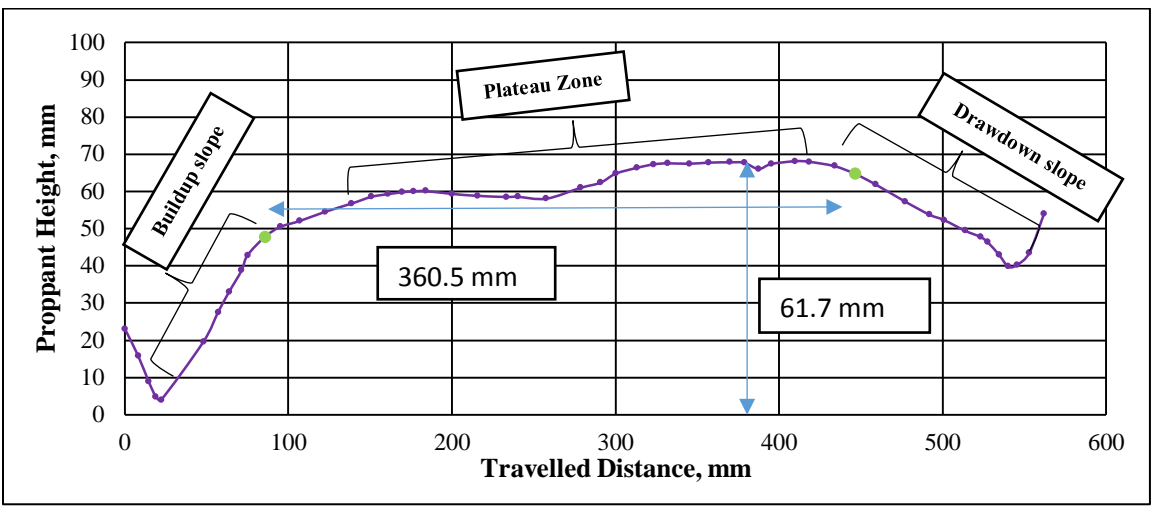
Figure 4.39. Proppant Distribution along the High Roughness after Reaching EDL (FPV17)

4.2.3.3. Comparison between smooth wall, low roughness and high roughness.

Figure 4.40 shows proppant distribution at the last slurry FPV for three fracture roughness models. The y-axis is for proppant height and x-axis is for the proppant travelling distance from the injection side to fracture tip side. The green points on the proppant distribution curves were used to determine the data range which included to calculate EDL and EDX. The lower curve in the plateau region is for the high-roughened wall fracture, and the upper curve is for the smooth fracture. Fracture model with smooth wall had higher proppant pile at the plateau than the other fracture model with rough wall. Additionally, proppant distribution along fracture with smooth wall was more uniformly distributed than the other fracture roughness models.
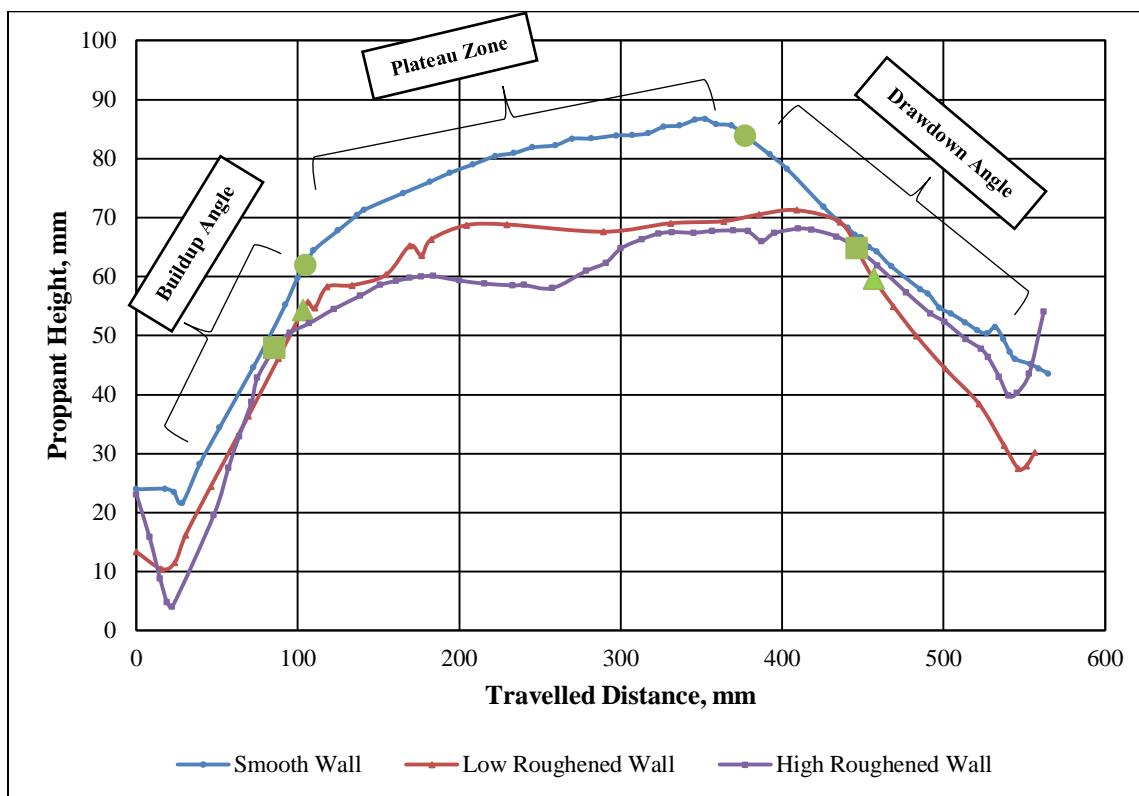
Figure 4.40. Effect of Fracture Wall Roughness on Proppant Distribution

Table 4.7 lists the proppant height measurements during the first slurry injection pore volume that was measured at the injection and at the fracture tip sides. The amount of proppant that settled close to the injection point decreased as fracture walls became rougher; e.g. proppant height that settled at the injection side dropped from 1.49 mm for the smooth walls to 0 mm in low and high roughened walls. Additionally, during the first slurry FPV, proppant in smooth wall fractures had larger proppant height than roughened fracture models at the fracture tip side. Proppant height at the tip side of the smooth fracture was 16.18 mm whereas it was 11.18 mm and 6.6 mm for the low and high roughened wall fracture respectively. The tip pile height for the slurry in smooth wall reinforced the conclusion that shared by Liu and Sharma (2005). They observed that increasing wall roughness reduces proppant horizontal velocity. In this study, proppant movement was restricted in horizontal and vertical direction as fracture wall roughness was increased. Proppant-settling velocity was impeded by increasing wall roughness more than proppant horizontal velocity, which can be implied from the proppant height that measured in low and high roughened wall at the injection and tip sides.

Table 4.7. Comparison between Three Fractures with Different Roughness

	Smooth Wall	Low Roughened Wall	High Roughened Wall
Pile height at the injection point for 1st FPV, mm	1.49	0.00	0.00
Pile height at the tip fracture point for 1st FPV, mm	16.18	11.18	6.60
Pile length, mm	272.14	340.96	360.59
Pile height, mm	79.47	64.77	61.73

Table 4.7. Comparison between Three Fractures with Different Roughness (cont)

EDL, fraction	0.81	0.67	0.64
EDX, fraction	0.48	0.61	0.64
Buildup slope, fraction	0.50	0.52	0.60
Buildup angle, degree	26.55	27.40	31.13
Drawdown slope, fraction	-0.22	-0.29	-0.29
Drawdown angle, degree	-12.55	-15.91	-16.15
Number of FPV	18	17	17
Proppant volume inside the slot, cm^3	97.58	70.62	71.15
Apparent concentration, lb/ft^2	0.93	0.69	0.69
Real concentration, lb/ft^2	1.39	1.20	1.25
Concentration fraction	0.66	0.57	0.55

The effect of fracture wall roughness on EDL and EDX is shown in Figure 4.41(a) and Figure 4.41(b) respectively. Increasing wall roughness decreased EDL value. EDL was 0.81 for smooth wall, but it was 0.64 for high roughness. However, EDX showed an opposite behavior. It was 0.48 for smooth wall and 0.64 for high-roughened wall. This observation reinforced the previous conclusion (Table 4.7) about wall roughness effect on proppant movement in both horizontal and vertical direction. Erosion and settling rate are

a function of horizontal and settling velocity; therefore, the high erosion rate in high-roughened wall prevented proppant to build as a high a dune as in smooth wall fractures.
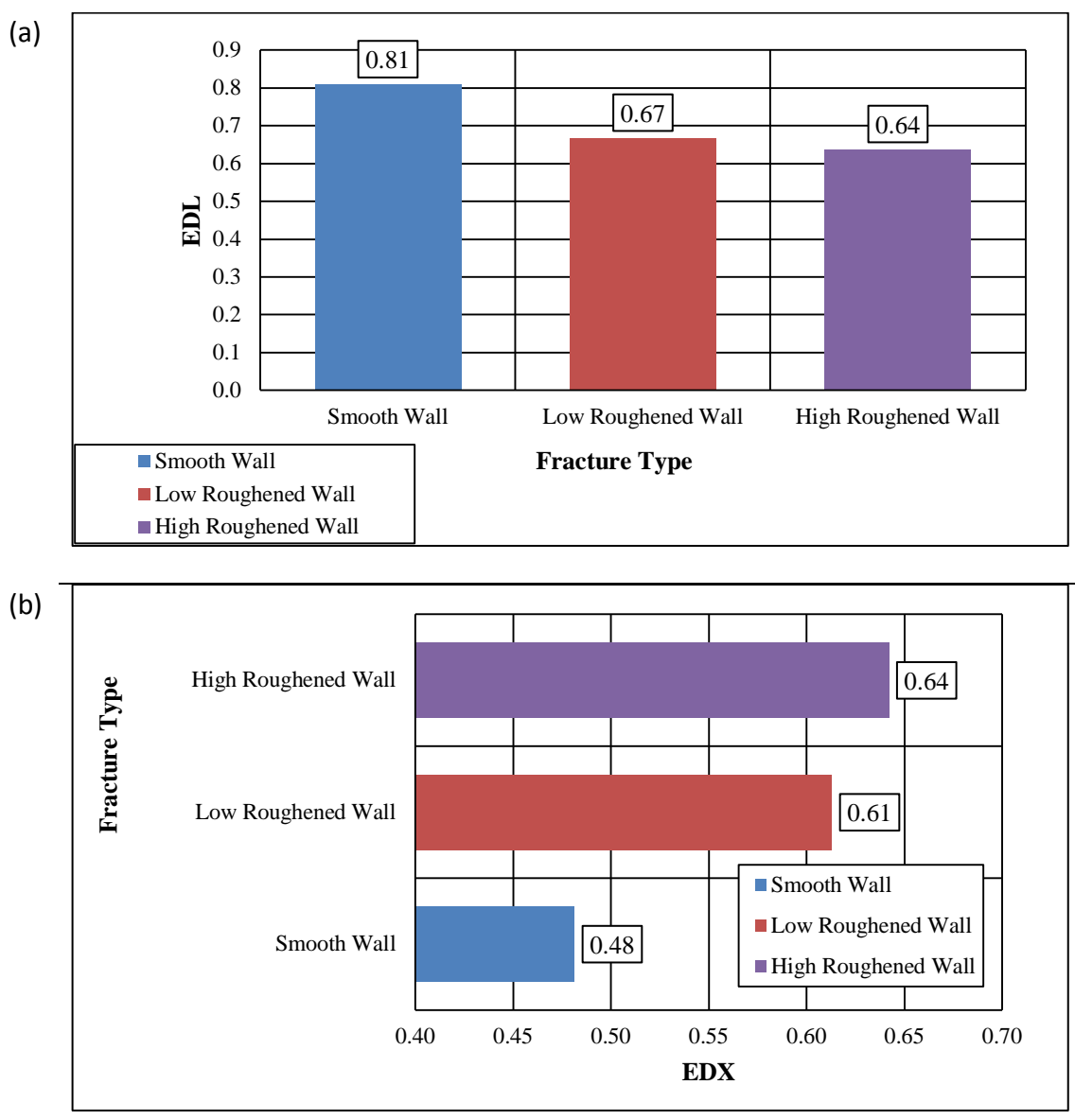
Figure 4.41. Wall Roughness Effect on EDL and EDX. (a) Effect of Wall Roughness on EDL (b) Effect of Wall Roughness on EDX

Referring to the results shown in Figure 4.40 and Figure 4.41, propped surface area improved due to increasing wall roughness. Figure 4.42 shows the development of surface

area fraction as a function of slurry injection pore volume for three fracture wall roughness models. Increasing wall roughness increased propped surface area. Additionally, low and high roughness had approximately the same propped surface area until slurry injection volume reached 15. When slurry injection fracture pore volume reached 15, propped surface area for high roughness fracture became larger than low roughness fracture model.

Kern et al. (1959) indicated that settled proppant is the only contributor to enhance production rate. Production rate increases as propped surface area increases. Our experimental results showed that fractures with high roughness had larger surface area than low and smooth walls. As a result, fractures with high roughness would have better fracture conductivity and production rate than fractures with less roughness.
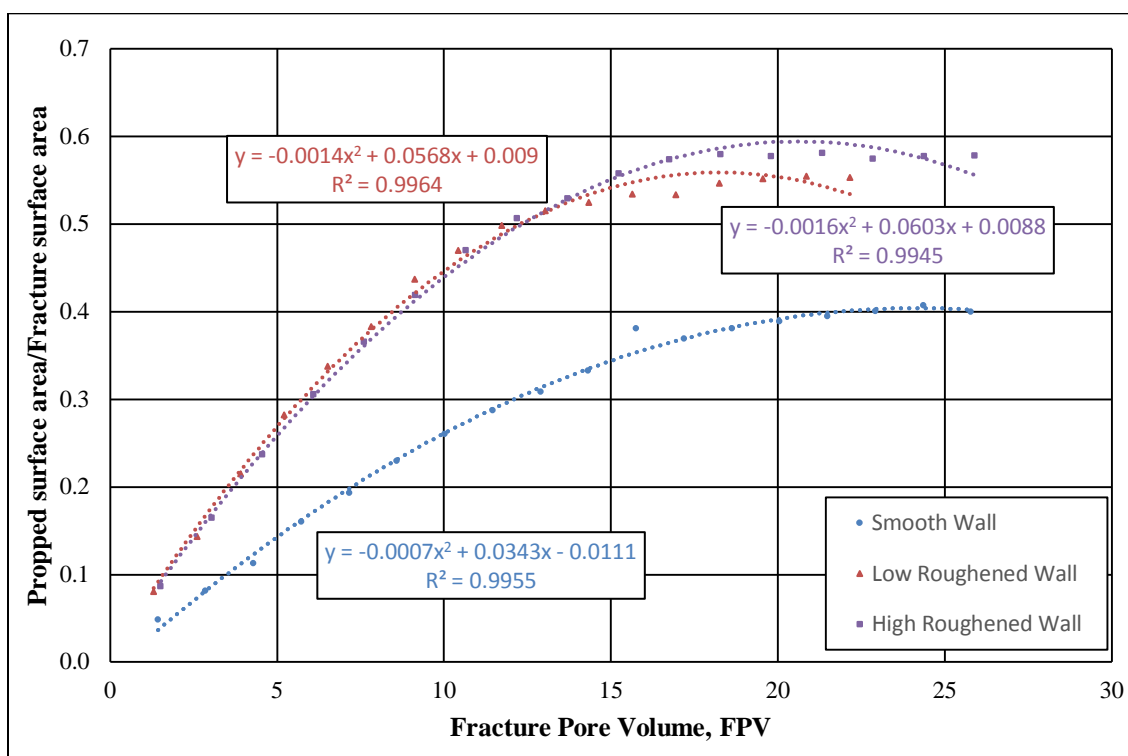
Figure 4.42. Effect of Wall Roughness on Surface Area Fraction for Three Fractures Differ in Wall Roughness

For better explanation, the relationship between propped surface area and fracture roughness at the last slurry FPV was explained in Figure 4.43. Surface area fraction increased from 0.4 for the smooth wall fracture to 0.58 for the high-roughened wall fracture.
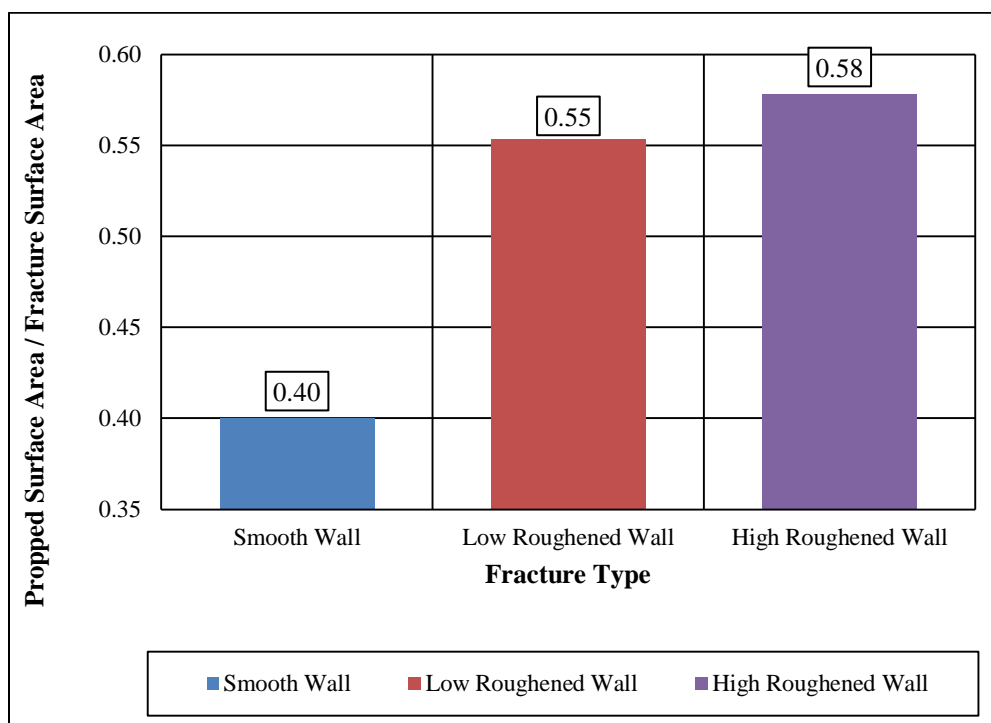
Figure 4.43. Effect of Wall Roughness on Surface Area Fraction for Last FPV of Three Fractures Differ in Wall Roughness

Figure 4.44(a) and Figure 4.44(b) reveal the effect of wall roughness on buildup and drawdown angles respectively. In Figure 4.44(a), buildup angle increased from 26.5° for the smooth wall to 31.1° for high roughened wall. Figure 4.44(b) showed that drawdown angle increased from -12.5° for the smooth wall to -16.1° for high roughened wall. That means that roughness helped proppant stick on the wall to give a steeper build-up and drawdown slope, which is what makes proppant more stable inside the fracture.

Increasing proppant consolidating inside the fracture can give better results in flowback process or production.
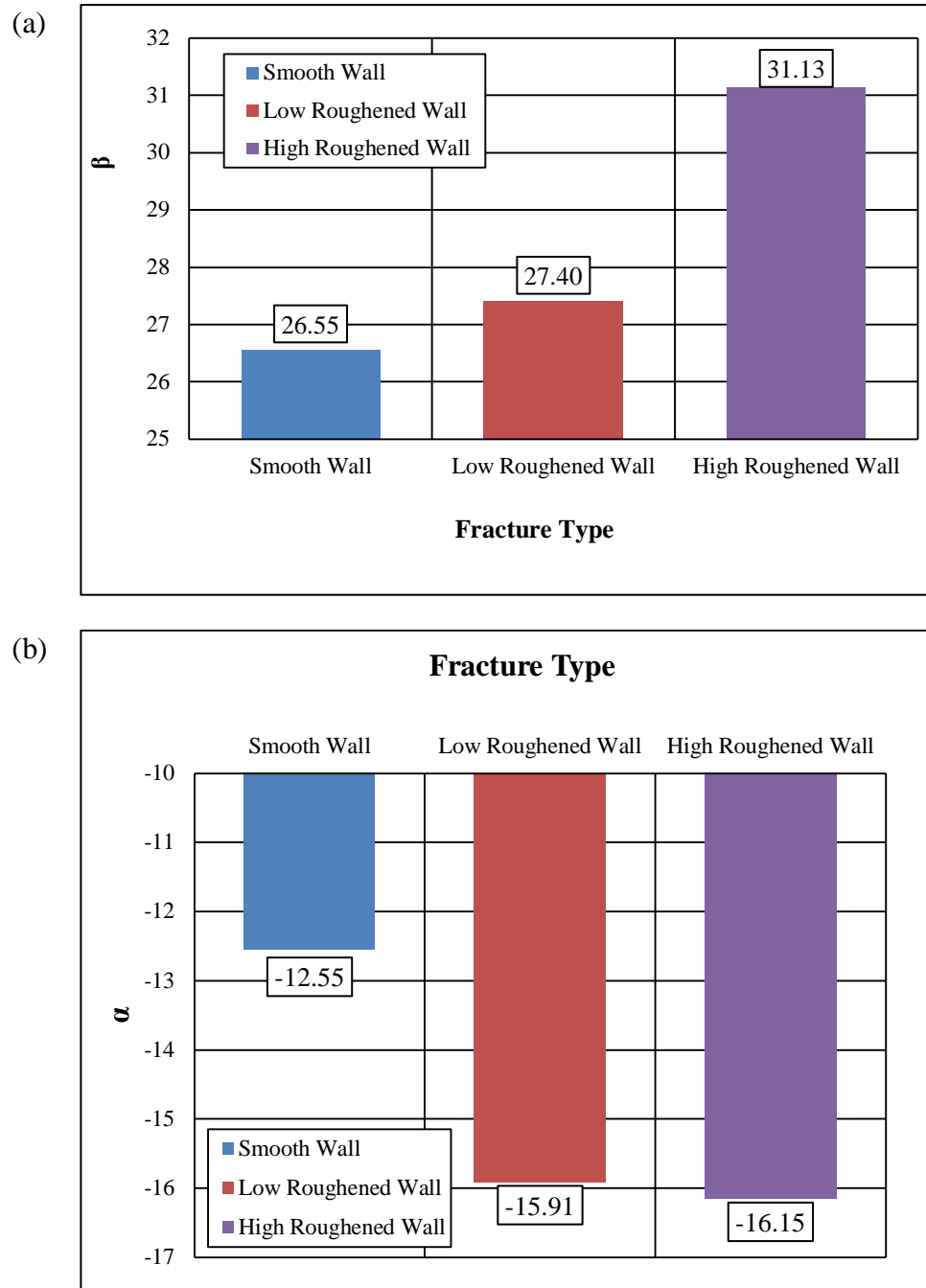
Figure 4.44. Effect of Fracture Wall Roughness on Buildup and Drawdown Angle. (a) Roughness Effect on Buildup Angle (b) Roughness Effect on Drawdown Angle

Figure 4.45 shows how proppant stuck at the rough surface. After finishing the experiment, this slice was exposed to flowing water to release the stuck proppant from this surface. No effect was observed during one day of flowing water. That was the exact opposite of what happened with smooth wall fractures. This observation emphasized the previous conclusion about the effect of roughness on the injected proppant stability inside a fracture. Thus, roughness can increase well productivity by supporting proppant during flowback process or production.
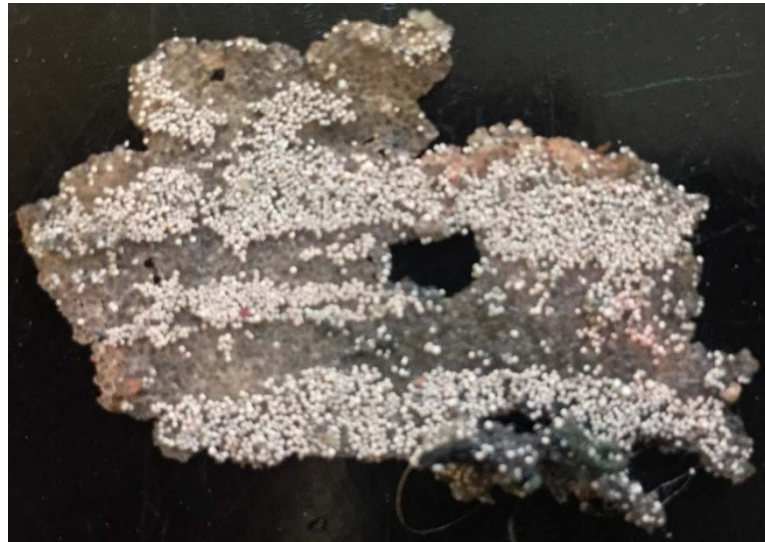
Figure 4.45. Sticking Proppant at the Rough Surfaces

4.2.4. Effect of Fracture Leak-off. This factor has been studied by drilling a different number of holes in one plexiglass sheet to give different fracture leak-off factors, as discussed in Section 4.1.4. In this section, the results of low leak-off fracture and high leak-off fracture will be explained, while no leak-off fracture, which is the base case of this study, is explained in Section 4.2.1.2. Table 4.8 illustrates the magnitude of each slurry FPV for $W_{in}/W_{out}=2$, $W_{in}/W_{out}=3$, and $W_{in}/W_{out}=4$.

Table 4.8. FPV Number and Magnitude for the Effect of Changing Fracture Leak-off

FPV Number	FPV Magnitude		
	No leak-off	Low Leak-off	High Leak-off
FPV1	1.43	1.50	1.50
FPV2	2.87	3.00	3.00
FPV3	4.30	4.49	4.50
FPV4	5.73	5.99	6.00
FPV5	7.17	7.49	7.50
FPV6	8.60	8.99	9.00
FPV7	10.03	10.48	10.50
FPV8	11.47	11.98	12.01
FPV9	12.90	13.48	13.51
FPV10	14.33	14.98	15.01
FPV11	15.77	16.47	16.51
FPV12	17.20	17.97	18.01
FPV13	18.63	19.47	19.51
FPV14	20.06	20.97	21.01
FPV15	21.50	22.46	
FPV16	22.93		
FPV17	24.36		
FPV18	25.80		

4.2.4.1. Low leak-off fracture. This model was constructed by drilling three apertures in the middle height of the slot to drain only water and keep proppant inside the slot. Figure 4.46 shows proppant distribution along the slot at the first slurry FPV. The red arrows in the figure mark each aperture spot. A captured photo for the slot at this stage was inserted at the top of this figure. The purple line in the photo pointes to the proppant bed. At the beginning of the slot, no settled proppant was observed. Three domes were recognized along the proppant pile. These domes were located below leak-off spots directly. Proppant along the slot was distributed in this manner because water drained through the apertures that forced proppant to change its pathway.
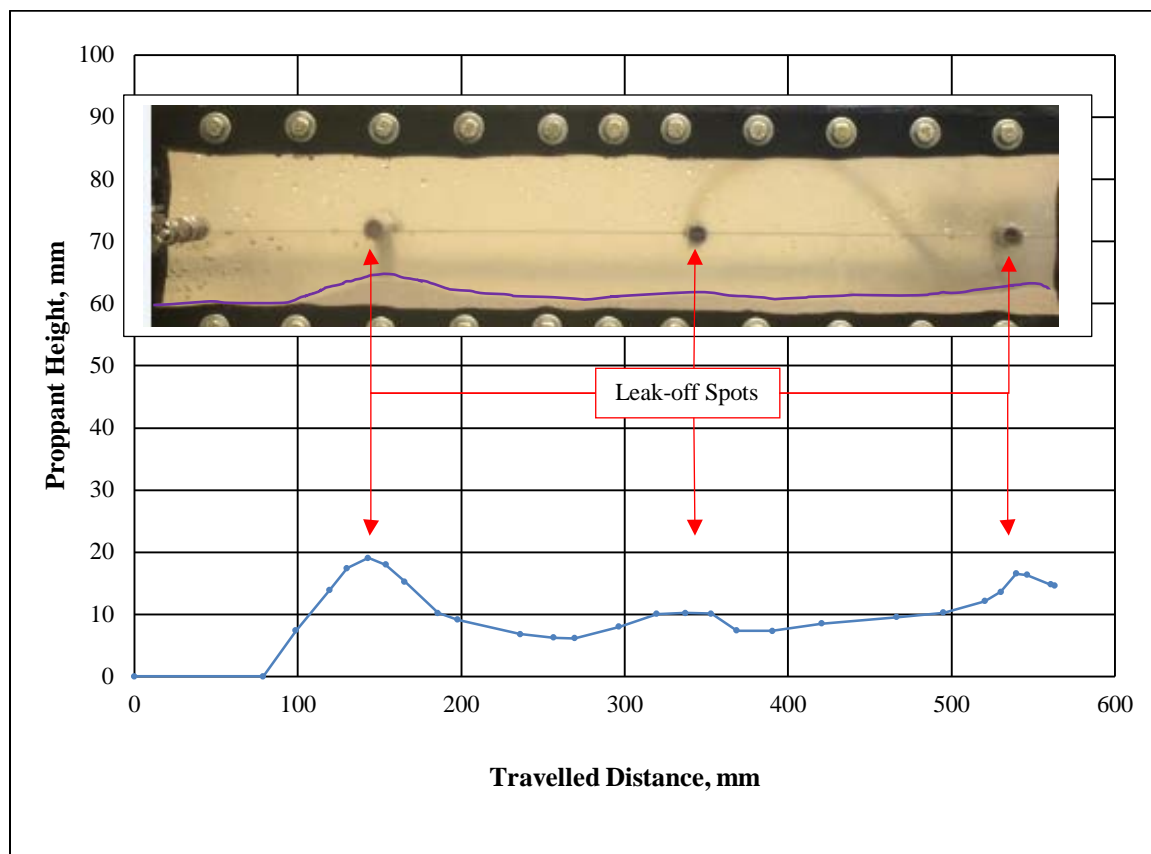
Figure 4.46. Proppant Distribution along the Low Leak-off Slot for the First FPV

Figure 4.47 shows proppant distribution along the low leak-off fracture during seven slurry FPVs. The effect of proppant settling at the holes became more pronounced as more proppant was injected until the three holes were covered completely. Proppant first covered the leak-off spot closest to the injection side and then covered the second one. The last aperture, which was close to the fracture-tip side, was covered later in FPV7.
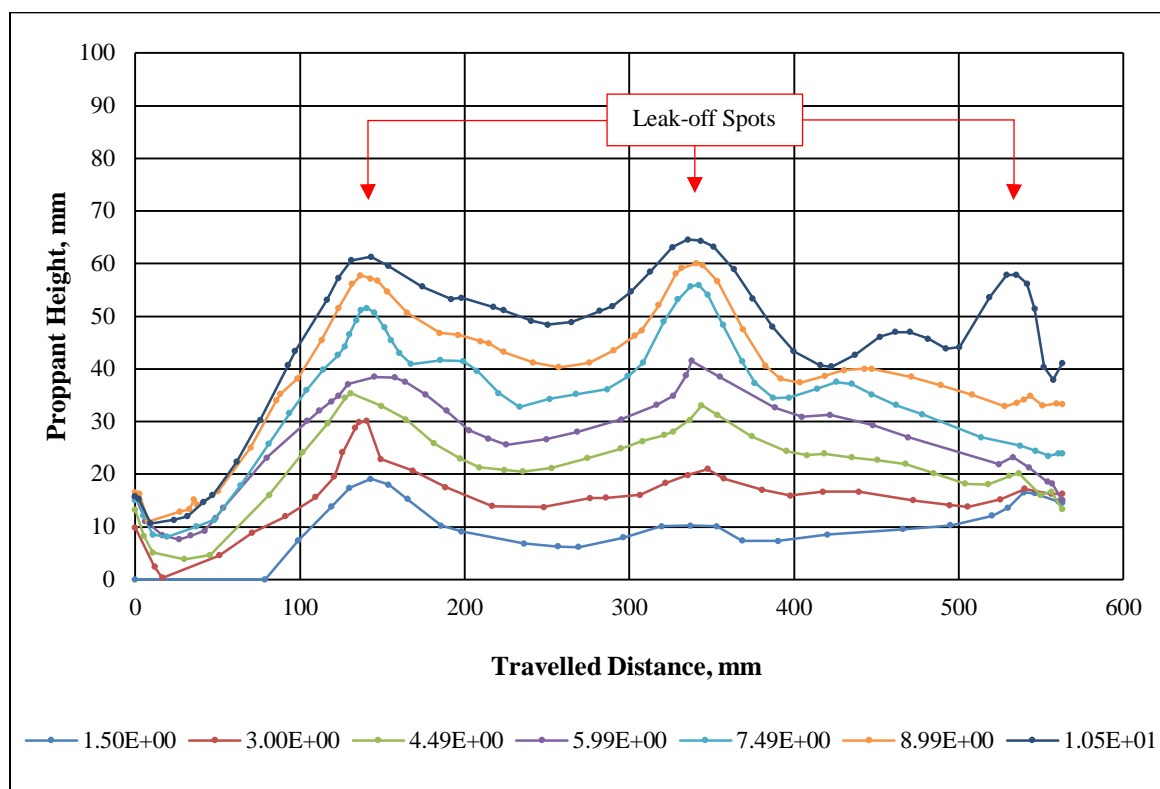
Figure 4.47. Proppant Distribution along the Low Leak-off Slot until all Leak-off Spots were Covered (after FPV7)

Figure 4.48 shows how leak-off spots have an effect on proppant settling and distribution from FPV1 to FPV10. After covering the three apertures, the two dips that formed between the three domes became dominant. Close to each dip, cross-sectional flow area became bigger than that close to each dome. Increasing cross-sectional area decreased

slurry horizontal velocity. On the other hand, each dome was working as a buffer to hinder slurry movement in general and proppant in particular. These two factors caused increasing proppant settling rate in each dip until it reached the same height as the domes.
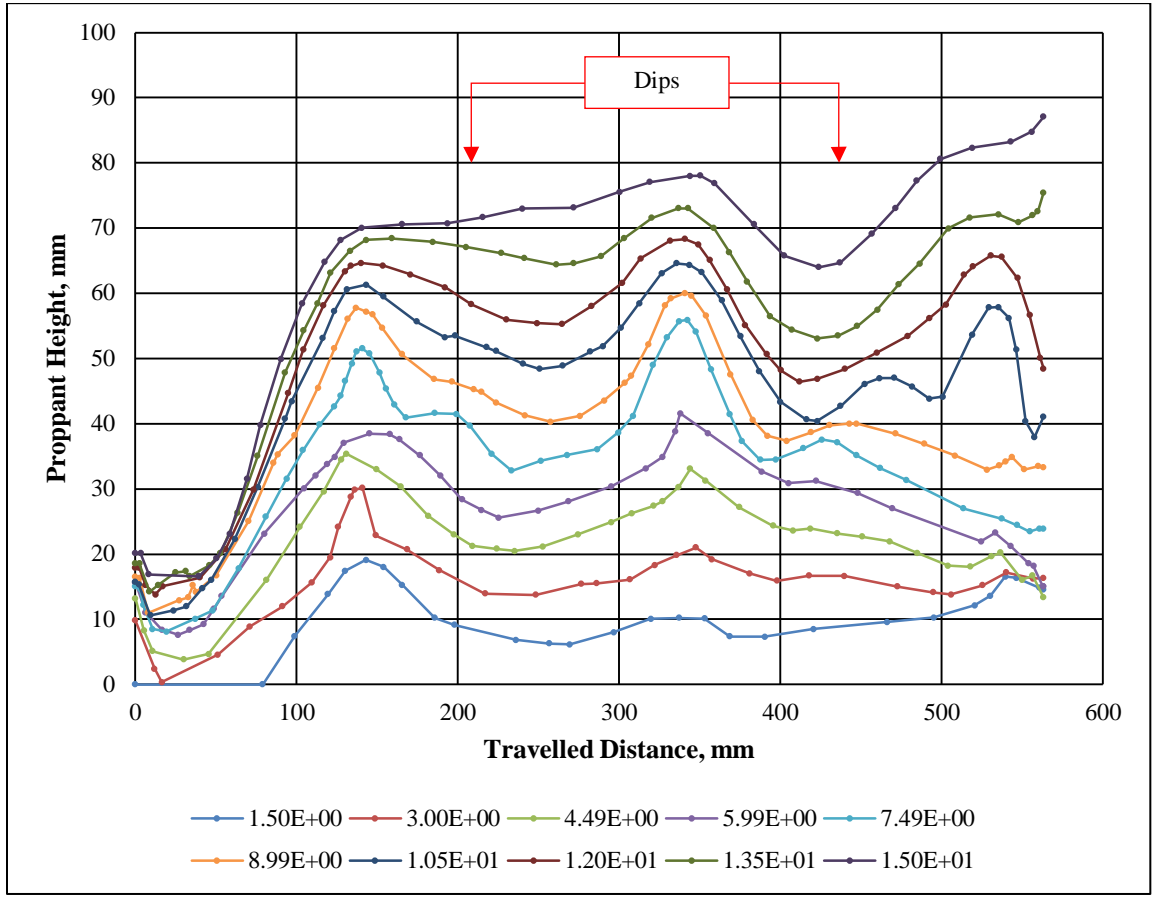
Figure 4.48. Proppant Distribution along the Low Leak-off Slot until Filling the Dips (after FPV10)

These holes, which were designed to permit water to flow through them but prevent proppant from exiting the slot, provided an opportunity to fill the slot completely. Figure 4.49 shows all of the aforementioned stages of filling a leak-off fracture. This stage

started by filling the fracture-tip side, then heading backward to fill the whole fracture until the injection point to reach tip screen out.
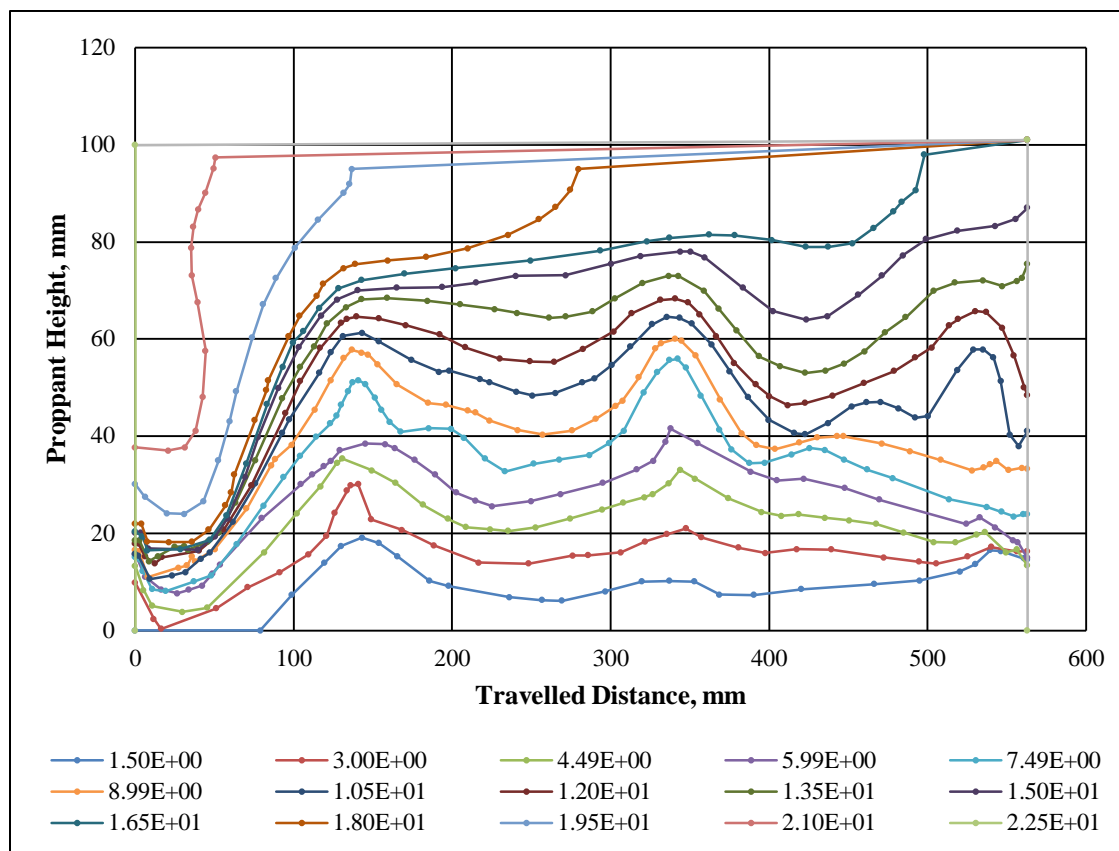
Figure 4.49. Proppant Distribution along the Low Leak-off Slot until Filling the Slot (after FPV15)

4.2.4.2. High leak-off fracture. This model was constructed by drilling nine apertures to drain only water from the slot, as explained in Section 4.1.4. Figure 4.50 clarifies proppant distribution along high leak-off fracture at the first slurry FPV. The red arrows in the figure pointed to the leak-off apertures' location. A captured photo for the slot at this stage was inserted at the top of this figure. The purple line in the photo pointes to the proppant bed. Because of the short distance between the apertures and the bottom of the slot, the effect of leak-off on proppant distribution is not clear.
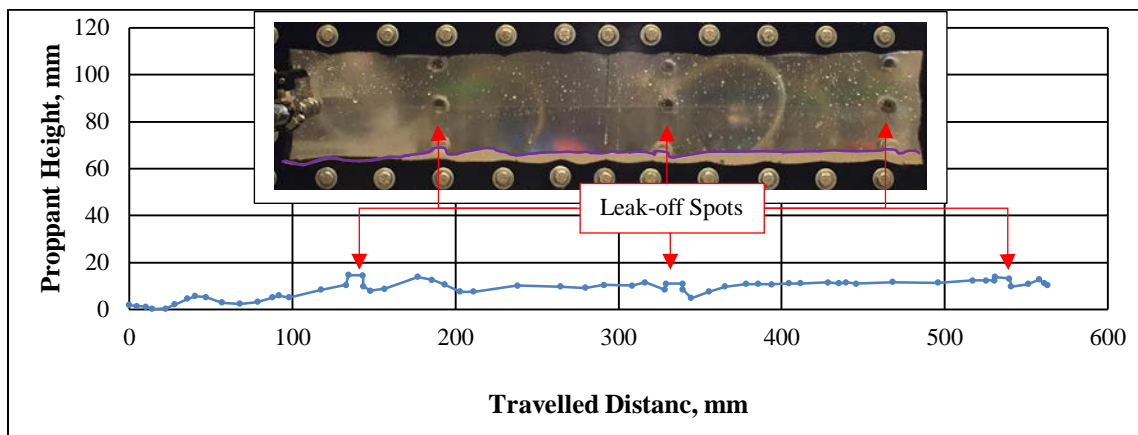
Figure 4.50. Proppant Distribution along the High Leak-off Fracture at the First FPV

Figure 4.51 explains proppant distribution along the slot during nine slurry FPVs. The red lines indicate the locations of the apertures. The captured photo that was inserted into the figure was for slurry FPV9. In this experiment, proppant was following water and settling close to the leak-off apertures. Aperture lines were plugged by proppant one after another; the bottom line (line 3) was first plugged, then line 2, and finally line 1. The first aperture in line 1 that was plugged by proppant was $Z_{3/3L}$l. The aperture, $Z_{1/3L}$1, was located at the top of the fracture tip side, and it is marked in the inserted captured photo.
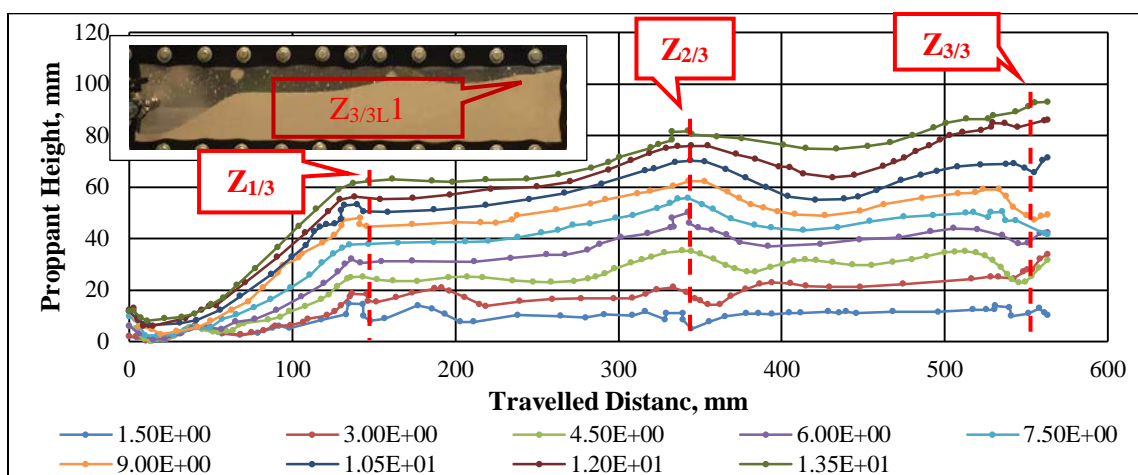
Figure 4.51. Proppant Distribution along the High Leak-off Fracture after FPV9

Figure 4.52 typifies all steps of proppant pile development until filling the slot. After covering $Z_{3/3L}1$ aperature in FPV9, proppant filled the whole slot starting from the fracture-tip side and ending with injection point to reach the tip screen out.
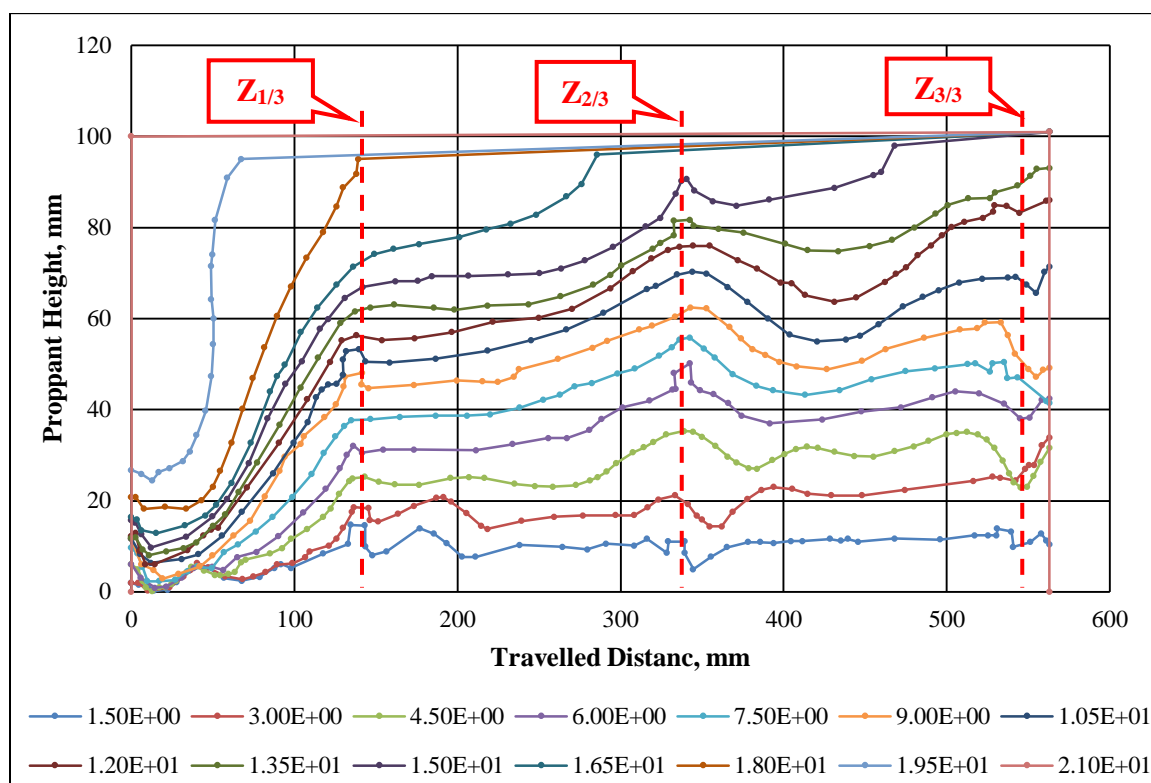
Figure 4.52. Proppant Distribution along the High Leak-off Slot until Filling the Slot (after FPV14)

Novotny (1977) found that fluid loss occurs along the entire permeable zone even if it was covered by proppant. In this study, in high leak-off fracture, the effect of covering a leak-off aperture by proppant was investigated. Water volume was collected separately from the nine apertures to determine water volume that was produced from each aperture. Figure 4.53 depicts water propensity to leave the slot from all leak-off spots as a function of slurry FPV. At the first slurry FPV, most produced water was from $Z_{3/3L}$. At 14 slurry

FPV, most produced water from the nine apertures was from $Z_{1/3L}$, while no produced water was observed from $Z_{3/3L}$.
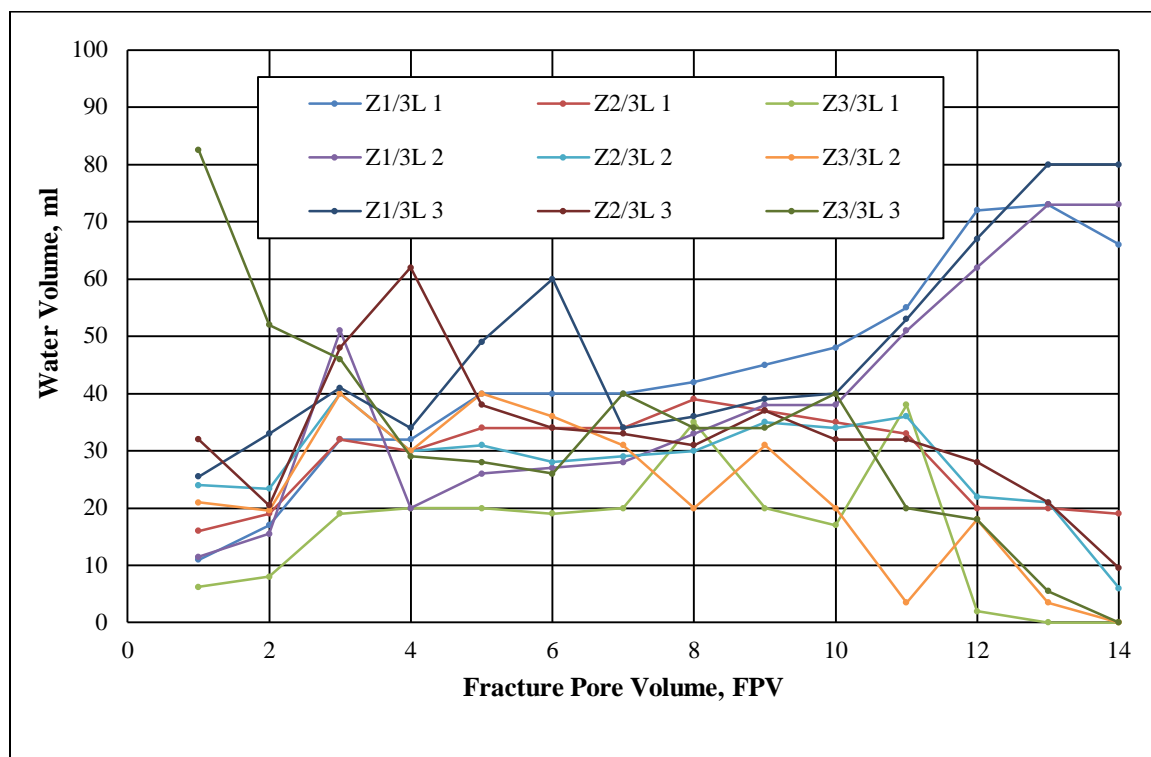
Figure 4.53. Water Volume Leaving the Slot from Each Spot of High Leak-off Fracture

Figure 4.54 shows the water volume fraction produced from each zone as a function of slurry injection pore volume. Water volume fraction is the ratio of the produced water volume from one zone to the total produced water volume from the three zones. The first slurry FPV showed that about 0.48 of the total produced water from the slot was from $Z_{3/3L}$ because of low pressure in this zone. The highest pressure was recorded at the injection side, $Z_{1/3L}$. Table 4.9 illustrates pressure distribution at these points. Pressure is calculated by (27) through (32). However, at the 14 FPV, $Z_{3/3L}$ apertures were plugged completely, and no water was produced from this zone. $Z_{2/3L}$ and $Z_{1/3L}$ apertures were the alternative

pathways for water to be produced from the fracture. $Z_{1/3L}$ produced 0.86 of the total produced water from the fracture slot. Additionally, Figure 4.54 shows that $Z_{1/3L}$ was the main conduit allowing water to leave the slot.
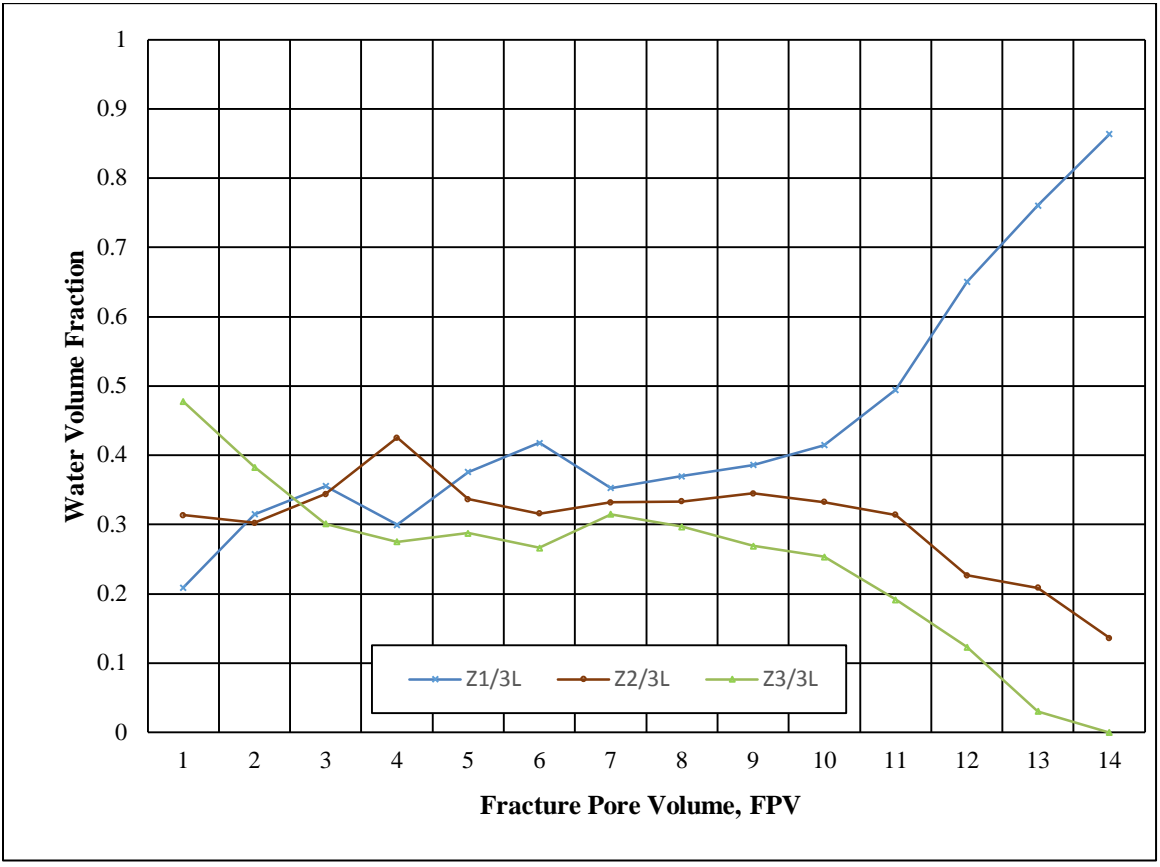
Figure 4.54. Effect of Location of the Apertures on the Amount of Existing Water

Table 4.9. Pressure Distribution along the Slot

Pressure inside the pipes before entering the slot, psi	Pressure at the injection side of the slot, psi	Pressure at $Z_{1/3L}$ spot, psi	Pressure at $Z_{2/3L}$ spot, psi	Pressure at $Z_{3/3L}$ spot, psi
27.09	27.06	27.03	27.00	26.96

Note that pressure in pipes was measured by the pressure gauge, while pressure distribution inside the slot was calculated through [(27)-(32)] where pressure loss due to changing the flow area, which represents the pressure at the injection side of the slot, is defined in (27) and (28):

$$P = \rho g h_m x 1.45 x 10^{-5} \tag{27}$$

$$\rho = \frac{m_p + m_w}{V_p + V_w} \tag{28}$$

where

P: Pressure, psi

ρ: Slurry density, m/cc

m_p: Proppant mass, gm

m_w: Water mass, gm

V_p: Proppant volume, cc

V_w: Water volume, cc

g: Acceleration due to gravity = 980.6 cm/s^2

1.45x10^{-5}: Conversion factor from dyne/cm^2 to psi.

The minor loss is h_m, which is calculated by (29) and (30) (White, 2010):

$$h_m = \frac{K_L v^2}{2g} \tag{29}$$

where

v: Slurry horizontal velocity, ft/s

$$K_L = 1 - \left(\frac{d^2}{D^2}\right)^2 \tag{30}$$

where

K_L: Loss coefficient, dimensionless

d: Smaller diameter pipe, cm

D: Bigger diameter pipe, cm.

Since the slot is a rectangular shape, its equivalent diameter was calculated by (31) (Saleh, 2002; White, 2010):

$$D_e = \frac{4 * area}{Perimeter} = \frac{4\,h * w}{2(h + w)} = \frac{2}{\left(\frac{1}{h} + \frac{1}{w}\right)} \tag{31}$$

where

D_e: Equivalent diameter, cm

h: Slot height, cm

w: Slot width, cm.

Pressure losses along the slot were calculated by (32) (Clark and Zhu, 1996):

$$\Delta P = \frac{12l\mu Q_s}{hw^3} \tag{32}$$

where

μ: Slurry viscosity, poise

Q_s: Slurry flowrate, cm³/s

l: Slot length, cm.

4.2.4.3. Comparison between no leak-off, low leak-off, and high leak-off fractures. Proppant followed water. Wherever water went, proppant flowed with it. When water changed its movement/direction to go through a leak-off spot, three factors played roles in proppant movement and settlement:

1. Proppant was forced to go in a normal direction to its original horizontal direction toward fracture wall, which made proppant lose its kinetic energy and settle down close to that spot.

2. The concentration of proppant close to the wall increased. As a result, proppant settling velocity also increased as it is represented by (33), which is a correlation proposed by Gadde et al. (2004):

$$V_\emptyset = V_s(2.37\emptyset^2 - 3.08\emptyset + 1) \tag{33}$$

where

$V_\emptyset$: settling rate of concentrated particle, cm/s

$\emptyset$: Proppant concentration (Volume of solid/Volume of mixture).

3. Water leaving a fracture meant less proppant-carrying fluid inside that fracture. Consequently, more settled proppant could be found close to leak-off zones.

Figure 4.55 explains proppant distribution along the slot at the first slurry FPV for no leak-off, low leak-off, and high leak-off fractures. The black circles mark the leak-off locations. Results show that proppant domes were not formed in the middle of fracture, but only occurred at the injection and fracture-tip sides. The first dome was observed close to $Z_{1/3L}3$ aperture even if no leak-off spots existed. This dome was formed due to the poor efficiency of slickwater in carrying proppant for a long distance, which caused most proppant to settle after a short distance. Another dome for the accumulated proppant was observed at the fracture-tip side (550 mm from the injection side) for all fracture types. At the fracture-tip side, small and large proppant sizes were accumulated together and formed the dome. Small-sized proppant reached and collided with the fracture-tip side before it

settled. Large-sized proppant settled along different locations of the slot and crept until reaching the fracture tip side to be settled with small-sized proppant. Figure 4.55 also shows that leak-off had no effect on proppant height distribution during the first FPV. This occurred because of the long distance between settled proppant height and apertures.
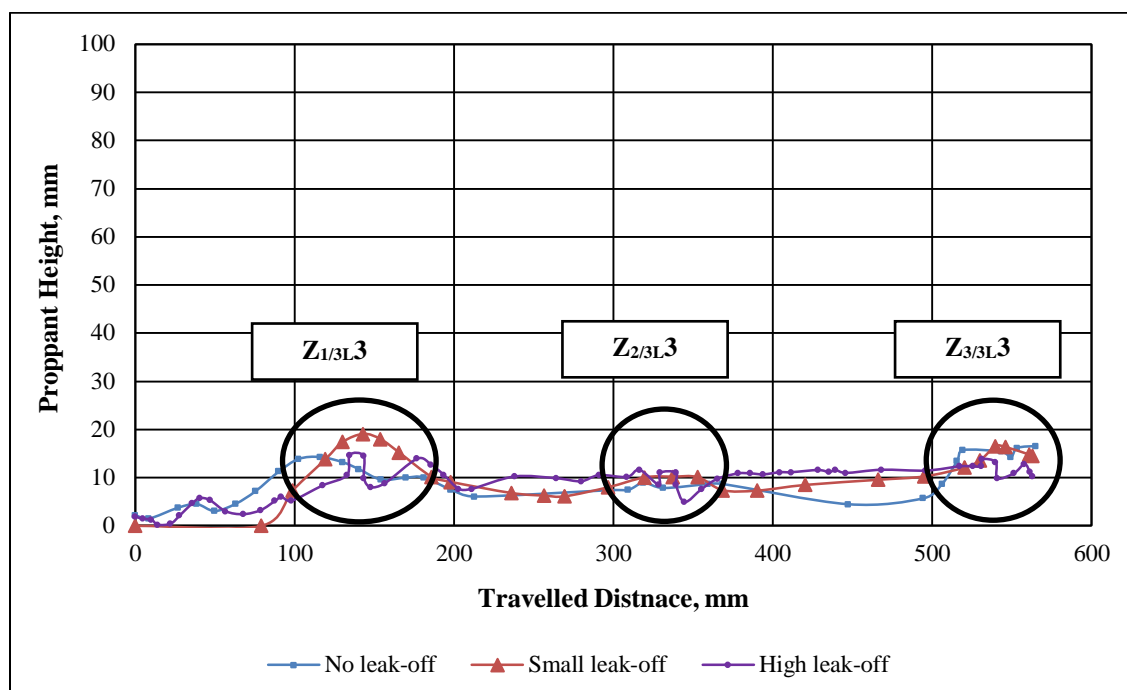
Figure 4.55. Leak-off Effect on Proppant Settling and Distribution for FPV1

Figure 4.56 illustrates proppant height along three fracture leak-off slot models after the proppant pile reached the middle of the fracture slots. Leak-off had a considerable effect on proppant height distribution, which was an opposite trend to the settling mechanism that occurred during the first FPV (Figure 4.55). The effect of fracture leak-off was more noticeable in the high leak-off fracture (the upper curve in Figure 4.56) than the other fractures. In the high leak-off fracture, proppant and water flowed together until both were discharged from the fracture.
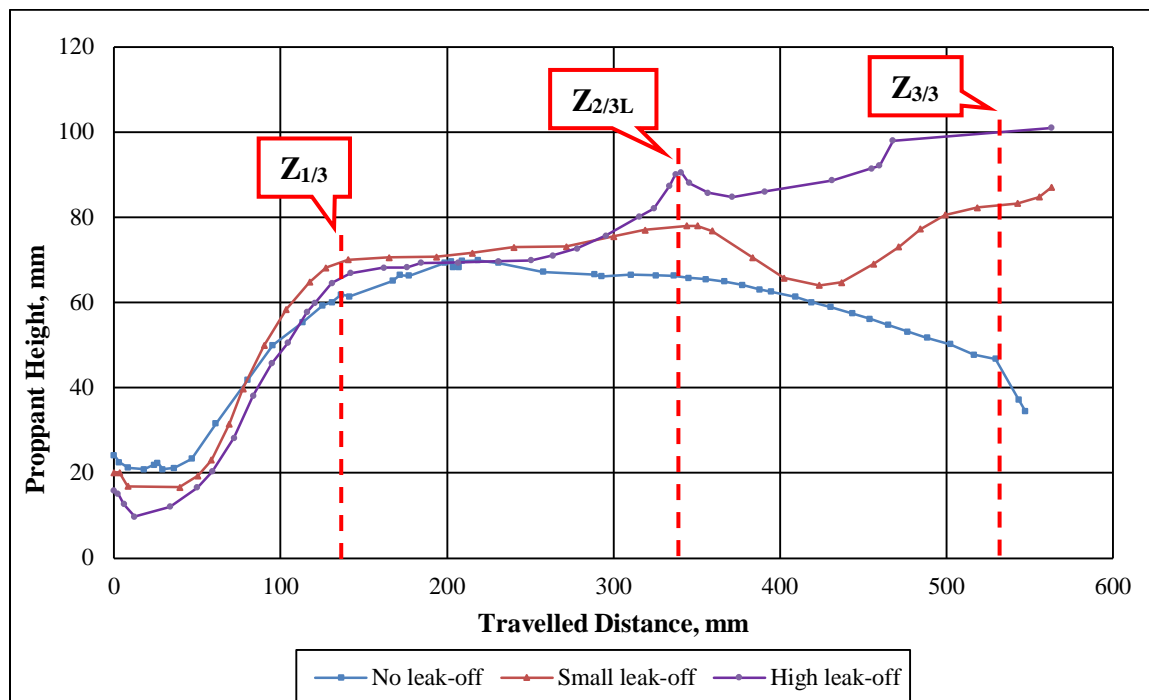
Figure 4.56. Proppant Distribution along Three Slots Differ in Fluid Efficiency

Figure 4.57 shows that the slurry injection pressure was varied and based on the leak-off intensity. At the first few slurry injection pore volumes, slurry injection pressure with no leak-off model had higher slurry injection pressure than slurry injection with high leak-off model. Slurry injection pressure decreased as the leak-off intensity increased. The presence of leak-off apertures lessened injected pressure because they provided surrogate channels to discharge water and accompanied pressure. At 1 FPV, the injection pressure was 32.8 psi for no leak-off fracture, while it was 21.7 psi for high leak-off fracture. However, at the last stage of injection at approximately 13 FPV (approaching the EDL), the slurry injection pressure trend changed. Recorded slurry injection pressure at fracture with high leak-off became higher than other leak-off models. This pressure change occurred because the slurry inside the fracture became more compactd due to the continuous loss of water from the fracture.
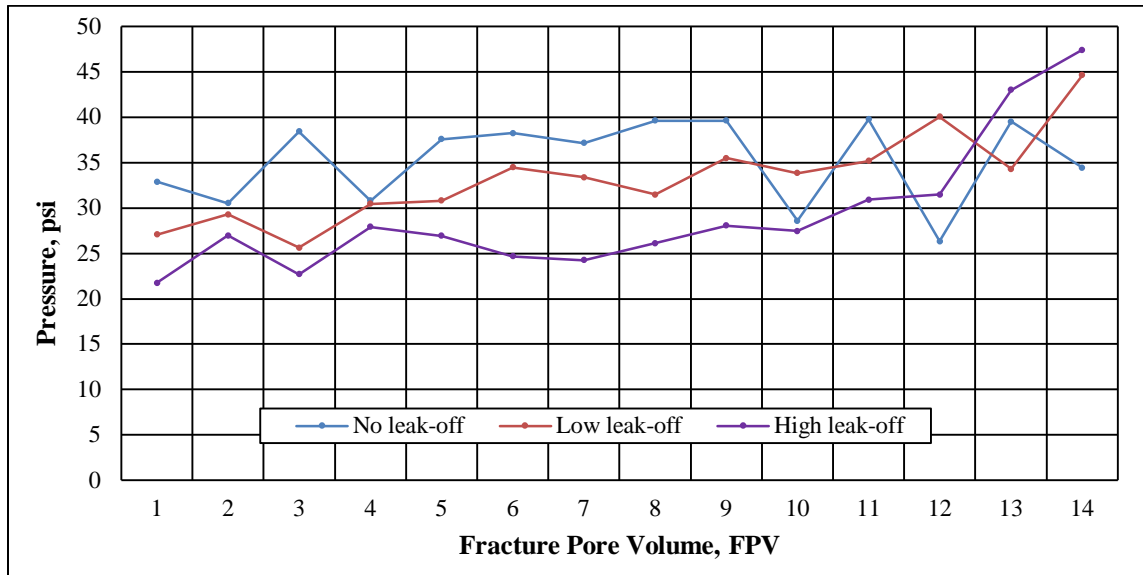
Figure 4.57. Pressure Profile for All FPVs of Different Leak-off Fractures

4.2.5. Settling and Transport Proppant Mechanisms. To facilitate understanding of proppant settling mechanisms in a fracture, Table 4.10 summarizes the five stages of proppant settling and dune shape development based on our experimental observations. Each of these five stages was determined by the upper and lower limit of proppant dune level development (PDLD). PDLD is the ratio of dune level before reaching the equilibrium dune level (EDL) to EDL as in (34):

$$\text{PDLD} = \frac{Dune\ Level\ (DL)}{Equilibrium\ Dune\ Level\ (EDL)}. \tag{34}$$

4.2.5.1. Stage 1: Friction and gravity. This stage occurred when PDLD was between 0.0 and 0.25 and drawdown angle was from -0° to -3.4°. At the beginning of this stage, most injected proppant spread along the fracture. Larger-size proppant settled first as clusters, obliging some smaller-size proppant to settle down to the bottom of the slot. This mechanism can be described as restricted or hindered settling. The rest of the small-

sized proppant traveled through the fracture to settle farther and singularly, which can be described as a free-settling mechanism.

4.2.5.2. Stage 2: Building dune height.   This stage occurred when PDLD was between 0.26 and 0.55. Proppant pile development was the fastest among the other five stages. In stage 1, proppant spread horizontally more than vertically (i.e., proppant pile height increment could be ignored). In stages 3, 4, and 5, flow area was reduced. The reduction in flow area caused very high slurry horizontal velocity that resulted in high erosion rate for proppant compared to settling rate. In stage 2, the dominant mechanism was creep and saltation. Drawdown angle ranged from -3.7° to -7.4°. Most of the dune height was built in this stage.

4.2.5.3. Stage 3: Extension the plateau and drawing the dune shape.   This stage started when EDL was 0.56 and ended when PDLD reached 0.89. Drawdown angle ranged from -7.4° to -8.6°. Since the proppant pile height exceeded the outlet point, proppant falling back was easily observed at this stage. The effect of this stage was noticed by the horizontal extension of the proppant mound and drawing the proppant pile shape.

4.2.5.4. Stage 4: Packing and sparse change.   This stage was observed when PDLD increased from 0.90 to 0.98. Drawdown angle was between -8.6° and -14.4°. High injection velocity of slurry caused some settled proppant to be carried and suspended with the newly injected slurry. When the slurry injection velocity became slow, more proppant settled.

4.2.5.5. Stage 5: EDL and EDX.   A negligible change in proppant height along the slot was observed during this stage. The PDLD ranged from 0.99 to 1.0, and the cross sectional area was smaller than previous stages. The reduction in cross section area

increased slurry horizontal velocity. This high velocity reduced proppant-settling rate. Essentially, all injected proppant left the fracture or was exchanged with old settled proppant because of the high slurry velocity. High injection slurry velocity suspended proppant grains to be produced at the outlet. Drawdown angle was -14.4° at the beginning of this stage and -14.5° at the end. Figure 4.58 shows how EDL fraction developed for each FPV.

Table 4.10. Five Stages Mechanisms to Reach EDL

Stage Number	Mechanism	Mechanism Description	PDLD, Fraction	Drawdown Angle, degree	Picture
1	Hindered and Free Settling	Friction and Gravity	0.0-0.25	0-3.4	
2	Creep and Saltation	Building Dune Height	0.26-0.55	3.4-7.4	
3	Rolling and Falling Back	Extension the Plateau and Drawing Dune Shape	0.56-0.89	7.4-8.6	
4	Suspension and Swirl at the Outlet	Packing and Sparse Change	0.90-0.98	8.6-14.4	
5	Severe Suspension and Swirl at the Outlet	EDL and EDX	0.99-1.0	14.4-14.5	
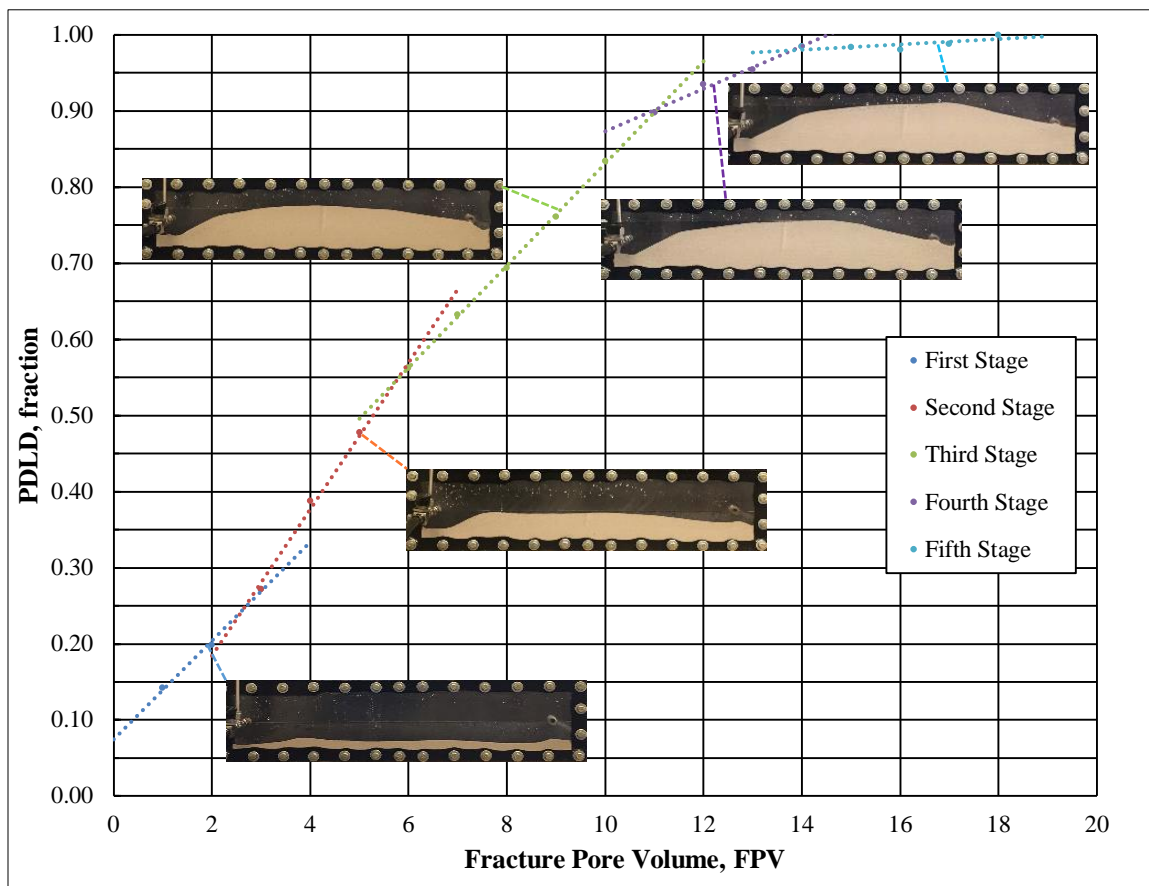
Figure 4.58. EDL Progress for Each FPV

4.2.5.6. Proppant movement and its effect on injected slurry composition.
Proppant transport along the fracture was observed starting from the injection point until proppant settled or left the slot from the outlet. When proppant entered into the slot, it underwent four types of forces: 1) thrust force to drive it to the fracture tip, 2) drag force to stop it from any propagation, 3) lift force to carry it upward, and 4) gravity force to settle at the bottom of the slot. Lighter proppant floated and rose up until it touched the upper bound of the slot. Then, its direction was changed to pass through the slot and finally settled at the end of the slot, as shown in Figure 4.59. Touching the upper bound of the fracture could abrade the fractured formation especially in fracturing shales or chalk formations.

On the other hand, touching the upper bound of the fracture, or any point of a formation, causes some proppant to adhere to or embed in the shale grains due to the roughness effect. Thus, sloughing and sticking processes could happen between shale grains and injected proppant. Since fracture conductivity is a function of proppant type and proppant/shale grains-packing pattern, this exchange will affect fracture conductivity.

Figure 4.59. Small Proppant Floated High up to the Upper Bound of the Slot, While Most of Large Proppant Settled Rapidly

5. CONCLUSIONS AND RECOMMENDATIONS

5.1. CONCLUSIONS

The following conclusions are obtained from this study:

1. Fracture heterogeneity, fracture width, fracture wall roughness, and fluid efficiency have significant effects on settling velocity, horizontal velocity and proppant distribution along a fracture.

2. Increasing fracture heterogeneity increases equilibrium dune level (EDL) and equilibrium dune length (EDX).

3. Increasing W_{in}/W_{out} increases EDL, while EDX will be decreased after reaching an optimum W_{in}/W_{out} value.

4. Increasing fracture width heterogeneity or W_{in}/W_{out} would increase settling velocity, but decrease horizontal velocity. That is observed by measuring the height of proppant pile at both injection and fracture tip side.

5. Fracture wall properties have more influence on settling velocity than horizontal velocity.

6. EDL decreased due to increasing fracture wall roughness, while EDX showed an opposite behavior because of the reduction in settling velocity due to increasing wall roughness compared to horizontal velocity recession.

7. Settled proppant can be more stable inside a fracture when the fracture wall is rougher; therefore, the higher fracture roughness, the better fracture conductivity.

8. Increasing fracture leak-off developed proppant-settling velocity that increased the amount of participated proppant around leak-off spots.

9. At FPV1, most proppant settled close to the first leak-off spot even though it is a high-pressure zone and water tends to skip it and leave the slot from the last zone because of low proppant-carrying slickwater efficiency.

10. Increasing fracture width heterogeneity, injection side width or roughness would increase propped surface area and therefore fracture conductivity improvement.

11. The proppant pile development can be divided into five stages based on pile buildup rate. Each stage has specific parameters and proppant movement mechanisms.

5.2. RECOMMENDATIONS

Hydraulic fracturing by using slickwater is an important research area. Although many studies were dedicated to proppant placement through a fracture, more efforts are needed to provide better comprehension about proppant settling in slickwater. The following lists suggestions for future work to expand the conclusions of this work:

1. During this work, it was observed that proppant pile height has an effect on proppant placement and settlement. This study suggests that fracture height should be investigated as well.

2. The effect of fracture width heterogeneity, injection side width, wall roughness, and leak-off should be studied collectively to give better understanding about proppant behavior inside an induced fracture

3. Due to the difference between the results of Alotaibi and Miskimins (2015) and this work about proppant pile mechanisms, more work should be added using FPV technique with sand to cover this research area.

4. Adding polyacrylamide (slickening agent).

APPENDIX

After explaining experimental procedure and results, it is important mention to the method by which proppant height and distribution were measured, and propped surface area was calculated. This section will deal with each one in detail.

A.1. MEASURING PROPPANT HEIGHT.

For more precise measurement, the program PlotDigitzer has been used to digitize each photo captured for each FPV and transform it to x and y representing the traveled distance of proppant along the slot and proppant height at that point. Figure A.1 illustrates a sample for this method.

Figure A.1. Digitizing Photo Method

This method can be summarized by four steps:

1. Determine x-axis and y-axis

2. Identify the minimum and maximum value for each axis.

3. Click on each point on a photo to get the coordinate value for that point.

4. Click "Done" to get a table that represents the x-axis and y-axis value for each point.

A.2. CALCULATING PROPPED SURFACE AREA.

After measuring the height of proppant pile for each FPV, a trapezoidal code in MATLAB was used to derive the surface area covered by proppant[1]. The code is illustrated below. To complete this process, three steps should be followed:

1. Insert traveled distance and proppant height at that distance between the two parentheses located after equal signs for *x* and *y*, respectively.

2. Go to the "ERROR" ribbon. Then hit "Run," which is located in the " RUN" group.

3. The area under the curve, which represents the propped surface area, will be calculated immediately.

The code is as below:

X = [Travelled distance];

Y = [Proppant height];

%% Outputs

plot(X,Y,'Linewidth',2)

---

[1] This code was written by Mr. Ethar Al-Kamil, Ph.D. student in Missouri University of Science and Technology.

```
xlabel('Distance')

ylabel('Height')

% Area Under the Curve Using Trapezoidal Role

Int = trapz(X, Y)

% Format Outputs

a=ceil(min(X));

b=ceil(max(X));

c=ceil(min(Y));

d=ceil(max(Y));

axis([a b c d])
```

BIBLIOGRAPHY

Alotaibi, M. A., & Miskimins,, J. L. (2015, September). Slickwater Proppant Transport in Complex Fractures: New Experimental Findings & Scalable Correlation. *SPE*, 1-26. doi:10.2118/174828-MS

Alqatrani, G., Britt, L. K., Otzen, G., Guzman, M., Kusanovic, G., & Dunn-Norman, S. (2016). A Statistical Approach to Fracture Optimization of the Glauconite Formation in Southern Chile. *SPE*, 1-26. doi:doi:10.2118/181864-MS

Barree, R. D., & Conway, M. W. (1995). Experimental and Numerical Modeling of Convective Proppant Transport. *SPE, 47*(3), 216-223. doi:10.2118/28564-PA

Boyer, J., Maley, D., & O'Neil, B. (2014). Chemically Enhanced Proppant Transport. *SPE*, 18. doi:10.2118/170640-MS

Carroll Jr., H. B., & Baker, B. A. (1979). Particle Size Distributions Generated By Crushed Proppants And Their Effects on Fracture Conductivity. *SPE-AIME*, 127-137. doi:10.2118/7923-MS

Cinco-Ley, H., & Samaniego-V., F. (1981). Transient Pressure Analysis for Fractured Wells. *SPE*, 1749-1766. doi:10.2118/7490-PA

Clark, P. E., & Quadir, J. A. (1981). Prop Transport in Hydraulic Fractures: A Critical Review of Particle Settling Velocity Equations. *SPE/DOE Low Permeability Gas Reservoirs Symposium*, 343-347. doi:10.2118/9866-MS

Clark, P. E., & Zhu, Q. (1996). Convective Transport of Propping Agents During Hydraulic Fracturing. *SPE*, 229-235. doi:10.2118/37358-MS

Cobb, S. L., & Farrell, J. J. (1986). Evaluation of Long.:rerm Proppant Stability. *SPE*, 483-492. doi:10.2118/14133-MS

Dayan, A., Stracener, S. M., & Clark, P. E. (2009). Proppant Transport in Slick-Water Fracturing of Shale-Gas Formations. *SPE*, 9. doi:10.2118/125068-MS

Economides, M. J., Hill, A. D., Ehlig-Economides, C., & Zhu, D. (2013). *Petroleum Production Systems.* (Second, Ed.) doi:0-13-703158-0

Examining Our Assumptions - Have Oversimplifications Jeopardized Our Ability To Design Optimal Fracture Treatments? (2009, January). *SPE Hydraulic Fracturing Technology Conference*, 1-31. doi:10.2118/119143-MS

Fracturing-Fluid Additives. (1988, October). *SPE*, 1277-1279. doi:10.2118/17112-PA

Gadde, P. B., Liu, Y., Norman, J., Bonnecaze, R., & Sharma, M. M. (2004, September). Modeling Proppant Settling in Water-Fracs. *SPE*, 1-10. doi:10.2523/89875-MS

Jones, J., & Britt, L. K. (2009). *Design and Appraisal of Hydraulic Fractures.* Richardson, Texas: Spciety of Petroleum Engineers. Retrieved from http://store.spe.org/Design-and-Appraisal-of-Hydraulic-Fractures-P17.aspx

Kern, L. R., Perkins, T. K., & Wyant, R. E. (1959). The Mechanics of Sand Movement In Fracturing. *Journal of Petroleum Technology, 11*(07), 55-57. doi:10.2118/1108-g

King, G. E. (2012, February). Hydraulic Fracturing 101: What Every Representative, Environmentalist, Regulator, Reporter, Investor, University Researcher, Neighbor and Engineer Should Know About Estimating Frac Risk and Improving Frac Performance in Unconventional Gas and Oil Wells. *SPE*, 1-80. doi:10.2118/152596-MS

Liang, F., Sayed, M., Al-Muntasheri, G. A., Chang, F. F., & Li, L. (2016, March). A comprehensive review on proppant technologies. *Petroleum, 2*(1), 26e39 Contents. doi:10.1016/j.petlm.2015.11.001

Liu, Y., & Sharma, M. M. (2005, October). Effect of Fracture Width and Fluid Rheology on Proppant Settling and Retardation: An Experimental Study. *Proceedings of SPE Annual Technical Conference and Exhibition*, 1-12. doi:10.2523/96208-MS

Mack, M. G., & Coker, C. E. (2013). Proppant Selection for Shale Reservoirs: Optimizing Conductivity, Proppant Transport and Cost. *SPE*, 14. doi:10.2118/167221-MS

Mack, M. G., & Coker, C. E. (2013, November). Proppant Selection for Shale Reservoirs: Optimizing Conductivity, Proppant Transport and Cost. *SPE Unconventional Resources Conference*, 1-14. doi:10.2118/167221-MS

Mack, M., Sun, J., & Khadilkar, C. (2014.). Quantifying Proppant Transport in Thin Fluids – Theory and Experiments. *SPE Hydraulic Fracturing Technology*, 1-14. doi:10.2118/168637-MS

Marquardt, D., Thompson, J., & Brown, E. (1991). Delayed Breaker Systems Improve Fracture Conductivity. *PETROLEUM SOCIETY OF CIM and AOSTRA* . doi:10.2118/91-93

McDaniel, B. W. (1986). Conductivity Testing of Proppants at High Temperature. *SPE California Regional Meeting*, 197-208. doi:10.2118/15067-MS

Me Meehan, D. E., & Shah, S. N. (1991, August). Static Proppant-Settling Characteristics of Non-Newtonian Fracturing Fluids in a Large-Scale Test Model. *SPE Production Engineering*, 305-312. doi:10.2118/19735-PA

Novotny, E. J. (1977). Proppant Transport. *Society of Petroleum Engineers of AIME*, 1-12. doi:10.2118/6813-MS

Paktinat, J., O'Neil, B., Aften, C., & Hurd, M. (2011). High Brine Tolerant Polymer Improves the Performance of Slickwater Frac in Shale Reservoirs. *Society of Petroleum Engineers*, 1-18. doi:doi:10.2118/144210-MS

Saleh, J. (2002). *Fluid Flow Handbook.* New York: McGraw-Hill.

Shelley, B., Grieser, B., Johnson, B. J., Fielder, E. O., Heinze, J. R., & Werline, J. R. (2008, September). Data analysis of Barnett shale completions. *SPE Journal*, 366-374. doi:10.2118/100674-PA

Smith, M. B., Bale, A. B., Britt, L. K., Klein, H. H., Siebrits, E., & Dang, X. (2001). Layered Modulus Effects on Fracture Propagation, Proppant Placement, and Fracture Modeling. *Proceedings of SPE Annual Technical Conference and Exhibition*, 1-14. doi:http://dx.doi.org/10.2118/71654-MS

Sun, H., Zhou, J., Brannon, H., Gupta, D. V., Ault, M., Carman, P., & Wheeler, R. (2015). Case Study of Soft Particle Fluid to Improve Proppant Transport and Placement. *SPE Annual Technical Conference and Exhibition*, 1-16. doi:10.2118/174801-MS

Swanson, V. F. (1967). The development of Formula For Direct Determination of Free Settling Velocity of Any Size Particle. *SME/AIME*, 160-166. Retrieved from http://www.onemine.org/document/document.cfm?docid=27298

Team, T. O. (1999). Principles and Processes of Sediment Transport. In *Waves, Tides and Shallow-Water Processes* (pp. 96-124). Oxford: Butterworth Heinemann.

Tsai, K., Fonseca, E., Degaleesan, S., & Lake, E. (2013, February). Advanced Computational Modeling of Proppant Settling in Water Fractures for Shale Gas Production. *SPE Hydraulic Fracturing Technology Conference, 18*(01), 50-56. doi:10.2118/151607-PA

Warpinski, N. R., Schmidt, R. A., & Northrop, D. A. (1982, March). In.;.Situ Stresses: The Predominant Influence on Hydraulic Fracture Containment. *Journal of Petroleum Technology, 34*(03), 653-664. doi:10.2118/8932-PA

White, F. (2010). *Fluid Mechanics* (7th ed.). 862. doi:10.1111/j.1549-8719.2009.00016.x.Mechanobiology

Zhou, J., Sun, H., Qu, Q., Guerin, M., & Li, L. (2014, February). Benefits of Novel Preformed Gel Fluid System in Proppant Placement for Unconventional Reservoirs. *SPE/EAGE European Unconventional Conference and Exhibition*, 1-7. doi:10.2118/167774-MS

VITA

Dhurgham Abdulameer Kadhim was born in Najaf, Iraq in 1984. He received his bachelor's degree in petroleum engineering from Baghdad University in 2010. He has been working with Midland Refineries Company/Najaf Refinery as a production monitor engineer since November 2010.

In September 2015, he was awarded a fully funded scholarship from The Higher Committee for Education Development in Iraq (HCED) to obtain his master's degree in petroleum engineering.

Kadhim joined Missouri University of Science and Technology in August 2015. He worked with Dr. Shari Dunn Norman and Dr. Abdulmohsin Imqam in hydraulic fracturing. He received his master's degree in Petroleum Engineering from Missouri University of Science and Technology in July 2017.